Effects of Lower Drying-Storage Temperature on the Ductility of High-Burnup PWR Cladding

Fuel Cycle Research & Development

Prepared for
U.S. Department of Energy
Used Fuel Disposition Campaign

M.C. Billone and T.A. Burtseva

Argonne National Laboratory
August 30, 2016
FCRD-UFD-2016-000065
ANL-16/16

Reviewed by:

Signature on file

Brady D. Hanson
(Pacific Northwest National Laboratory)
Technical Reviewer

Submitted by:

Michael C. Billone
(Argonne National Laboratory)
Work Package Manager

Page intentionally blank

Executive Summary

The purpose of this research effort is to determine the effects of canister and/or cask drying and storage on radial hydride precipitation in, and potential embrittlement of, high-burnup (HBU) pressurized water reactor (PWR) cladding alloys during cooling for a range of peak cladding temperatures (PCTs) and hoop stresses. Extensive precipitation of radial hydrides could lower the failure hoop stresses and strains, relative to limits established for as-irradiated cladding from discharged fuel rods stored in pools, at temperatures below the ductile-to-brittle transition temperature (DBTT).

HBU PWR cladding alloys have a wide range of hydrogen contents and hydride distributions after in-reactor service. Cooling from PCTs during drying and storage may result in the precipitation of radial hydrides. These radial hydrides are a potential embrittlement mechanism for HBU cladding subjected to hoop-stress loading, which may occur during post-storage cask transport. Ring compression tests (RCTs), which simulate pinch-type loading at grid spacers, are used as screening tests to determine cladding ductility as a function of RCT temperature and the corresponding DBTT. Previous tests were conducted with pressurized and sealed cladding rodlets heated to 400°C (the NRC ISG-11, Rev. 3, limit for all fuel burnups under normal conditions of storage and short-term loading operations) and 350°C followed by slow cooling at 5°C/h. After simulation of drying-storage conditions, the DBTT was determined as a function of the peak hoop stress for HBU PWR cladding alloys: M5® (400°C PCT), ZIRLO™ (400°C and 350°C PCT), and Zircaloy-4 (Zry-4, 400°C PCT). The results for 400°C-PCT samples indicated that radial-hydride-induced embrittlement was insignificant (i.e., DBTT <25°C) for peak hoop stresses ≤90 MPa even with temperature cycling, but it was potentially significant for hoop stresses ≥110 MPa. However, the DBTT results for M5® cladding were not conclusive because the hydrogen content in the samples decreased as the hoop stresses were lowered. Also, test results for ZIRLO™ (now ZIRLO®) heated to 350°C PCT at modest peak hoop stress levels of 93–94 MPa resulted in a high DBTT (125±5°C) compared to the DBTT (23°C) measured for samples subjected to 400°C PCT and peak stresses of 88–89 MPa. The previous data for ZIRLO™ were insufficient to interpret these results with regard to the cause or causes of the 100°C increase in DBTT: (a) very high sensitivity of the ZIRLO™ DBTT to hoop stress level; (b) degrading effects of the very high hydrogen content for the 350°C-PCT samples; and (c) potential decrease in radiation-hardening annealing for the 350°C-PCT samples.

Two new tests were conducted to close or at least narrow the gaps identified above for HBU M5® and ZIRLO™ cladding alloys. An 80-wppm HBU M5® rodlet was subjected to 350°C PCT and 89 MPa prior to cooling at 5°C/h under conditions of decreasing pressure and stress. These test parameters were chosen to support the hypothesis that hydrogen content has a more detrimental effect on the DBTT for M5® than the hoop-stress level for the range of conditions tested. For the HBU ZIRLO™ test, a 387-wppm rodlet was subjected to 350°C PCT and 87 MPa prior to cooling at 5°C/h under conditions of decreasing pressure and stress. These conditions were chosen to test the hypothesis that the DBTT for ZIRLO™ is highly sensitive to peak stress level within the narrow range of 90±3 MPa.

The results of the new M5® test indicated an increase in DBTT from <20°C to 70°C at about 90-MPa peak stress with the increase in hydrogen content from 58 wppm to 80 wppm. These results are comparable to those obtained for the 72-wppm rodlet subjected to peak conditions of 400°C and 111 MPa (70°C DBTT) and very close to the results obtained for the 94-wppm rodlet subjected to peak conditions of 400°C and 142 MPa (80°C DBTT). From a mechanistic perspective, it is more significant to compare hoop stresses at the precipitation temperatures, which depend on total hydrogen content, as all the hydrogen goes into solution at temperatures <330°C: 67 MPa for the 58-wppm rodlet, 74 MPa for the 80-wppm rodlet, 84 MPa for the 72-wppm rodlet, and 113 MPa for the 94-wppm rodlet. The dependence of M5® DBTT on total hydrogen content is further illustrated by examining the effective lengths of radial

hydrides for each case. For the HBU M5® samples tested, essentially all the hydrogen precipitated as radial hydrides within the precipitation stress range of 67–113 MPa. The lengths (i.e., radial hydride continuity factor, RHCF) increased with increasing hydrogen content: 37% for 58 wppm, 54% for 72 wppm, 55% for 80 wppm, and 61% for 94 wppm. It is also speculated that the connectivity of radial hydrides in the axial direction increases with increasing hydrogen content. Stress levels appear to have a secondary effect on DBTT within the range of conditions studied. The potential decrease in annealing for 350°C-PCT samples appears to have a tertiary effect on ductility for the one-hour hold times used in these experiments.

The new ZIRLO™ test sample subjected to 350°C PCT had similar hydrogen content (387 wppm vs. 350 wppm) and the same hold time (24 h) as a sample previously tested at 400°C PCT. These hydrogen contents are more representative of the anticipated peak hydrogen contents in HBU ZIRLO™ irradiated to <60 GWd/MTU. The peak stress was reduced to 87 MPa (vs. 111 MPa). The results were encouraging in that the DBTT was about 27°C, which is comparable to results for samples with about 500-wppm hydrogen heated to 400°C PCT at peak stresses of 88-89 MPa. The DBTT for these three samples was <30°C. However, the DBTT for samples heated to 350°C at 93–94 MPa and to 400°C at 111 MPa was >120°C. Thus, the rapid increase (≈100°C) in DBTT occurred within the narrow peak stress range of 90±3 MPa. In terms of stresses at initiation of precipitation, the transition occurred within the narrow stress range of about 80±2 MPa. Concurrent with the increase in DBTT, the effective length of radial hydrides increased from 20% for peak stresses of 87–89 MPa to ≥30% for peak stresses of 93–94 MPa at 350°C and 111 MPa at 400°C. This observation further supports the high sensitivity of ZIRLO™ DBTT to peak and precipitation stresses. Data trends for the ductility of HBU ZIRLO™ following simulated drying and storage indicate the following: (a) the DBTT for HBU ZIRLO™ has a high sensitivity to peak stress within the range of 90±3 MPa; (b) excessive hydrogen (>600-wppm average, >800 wppm local) can reduce ductility and increase the DBTT; and (c) no significant effects of annealing were observed on ductility and DBTT for samples heated to 350°C and 400°C for periods of 1–24 hours.

For standard PWR fuel rods, the upper-bound hoop stress during drying and storage is estimated to be <80 MPa on the basis of the end-of-life rod-internal-pressure (RIP) data currently available. The 3-sigma upper bound of these data, along with fuel-rod code predictions, is 5 MPa for burnup levels ≤60 GWd/MTU. This upper bound is below the critical stress of about 90 MPa for radial-hydride-induced embrittlement of HBU ZIRLO™ cladding. It is likely below the stress needed to embrittle M5® cladding, as well, although this should be confirmed by conducting a test with a 100-wppm sample subjected to peak conditions of 350°C/80-MPa. The PWR RIP database does not include data for M5®-clad fuel rods nor does it include data for fuel rods irradiated under more modern reactor conditions. However, ORNL plans to generate additional data for 25 PWR standard fuel rods irradiated to 50–60 GWd/MTU under more modern conditions: 4 Zry-4-clad rods, 9 M5®-clad rods and 12 ZIRLO™-clad rods. The expectation is that the measured plenum pressures will be ≤5 MPa, the upper-bound hoop stress will remain at <80 MPa and radial-hydride-induced embrittlement will not be an issue for standard PWR fuel rods.

No end-of-life gas-pressure data are available for PWR Integral Fuel Burnable Absorber (IFBA) ZIRLO™-clad fuel rods. Gas pressures are predicted to be higher for IFBA rods due to the transmutation of the B-10 neutron absorber to helium within the rods. It is anticipated that peak cladding hoop stresses for these rods will exceed the DBTT-transition stress (about 90 MPa) for HBU ZIRLO™. Radial-hydride-induced embrittlement should be considered in setting the failure stress and strain limits for ZIRLO™-clad IFBA fuel rods.

CONTENTS

Executive Summary iii
Contents v
Figures v
Tables viii
1. Introduction 1
2. HBU Cladding Materials and Test Methods 5
   2.1 HBU Cladding Materials 5
   2.2 Test Methods 5
3. Previous Results for HBU M5® and HBU ZIRLO™ 11
   3.1 HBU M5® 11
   3.2 HBU ZIRLO™ 12
4. Results from Current Tests 14
   4.1 HBU M5® following cooling from 350°C PCT 14
   4.2 HBU ZIRLO™ Following cooling from 350°C PCT 23
5. Discussion and Summary 33
References 37
Appendix A Metallographic Images of ZIRLO™ Cross Section 646D6 from 350°C/87-MPa Rodlet 646D 39

FIGURES

1 Steady-state curves for hydrogen dissolution and precipitation in Zr alloys 3
2 RCT measured load (P) and controlled displacement (δ). 7
3 Load-displacement curve for non-irradiated M5® ring tested at RT and 5 mm/s to 1.7 mm displacement. 7
4 RCT benchmark results for determining the ratio of unloading/loading stiffness as a function of the traditional offset strain. 8
5 Summary of ductility data for HBU M5® in the as-irradiated condition and following RHT at 400°C PCT 11
6 Summary of ductility data for HBU ZIRLO™ following RHT at 400°C and 350°C PCTs and peak hoop stresses in the narrow range of 88–94 MPa. 13
7 Sectioning diagram for HBU M5® rodlet 652F2 following RHT at 350°C PCT. 14
8 Longest radial hydride observed for the 652F2F cross section at the reference axial location: (a) 100X and (b) 200X. 15
9 Longest radial hydride observed for the 652F2F cross section at the -0.5-mm axial location. 16
10 Radial hydrides observed on the -0.6-mm 652F2F cross section: (a) longest length (95% RHCF) and (b) average length (55% RHCF). 17

11 Load-displacement curve for the 652F2H sample tested at 23°C.... 18
12 Load-displacement curve for the 652F2D sample tested at 60°C.... 19
13 Load-displacement curve for the 652F2C sample tested at 90°C.... 19
14 Load-displacement curve for the 652F2G sample tested at 120°C.... 20
15 RCT ductility curves for HBU M5® in the as-irradiated condition and following RHT at 350°C and 400°C PCTs.... 22
16 DBTT for HBU M5® vs. hydrogen content following RHT at 350°C and 400°C PCTs.... 22
17 Sectioning diagram for the HBU ZIRLO™ rodlet 646D following RHT at 350°C PCT.... 23
18 Longest radial hydrides observed for the 646D6 cross section: (a) 100X and (b) 200X.... 24
19 Average-length radial hydrides observed for the 646D6 cross section: (a) 100X and (b) 200X.... 25
20 Circumferential orientation of the 652F2F cross section with essentially no radial hydrides.... 26
21 Load-displacement curve for the 646D8 sample tested at 27°C.... 27
22 Load-displacement curve for the 646D4 sample tested at 60°C.... 27
23 Load-displacement curve for the 646D7 sample tested at 90°C.... 28
24 Load-displacement curve for the 646D3 sample tested at 120°C.... 28
25 Summary of ductility data for HBU ZIRLO™ following RHT at 400°C and 350°C PCTs.... 30
26 DBTT vs. hoop stress for HBU ZIRLO™ following RHT at 400°C and 350°C PCTs.... 30
27 DBTT vs. the effective lengths of radial hydrides (RHCF) for HBU ZIRLO™ following RHT at 400°C and 350°C PCTs.... 31
28 Data and FRAPCON predictions for end-of-life (EOL) PWR rod-internal pressures (RIPs) at 25°C as a function of burnup.... 35
A.1 Image (100X) of ZIRLO™ sample 646D6 in Area 1 (12:00 o'clock orientation) from 1-cycle 350°C/87-MPa rodlet 646D.... 41
A.2 Image (100X) of ZIRLO™ sample 646D6 in Area 2 from 1-cycle 350°C/87-MPa rodlet 646D.... 42
A.3 Image (100X) of ZIRLO™ sample 646D6 in Area 3 from 1-cycle 350°C/87-MPa rodlet 646D.... 43
A.4 Image (100X) of ZIRLO™ sample 646D6 in Area 4 from 1-cycle 350°C/87-MPa rodlet 646D.... 44
A.5 Image (100X) of ZIRLO™ sample 646D6 in Area 5 from 1-cycle 350°C/87-MPa rodlet 646D.... 45
A.6 Image (100X) of ZIRLO™ sample 646D6 in Area 6 from 1-cycle 350°C/87-MPa rodlet 646D.... 46
A.7 Image (100X) of ZIRLO™ sample 646D6 in Area 7 from 1-cycle 350°C/87-MPa rodlet 646D.... 47
A.8 Image (100X) of ZIRLO™ sample 646D6 in Area 8 from 1-cycle 350°C/87-MPa rodlet 646D.... 48
A.9 Image (100X) of ZIRLO™ sample 646D6 in Area 9 from 1-cycle 350°C/87-MPa rodlet 646D.... 49
A.10 Image (100X) of ZIRLO™ sample 646D6 in Area 10 from 1-cycle 350°C/87-MPa rodlet 646D.... 50
A.11 Image (100X) of ZIRLO™ sample 646D6 in Area 11 from 1-cycle 350°C/87-MPa rodlet 646D.... 51
A.12 Image (100X) of ZIRLO™ sample 646D6 in Area 12 from 1-cycle 350°C/87-MPa rodlet 646D.... 52
A.13 Image (100X) of ZIRLO™ sample 646D6 in Area 13 from 1-cycle 350°C/87-MPa rodlet 646D.... 53

A.14 Image (100X) of ZIRLO™ sample 646D6 in Area 14 from 1-cycle 350°C/87-MPa rodlet 646D..... 54
A.15 Image (100X) of ZIRLO™ sample 646D6 in Area 15 from 1-cycle 350°C/87-MPa rodlet 646D..... 55
A.16 Image (100X) of ZIRLO™ sample 646D6 in Area 16 from 1-cycle 350°C/87-MPa rodlet 646D..... 56
A.17 Image (100X) of ZIRLO™ sample 646D6 in Area 17 from 1-cycle 350°C/87-MPa rodlet 646D..... 57
A.18 Image (100X) of ZIRLO™ sample 646D6 in Area 18 from 1-cycle 350°C/87-MPa rodlet 646D..... 58
A.19 Image (100X) of ZIRLO™ sample 646D6 in Area 19 from 1-cycle 350°C/87-MPa rodlet 646D..... 59
A.20 Image (100X) of ZIRLO™ sample 646D6 in Area 20 from 1-cycle 350°C/87-MPa rodlet 646D..... 60
A.21 Image (100X) of ZIRLO™ sample 646D6 in Area 21 from 1-cycle 350°C/87-MPa rodlet 646D..... 61
A.22 Image (100X) of ZIRLO™ sample 646D6 in Area 22 from 1-cycle 350°C/87-MPa rodlet 646D..... 62
A.23 Image (100X) of ZIRLO™ sample 646D6 in Area 23 from 1-cycle 350°C/87-MPa rodlet 646D..... 63
A.24 Image (100X) of ZIRLO™ sample 646D6 in Area 24 from 1-cycle 350°C/87-MPa rodlet 646D..... 64
A.25 Image (100X) of ZIRLO™ sample 646D6 in Area 25 from 1-cycle 350°C/87-MPa rodlet 646D..... 65
A.26 Image (100X) of ZIRLO™ sample 646D6 in Area 26 from 1-cycle 350°C/87-MPa rodlet 646D..... 66
A.27 Image (100X) of ZIRLO™ sample 646D6 in Area 27 from 1-cycle 350°C/87-MPa rodlet 646D..... 67
A.28 Image (100X) of ZIRLO™ sample 646D6 in Area 28 from 1-cycle 350°C/87-MPa rodlet 646D..... 68
A.29 Image (100X) of ZIRLO™ sample 646D6 in Area 29 from 1-cycle 350°C/87-MPa rodlet 646D..... 69
A.30 Image (100X) of ZIRLO™ sample 646D6 in Area 30 from 1-cycle 350°C/87-MPa rodlet 646D..... 70
A.31 Image (100X) of ZIRLO™ sample 646D6 in Area 31 from 1-cycle 350°C/87-MPa rodlet 646D..... 71
A.32 Image (100X) of ZIRLO™ sample 646D6 in Area 32 from 1-cycle 350°C/87-MPa rodlet 646D..... 72
A.33 Image (100X) of ZIRLO™ sample 646D6 in Area 33 from 1-cycle 350°C/87-MPa rodlet 646D..... 73
A.34 Image (100X) of ZIRLO™ sample 646D6 in Area 34 from 1-cycle 350°C/87-MPa rodlet 646D..... 74
A.35 Image (100X) of ZIRLO™ sample 646D6 in Area 35 from 1-cycle 350°C/87-MPa rodlet 646D..... 75
A.36 Image (100X) of ZIRLO™ sample 646D6 in Area 36 from 1-cycle 350°C/87-MPa rodlet 646D..... 76
A.37 Image (100X) of ZIRLO™ sample 646D6 in Area 37 from 1-cycle 350°C/87-MPa rodlet 646D..... 77
A.38 Image (100X) of ZIRLO™ sample 646D6 in Area 38 from 1-cycle 350°C/87-MPa rodlet 646D..... 78
A.39 Image (100X) of ZIRLO™ sample 646D6 in Area 39 from 1-cycle 350°C/87-MPa rodlet 646D..... 79
A.40 Image (100X) of ZIRLO™ sample 646D6 in Area 40 from 1-cycle 350°C/87-MPa rodlet 646D..... 80
A.41 Image (100X) of ZIRLO™ sample 646D6 in Area 41 from 1-cycle 350°C/87-MPa rodlet 646D..... 81
A.42 Image (100X) of ZIRLO™ sample 646D6 in Area 42 from 1-cycle 350°C/87-MPa rodlet 646D..... 82

TABLES

1 Summary of HBU M5® and ZIRLO™ cladding materials used in studies of cladding ductility following simulated drying and storage (RHT) at PCT. 5

2 Characterization results for HBU M5® cladding following cooling from 350°C and 400°C. 21

3 Characterization results for HBU ZIRLO™ cladding following cooling from 350°C and 400°C. 29

ACRONYMS, UNITS AND SYMBOLS

ACRONYMS

ANL	Argonne National Laboratory (Argonne)
CWSRA	cold-worked, stress-relief annealed
DBTT	ductile-to-brittle transition temperature
DOE	U.S. Department of Energy
DTT	ductility transition temperature
EOL	end of life
EPRI	Electric Power Research Institute
ESCP	Extended Storage Collaboration Program
HBU	high burnup
ID	inner diameter surface
IFBA	Integral Fuel Burnable Absorber
ISG	Interim Staff Guidance
NRC	Nuclear Regulatory Commission
OD	outer diameter surface
ORNL	Oak Ridge National Laboratory
PCT	peak cladding temperature
PNNL	Pacific Northwest National Laboratory
PWR	pressurized water reactor
RCT	ring compression test
RHCF	radial hydride continuity factor (in %); also called the effective radial hydride length
RHT	radial-hydride treatment
RIP	rod internal pressure
RT	room temperature
RXA	recrystallized-annealed
TMT	thermo-mechanical treatment
Zry-2	Zircaloy-2
Zry-4	Zircaloy-4

UNITS

°C	degree Celsius
GWd/MTU	giga-watt-days per metric tonne of uranium
h	hour
kN	kilo-newton
m	meter
mm	millimeter
µm	micro meter (micron)
MPa	mega-pascal
N	newton
s	second
wppm	weight parts per million

SYMBOLS

C_H	hydrogen content in weight parts per million (wppm)
C_{HD}	dissolved hydrogen in wppm
C_{HP}	amount of dissolved hydrogen needed to initiate hydride precipitation (in wppm)
D_{mi}	inner diameter of cladding alloy (mm)
D_{mo}	outer diameter of cladding alloy (mm)
D_o	cladding outer diameter (includes outer-surface corrosion layer if present, mm)
d_p	permanent displacement (pre-test diameter minus post-test diameter in loading direction, mm)
d_p/D_{mo}	RCT permanent strain (%)
δ	controlled RCT displacement at the 12 o'clock sample position (mm)
δ_{max}	maximum RCT displacement at the 12 o'clock sample position (mm)
Δp	pressure difference across cladding wall ($p_i - p_o$, MPa)
ΔP	load drop from crack initiation load (P_i) to minimum load (P_d) during load drop
δ_p	RCT offset displacement at 12 o'clock position relative to static support at 6 o'clock (mm)
δ_p/D_{mo}	RCT offset strain (%)
ΔT	temperature drop per drying cycle (°C)
ΔT_{PD}	difference between hydrogen precipitation (T_P) and dissolution (T_D) temperatures (°C)
$(\varepsilon_\theta)_{max}$	maximum hoop strain
h_m	cladding metal wall thickness (mm)
h_{ox}	thickness of outer surface corrosion (oxide) layer (μm)
K_{LC}	calculated linearized loading slope (also known as loading stiffness) for RCT samples (kN/mm)
K_{LM}	measured linearized loading slope (kN/mm)
K_U	calculated linearized unloading slope (kN/mm)
K_{UM}	measured linearized unloading slope (kN/mm)
L	length of RCT samples (mm)
M_{max}	maximum RCT bending moment (N•m)
P	measured RCT load at the 12 o'clock sample orientation (N)
p_i	absolute internal gas pressure (MPa)
P_d	minimum load during load drop (N)
P_i	peak load at crack initiation (N)
P_{max}	maximum RCT load (N)
p_o	external gas pressure
R_{mi}	inner radius of cladding alloy (mm)
σ_θ	hoop stress (MPa)
T	temperature (°C)
t_h	hold time at PCT for RHT (h)
T_D	hydrogen dissolution temperature (°C)
T_P	hydrogen precipitation temperature (°C)

1. INTRODUCTION

Structural analyses of high-burnup (HBU) fuel rods require cladding mechanical properties and failure limits to assess fuel behavior during long-term dry-cask storage, post-storage retrieval and transportation, and post-transport retrieval. License applications for transport casks containing HBU fuel assemblies have used properties and failure limits for as-irradiated cladding [1]. The Zircaloy-4 (Zry-4) properties and limits in Ref. 1 were based primarily on axial-tensile and pressurized-tube tests. Isotropic correlations were developed for stress vs. strain and failure limits. However, pre-storage drying-transfer operations and early stage storage subject cladding to higher tensile hoop stresses induced by higher temperatures and pressures relative to in-reactor operation and pool storage. Under these conditions, radial hydrides may precipitate during slow cooling and may introduce an embrittlement mechanism if the cladding temperature decreases below a critical point, which is defined in this work as the ductile-to-brittle transition temperature (DBTT). To avoid potential confusion among materials experts who associate DBTT with body-centered-cubic metals, the acronym DTT (ductility transition temperature) will be used in future documentation. If embrittlement is predicted, then cladding failure hoop stresses and strain would have to be revised to account for this effect.

In Interim Staff Guidance-11, Revision 3 (ISG-11, Rev. 3), the Nuclear Regulatory Commission (NRC) recommends a peak cladding temperature (PCT) limit of 400°C for all fuel burnups under normal conditions of storage and short-term loading operations (e.g., drying, backfilling with inert gas, and transferring the canister or cask to the storage pad) [2]. During loading operations, repeated thermal cycling (repeated heat-up/cool-down cycles) may occur but should be limited to fewer than 10 cycles, with cladding temperature variations that are less than 65°C per cycle, according to ISG-11, Rev. 3 (see Fig. 1 at the end of this section for justification of <65°C per cycle). One concern for HBU fuel cladding is the possible precipitation of radial hydrides, which could embrittle cladding in response to tensile hoop stresses caused by internal pressure loading and "pinch-type" loading during transport. Limits established in ISG-11, Rev. 3, relied on data available before 2002, which were primarily for low-burnup and non-irradiated/pre-hydrided Zry-4. At the time ISG-11, Rev. 3, was issued (2003), NRC recognized that data for HBU fuel cladding alloys were needed to determine the extent of radial-hydride embrittlement under conditions relevant to drying-transfer operations and storage. One concern was, and still is, whether or not HBU fuel will maintain cladding integrity and be readily retrievable after more than 20 years of storage, at which time the peak cladding temperatures would be ≈200°C or less.

Argonne National Laboratory has developed a test protocol for studying HBU cladding embrittlement that has been used to generate data for NRC. Experimentally, the protocol involves two steps: (a) radial-hydride treatment (RHT), during which HBU cladding is exposed to simulated drying-storage temperature and hoop stress conditions, including slow cooling with decreasing stress, followed by (b) ring compression testing, in which rings sectioned from RHT HBU cladding are compressed to determine strength and ductility as a function of the test temperature. The ring compression test (RCT) is used as a ductility screening test, and the RCT loading simulates the pinch-type loading on HBU cladding that occurs during normal cask transport and possible drop accidents. The protocol was used to generate DBTT data for HBU ZIRLO™ and Zry-4 [3, 4] (both efforts sponsored by NRC) and HBU M5® [sponsored by the U.S. Department of Energy (DOE)] [5]. Under DOE-sponsorship, Argonne has also generated baseline characterization data and data for the strength and ductility of as-irradiated Zry-4, ZIRLO™, and M5®. These data are important not only for determining the potentially degrading effects of drying and early stage storage, but also for serving as reference properties for future evaluations of the effects of drying storage on these cladding alloys [6–8]. Reference 9 includes Argonne data generated through September 30, 2013, including additional DOE-sponsored test results for HBU ZIRLO™ and M5® following cooling from 400°C and lower hoop stress levels (80 to 90 MPa). Reference 10 contains refined

interpretations of previously generated data, as well as new test results for HBU ZIRLO™ subjected to 3-cycle drying at 350°C PCT and 93-MPa peak hoop stress. Reference 11 contains additional data for as-irradiated Zry-4 and for HBU ZIRLO™ following 1-cycle drying at 350°C PCT and 94-MPa peak hoop stress.

In addition to the Argonne data sets for PWR cladding alloys, Aomi et al. [12] have generated data for Zircaloy-2 (Zry-2) and Zry-4 using test methods similar to the ones developed by Argonne. However, RHT samples were cooled under constant stress (vs. decreasing stress, as used by Argonne), and RCTs were conducted only at room temperature (RT) and at a very slow displacement rate (0.033 mm/s vs. 5 mm/s used by Argonne). Their results are both revealing and relevant in evaluating the effects of hydrogen content (C_H) and thermo-mechanical treatment (TMT) on the susceptibility of cladding alloys to radial-hydride formation. Argonne and Aomi et al. test results indicate that susceptibility to radial-hydride precipitation during cooling is dependent on cladding alloy, TMT, total C_H, C_H below the hydride rim, and peak RHT temperature and hoop stress. The combination of recrystallized-annealed (RXA) microstructure and low C_H (above the inner liner for Zry-2) makes Zry-2 and M5® more susceptible to precipitation of long radial hydrides during cooling. For cold-worked, stress-relief-annealed (CWSRA) alloys, ZIRLO™ was found by Argonne to be more susceptible to radial-hydride precipitation than Zry-4. The differences in the distribution of hydrides across the cladding wall (lower for ZIRLO™ below the hydride rim) may be partly responsible for this behavior [4].

Section 2 of this report describes the materials and test methods used in this program. It has been updated with additional RCT results for benchmark samples (as-fabricated and irradiated 17×17 M5®). Previous test results for HBU M5® and HBU ZIRLO™ are summarized in Section 3 for these materials following RHT at 400°C PCT for both alloys and at 350°C PCT for ZIRLO™.

Results of current best-estimate thermal analyses indicate that PCTs may not exceed 350°C during vacuum drying and storage for canisters and/or casks containing HBU fuel assemblies [13]. Starting with the 3-cycle/350°C RHT conducted in Fiscal Year 2014, the emphasis of current testing has been on peak RHT temperatures ≤350°C. It is also desirable to conduct tests within a relevant RHT hoop stress range. As the database for end-of-life (EOL) rod internal pressures (RIPs) is insufficient to determine this range with a reasonable degree of confidence, RHT hoop stresses for testing remain at 80 MPa to 110 MPa for standard PWR fuel rods. Efforts to improve this database are described in Section 5.

New test results for HBU M5® and HBU ZIRLO™ are presented in Section 4. The new M5® rodlet test was designed to support the hypothesis that the DBTT for this material was more sensitive to total hydrogen content than stress within the hydrogen and peak stress ranges of 58–94 wppm and 90–142 MPa, respectively. This rodlet contained 80-wppm hydrogen and was subjected to 350°C PCT and 89-MPa hoop stress prior to cooling at 5°C/h. For HBU ZIRLO™, the new test was designed to support the hypothesis that the DBTT for this cladding alloy was very sensitive to peak hoop stress in the narrow range of 90±3 MPa. As such, a rodlet with about 390-wppm hydrogen was fabricated, heated to 350°C at 87-MPa hoop stress and held for 24-hours prior cooling at 5°C/h. The RCT results for previous tests conducted with this material at 350°C PCT and 93–94 MPa prior to cooling contained a lot of scatter and were difficult to interpret because of their very high hydrogen contents (564±177 wppm with peak local value >840 wppm and 644±172 wppm with peak local value >960 wppm). For ZIRLO™-clad fuel rods irradiated to ≤60 GWd/MTU, the peak hydrogen content is anticipated to be <450 wppm.

To appreciate the influence of PCT (i.e., decrease from 400°C to 350°C), stress, temperature cycling, and hydrogen content on radial hydride precipitation and embrittlement, it is important to review literature results for hydrogen dissolution and hydride precipitation. Unlike most, if not all, studies of radial hydride precipitation and subsequent ductility, the Argonne RHT process includes decreasing internal

gas pressure and hoop stress with decreasing temperature during cooling, as would occur in fuel rods during storage. Most researchers have used an actively pressurized cladding tube for which the pressure is kept constant during cooling. As such, it is important to understand the dependence of hydrogen solubility (C_{HD}) on temperature (T_D) during the heating phase and the initiation of hydrogen precipitation (C_{HP} at T_P) during the cooling phase. Figure 1 summarizes the data of Kearns [14], Kammenzind et al. [15], and McMinn et al. [16] for these parameters, as well as the temperature gap (ΔT_{PD}) between precipitation and dissolution. The results in Fig. 1 are used in Sections 3 and 4 to determine the cladding temperature and stress at which precipitation, especially radial hydride precipitation, can initiate. In particular, the solubility of hydrogen at 400°C is 206±5 wppm and the precipitation temperature is 335°C. The hydrogen solubility at 350°C is 126±6 wppm and the precipitation temperature is 285°C. These results are directly applicable to the Zry-4 and ZIRLO™ test samples used in the Argonne test program because these samples contained ≥300 wppm for Zry-4 and ≥350 wppm for ZIRLO™. However, the M5® samples tested by Argonne contained lower hydrogen contents (58–94 wppm) for which total dissolution occurred during the heating ramp at temperatures in the range of 290–330°C. Corresponding temperatures at which precipitation initiated were in the low range of 225–265°C.

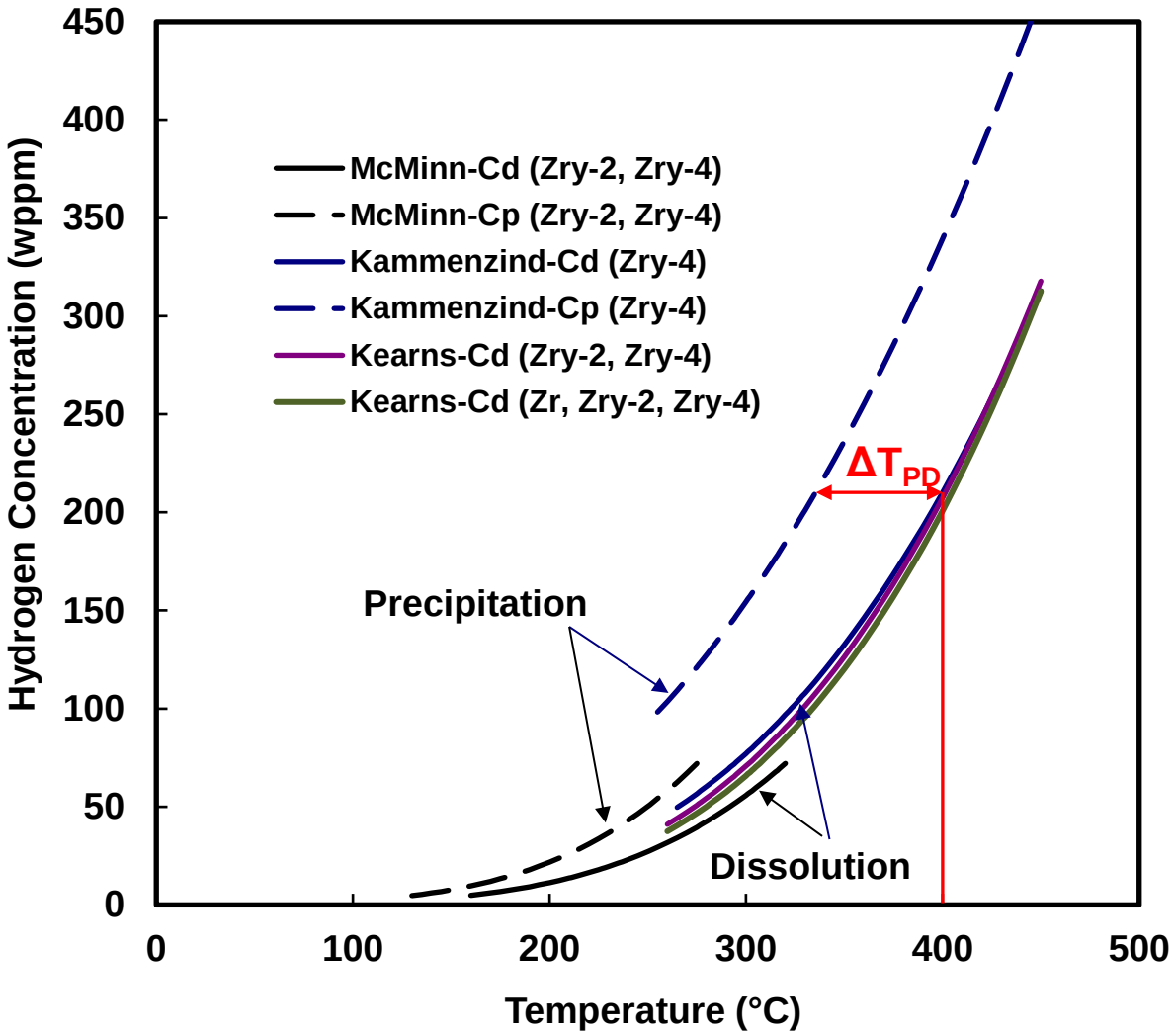

Figure 1: Steady-state curves for hydrogen dissolution and precipitation in Zr alloys.

Page intentionally blank

2. HBU CLADDING MATERIALS AND TEST METHODS

2.1 HBU CLADDING MATERIALS

References 9 and 10 contain detailed lists of defueled cladding materials used in previous testing. Relevant materials for the current work are listed in Table 1. New tests are listed in bold font. For rodlets subjected to three drying cycles, the hold time at PCT refers to the hold time per cycle. The materials came from fuel rods irradiated to HBU in commercial light water reactors. The M5® cladding segment listed at 63 GWd/MTU came from one fuel rod irradiated in one of the Ringhals reactors. The other cladding segments came from two fuel rods irradiated to 68–70 GWd/MTU in the same assembly in the North Anna reactors. ZIRLO™ cladding segments came from three fuel rods irradiated in the same assembly in the North Anna reactors. The $\pm C_H$ values represent one-sigma variations in data collected from multiple axial locations along each segment and quarter-ring samples at each axial location. In general, the large one-sigma values were due to circumferential variation in C_H, especially for average C_H values ≥350 wppm. Additional characterization results are presented in subsequent sections.

Table 1 Summary of HBU M5® and ZIRLO™ cladding materials used in studies of cladding ductility following simulated drying and storage (RHT) at PCT.

Cladding Alloy	TMT	Burnup, GWd/MTU	Hydrogen Content, wppm	Peak RHT Stress, MPa	PCT, °C	Hold Time (cycles), h
M5®	RXA	63	94±6	142	400	1 (1)
		68	72±10	111	400	1 (1)
		68	58±15	90	400	1 (1)
		70	**80±7**	**89**	**350**	**1 (1)**
ZIRLO™	CWSRA	70	425±63	111	400	1 (1)
		70	350±80	111	400	24 (1)
		66	**387±72**	**87**	**350**	**24 (1)**
		68	530±100	89	400	1 (1)
		68	480±131	88	400	1 (3)
		68	564±177	93	350	1 (3)
		68	644±172	94	350	1 (1)
		68	535±50	80	400	1 (1)

2.2 TEST METHODS

The protocol for single-cycle heating-cooling tests consisted of two steps: (a) simulated drying and storage testing (called "RHT") during which a sealed, pressurized rodlet is heated to and stabilized at 400°C within one hour, held at 400°C for one hour, cooled slowly at 5°C/h to 200°C (≈130°C for low-C_H M5®), and cooled at a higher rate to RT and (b) ring-compression testing at three to four temperatures from RT to 200°C and at 5 mm/s (reference value) displacement rate to a maximum displacement of 1.7 mm. For three-cycle heating-cooling RHTs, rodlets were heated to peak temperatures of 400°C or 350°C, held at the PCT for one hour, cooled at 5°C/h to 100°C below the PCT, reheated to the PCT, held at PCT for one hour, cooled at 5°C/h to 100°C below the PCT, reheated to the PCT, held at the PCT for one hour, and then cooled at the same rates used for the single-cycle tests. For 1-cycle ZIRLO™ tests conducted at 350°C PCT, the 5°C/h cooling was maintained down to 130°C to give the dissolved hydrogen (≈125 wppm) more time to precipitate, which possibly led to longer radial hydrides.

HBU cladding segments were used to fabricate sealed and pressurized (with argon) rodlets. Details of rodlet fabrication are given in Ref. 10.

Prior to rodlet pressurization, the outer diameter was measured for each corroded segment at two orientations (90° apart) and at three axial locations. These values were averaged to give the cladding outer diameter (D_o). The thickness of the corrosion (oxide) layer (h_{ox}) was estimated from sibling rod data or from interpolation and extrapolation of data from the same rod at different axial locations. The same approach was used to estimate the cladding metal wall thickness (h_m). The outer diameter of the cladding alloy (D_{mo}) was calculated from $D_o - 2\ h_{ox}$, and the inner diameter of the cladding alloy (D_{mi}) was calculated from $D_{mo} - 2\ h_m$. The ratio R_{mi}/h_m, where R_{mi} is the metal inner radius, was used in Eq. 1 to calculate the average hoop stress (σ_θ) from the pressure difference ($\Delta p = p_i - p_o$) across the cladding wall, where p_o was 0.1 MPa during RT (23°C) fabrication and 0.17 MPa in the RHT furnace.

$$\sigma_\theta = (R_{mi}/h_m)\ \Delta p - p_o \qquad (1)$$

The ideal gas law was used to relate the absolute internal gas pressure (p_i) at the RHT PCT to the RT pressure according to $p_i(\text{PCT}) = ([\text{PCT} + 273\ \text{K}]/296\ \text{K})\ p_i(23°\text{C})$. Given the target σ_θ value at the PCT, the fabricated RT pressure can be calculated using Eq. 1 and the information given above.

Following RHT, the rodlet was depressurized and sectioned for C_H samples, RCT samples, and metallographic imaging samples, which allowed precise determination of the geometrical factors in Eq. 1. Using this procedure, the calculated peak rodlet stress was within ±3 MPa of the target value.

The second phase of the test protocol consisted of RCTs. Figure 2 shows a schematic of RCT loading. The RCT load induces maximum hoop stresses (σ_θ) at the inner surfaces of the 12 (under load) and 6 (above support) o'clock positions. Tensile hoop stresses also occur at the 3 and 9 o'clock outer surfaces. Associated with these maximum tensile stresses are maximum tensile strains (ε_θ). Within the elastic range, these hoop stresses at 3 and 9 o'clock are about 60% of the maximum stresses at 12 and 6 o'clock. Also, because the length ($L \approx 8$ mm) of the rings is much greater than the cladding wall thickness (h_m = 0.54 to 0.57 mm for HBU ZIRLO™ and M5®), an axial stress is induced that is 0.37 times the hoop stress within the elastic deformation regime. The maximum displacement (1.7 mm) was chosen to give ≈10% offset strain at RT. The reference displacement rate was 5 mm/s.

Load-displacement curves and post-test examinations were used to determine offset displacements (δ_p) and permanent displacements (d_p), respectively. These were normalized to D_{mo} to give relative plastic displacement (i.e., plastic strain) for the ring structure. Permanent displacement is defined as the difference between pre- and post-test diameter measurements along the loading direction. Figure 3 shows how traditional and corrected offset displacements were determined from a benchmark load-displacement curve for an as-fabricated M5® ring. For the benchmark sample, D_{mo} = 9.50 mm, h_m = 0.61 mm, and L = 8.00 mm. The traditional offset methodology calls for unloading the sample at the same slope as the measured loading slope (K_{LM}). It should be noted that this slope is less than the calculated sample stiffness (K_{LC}) due to the influence of machine compliance. This approach gave a traditional δ_p = 0.94 mm, which is greater than the more accurate d_p = 0.83 mm. Thus, there is an inherent error in the traditional approach as the measured unloading slope (K_{UM} = 0.81 kN/mm) is always less than the measured loading slope. K_{UM} was determined from the slope of the line connecting the maximum displacement to the displacement axis value based on the measured value of d_p at zero load. Normalizing these displacements to D_{mo} gives 9.9% traditional offset strain and 8.7% permanent strain, which is also called the "corrected offset strain" for these benchmark tests.

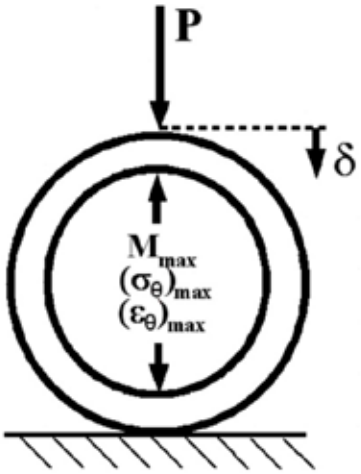

Figure 2: RCT measured load (P) and controlled displacement (δ).

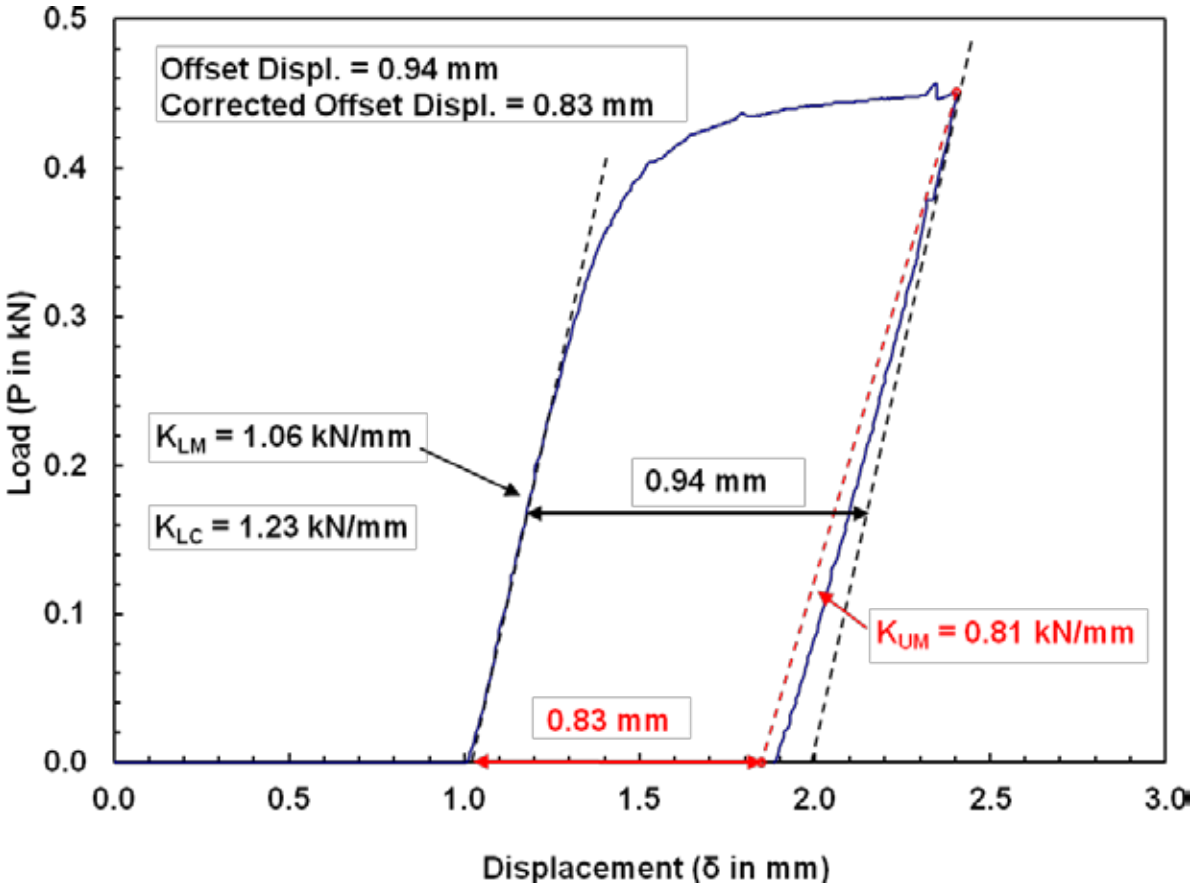

Figure 3: Load-displacement curve for non-irradiated M5® ring tested at RT and 5 mm/s to 1.7 mm displacement.

For HBU cladding rings that crack during the 1.7-mm displacement, d_p cannot be determined accurately. Thus, one must rely on a correlation for the unloading slope to determine the corrected offset displacement prior to the first significant crack, from which the ductility can be determined. The correlation developed for this application is based on the results from a large number of benchmark tests with permanent displacements ranging from 0.14 mm to 1.2 mm, with displacement rates in the range of 0.03–50 mm/s, and with temperatures ranging from 20–150°C. Results of these benchmark tests are shown in Fig. 4 in terms of the ratio of measured unloading/loading (K_{UM}/K_{LM}) slopes vs. traditional offset strain (δ_p/D_{mo}). Also shown in Fig. 4 are results from nine RCTs with HBU M5® (solid red circles) that exhibited no cracking after 1.7 mm of total displacement. One of these points is from the current test described in Section 4. The blue-circle data points are from benchmark tests conducted with as-fabricated 17×17 M5® (29 points) and 17×17 ZIRLO™ (6 points) cladding samples.

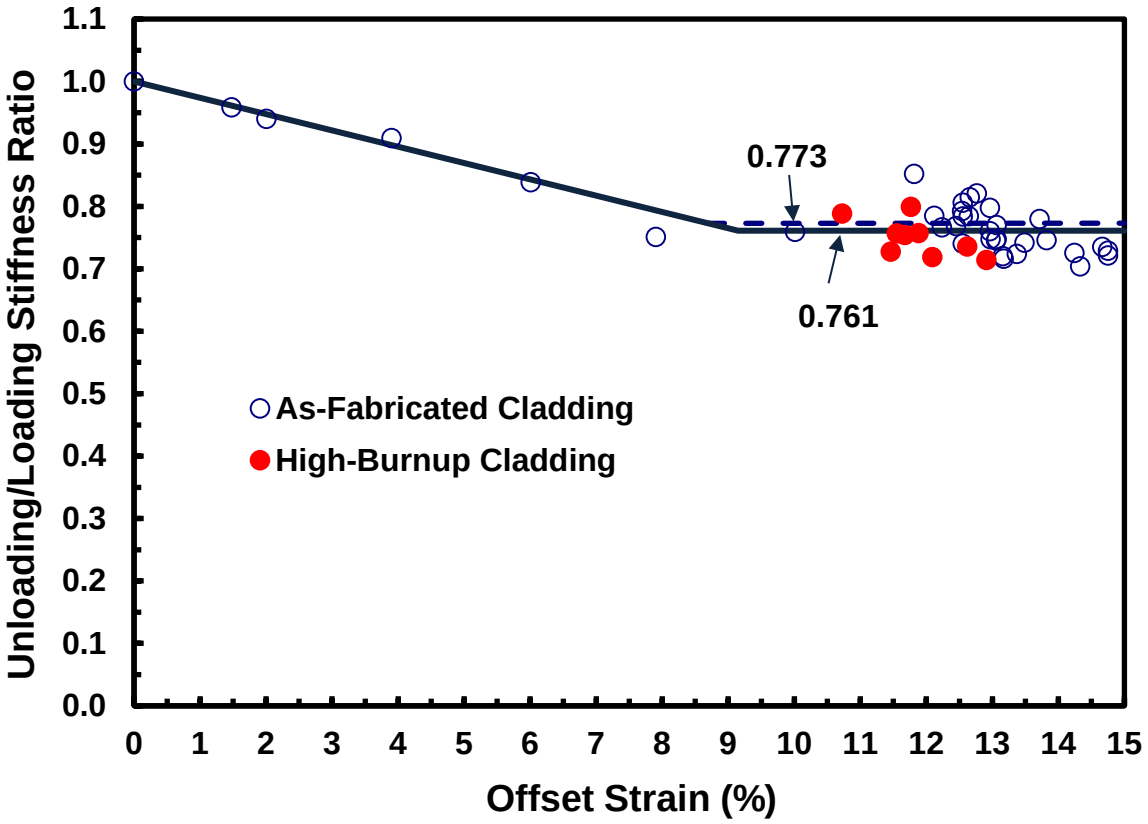

Figure 4: RCT benchmark results for determining the ratio of unloading/loading stiffness as a function of the traditional offset strain.

The correlation used for calculating the unloading slope (K_U in kN/mm) as a function of the measured loading slope (in kN/mm) and the measured traditional offset strain (in %) is given by:

$$K_U/K_{LM} = 1 - 0.02612\ \delta_p/D_{mo} \text{ for } \delta_p/D_{mo} \le 8.7\% \quad (2a)$$

$$K_U/K_{LM} = 0.773 \text{ for } \delta_p/D_{mo} > 8.7\% \quad (2b)$$

This correlation was based on a subset of the data in Fig. 4. For the complete data set in Fig. 4, the stiffness ratio is 0.761±0.036 at higher offset strains, which encompasses the 0.773 used in Eq. 2b.

The criteria for determining embrittlement remain the same for cladding with radial and circumferential hydrides: corrected δ_p/D_{mo} <2% prior to >25% load drop or >50% decrease in loading slope. In previous works [4–7], it was established that >25% load drop and >50% decrease in loading slope correspond to a crack or cracks extending through >50% of the wall thickness. The 2% offset strain limit is based on the uncertainty in measurement of the permanent strain (d_p/D_{mo} ≤1%) for as-fabricated cladding and the added uncertainty (≤1%) in the permanent displacement for HBU cladding due to flaking off of the corrosion (i.e., oxide) layer under the applied load and above the support plate. Multiple cracks through the oxide layer and cracks through the hydride rim lower the unloading stiffness to values less than shown in Fig. 4. As the HBU M5® tested had very thin oxide layers (≈10 µm) and no hydride rim, the 2% offset strain criterion is more conservative for this HBU alloy than for the HBU Zry-4 and ZIRLO samples tested, both of which had thicker oxide layers (30−100 µm) and thick hydride rims (30−100 µm).

Page intentionally blank

3. PREVIOUS RESULTS FOR HBU M5® AND HBU ZIRLO™

3.1 HBU M5®

Figure 5 summarizes the RCT ductility data measured for as-irradiated HBU M5® and for HBU M5® following cooling from peak RHT conditions of 400°C and 90–142 MPa hoop stresses. The as-irradiated material with 76-wppm hydrogen had high ductility at RT for a wide range of displacement rates (0.05–50 mm/s). None of the samples tested at RT or at 60°C and 90°C exhibited cracking through 1.7-mm displacement. Permanent and offset strains were in the range of 9–10% for these samples. Similar results were obtained for HBU M5® with 58-wppm hydrogen following cooling from 400°C and 90-MPa hoop stress. These results were somewhat surprising in that most of the hydrogen precipitated in the radial direction to give effective radial-hydride lengths (RHCF) of 37±17%. However, the low hydrogen content may have resulted in poor connectivity or continuity of radial hydrides in the axial direction and consequently enhanced ductility. The RHCF factor increased with increasing peak hoop stress: 54±20% for 111 MPa and 72 wppm and 61±18% for 142 MPa and 94 wppm. However, the DBTT values for these samples were very close (70–80°C). At these low hydrogen contents, the peak cladding stress is less important than the stress at the hydrogen precipitation temperature (T_P) because all the hydrogen remains in solution above T_P. T_P values and corresponding hoop stresses are: 226°C and 67 MPa for the 58-wppm sample; 242°C and 84 MPa for the 72-wppm sample; and 264°C and 113 MPa for the 94-wppm sample. It is hypothesized that the DBTT is more sensitive to hydrogen content than hoop stress for precipitation hoop stresses in the range of 67–113 MPa. However, without additional data, it could be argued that hoop stress is the dominant factor in determining DBTT.

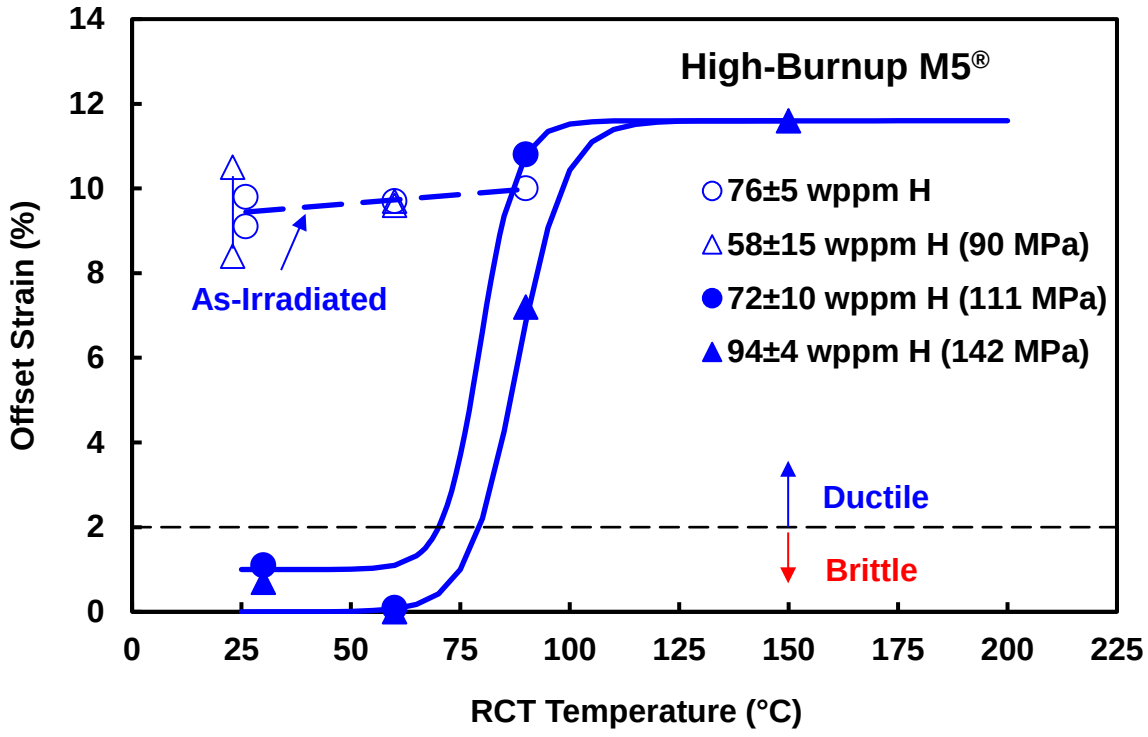

Figure 5: Summary of ductility data for HBU M5® in the as-irradiated condition and following RHT at 400°C PCT.

3.2 HBU ZIRLO™

HBU ZIRLO™ was subjected to RCTs in the as-irradiated condition and following RHT at 400°C PCT and 80–141 MPa. The hydrogen concentrations of the test samples ranged from about 350 wppm to 650 wppm. In the as-irradiated condition HBU ZIRLO™ had relatively high ductility of 6% to >11% offset strain for tests conducted at RT displacement rates of 0.05 mm/s to 50 mm/s and at 5 mm/s and RT to 150°C. For an 80-MPa peak RHT hoop stress, radial hydrides were short (9±4% RHCF) and ductility values were moderately high (5–7%) at RT and 60°C and high (>9%) at 90°C and 150°C [6,9]. Thus, for peak RHT conditions of 400°C and ≤80 MPa, the corresponding DBTT would be <20°C and radial-hydride-induced embrittlement would not be an issue. The two test samples subjected to peak RHT conditions of 400°C and 111 MPa exhibited longer radial hydrides (32±13%) and a higher DBTT value (122°C) [3]. For the peak RHT conditions of 400°C and 141–MPa hoop stress, the DBTT was >150°C (estimated to be 185°C) [4]. However, the hydrogen content of this sample was much higher (650±190 wppm) than anticipated for standard and IFBA ZIRLO™ fuel rods irradiated to less than the licensing limit (62 GWd/MTU). Also, the stress level was considerably higher than estimated for standard ZIRLO™ fuel rods irradiated to less than the licensing limit. However, the results for this highly degraded ZIRLO™ sample (65±17% RHCF and very thick hydride rim) can be used to set an upper bound of 200°C on the DBTT for ZIRLO™.

Following the tests described above, two rodlet tests were conducted with peak RHT conditions of 400°C and 88–89 MPa hoop stress: one with the standard 1-cycle heating-cooling temperature history (89 MPa) and one with a 3-cycle heating-cooling temperature history (88 MPa with 100°C temperature drop after the first and second heating cycles). The hold time was 1 h for the 1-cycle test and for each cycle of the 3-cycle test. The 1-cycle test was conducted first to demonstrate that the DBTT was low (23°C) and the radial-hydride lengths were modest (19±9% RHCF) for this peak stress level. Results following the 3-cycle test were 23°C DBTT and 18±7% RHCF, which are essentially identical to the results for the 1-cycle test sample. These tests demonstrated that temperature cycling at a peak stress of about 90 MPa had no effect on the DBTT or the RHCF for this cladding alloy. The test results also helped to narrow the range of stresses (89–111 MPa) for which the DBTT of HBU ZIRLO™ increased by about 100°C. The hydrogen contents (530±115 wppm for 1-cyle test and 480±131 wppm for 3-cycle test) of these samples were comparable to those measured for tests conducted with the as-irradiated sample (530±70 wppm), with the sample following cooling from 80 MPa (530±50 wppm), and with one of the samples following cooling from 111 MPa (425±63 wppm). The other 111-MPa sample had 350±80 wppm. No effects of total hydrogen content were discernable within the hydrogen-content range (350–550 wppm) for these samples.

Two subsequent tests (1-cycle and 3-cycle RHT) were conducted at lower PCT (350°C) and moderate peak hoop stress of 93-94 MPa. The reduction in PCT resulted in an 80-wppm reduction in dissolved hydrogen prior to cooling. The expectation was that the DBTT would be <20°C because less hydrogen would be available to precipitate as radial hydrides and the stresses at T_P (83-84 MPa) would be very close to the stress at T_P for the previous two tests (80 MPa). The results of these tests were quite different from expectations. The DBTT jumped to 125±5°C and the radial hydrides were longer than expected (30±11% for the 3-cycle test and 37±11% for the 1-cycle test). The average hydrogen content (564 wppm) of the 3-cycle sample was consistent with previous samples tested, but the maximum local hydrogen content (>840 wppm) was considerably higher. For the 1-cycle test, which exhibited very low ductility at 135°C, both the average (644 wppm) and maximum local (>960 wppm) hydrogen contents were considerably higher and well above anticipated values for ZIRLO™-clad fuel rods irradiated to less than the licensing limit. The ductility data for these tests, along with ductility data for the 400°C PCT tests at 88-89 peak hoop stresses, are compared in Fig. 6.

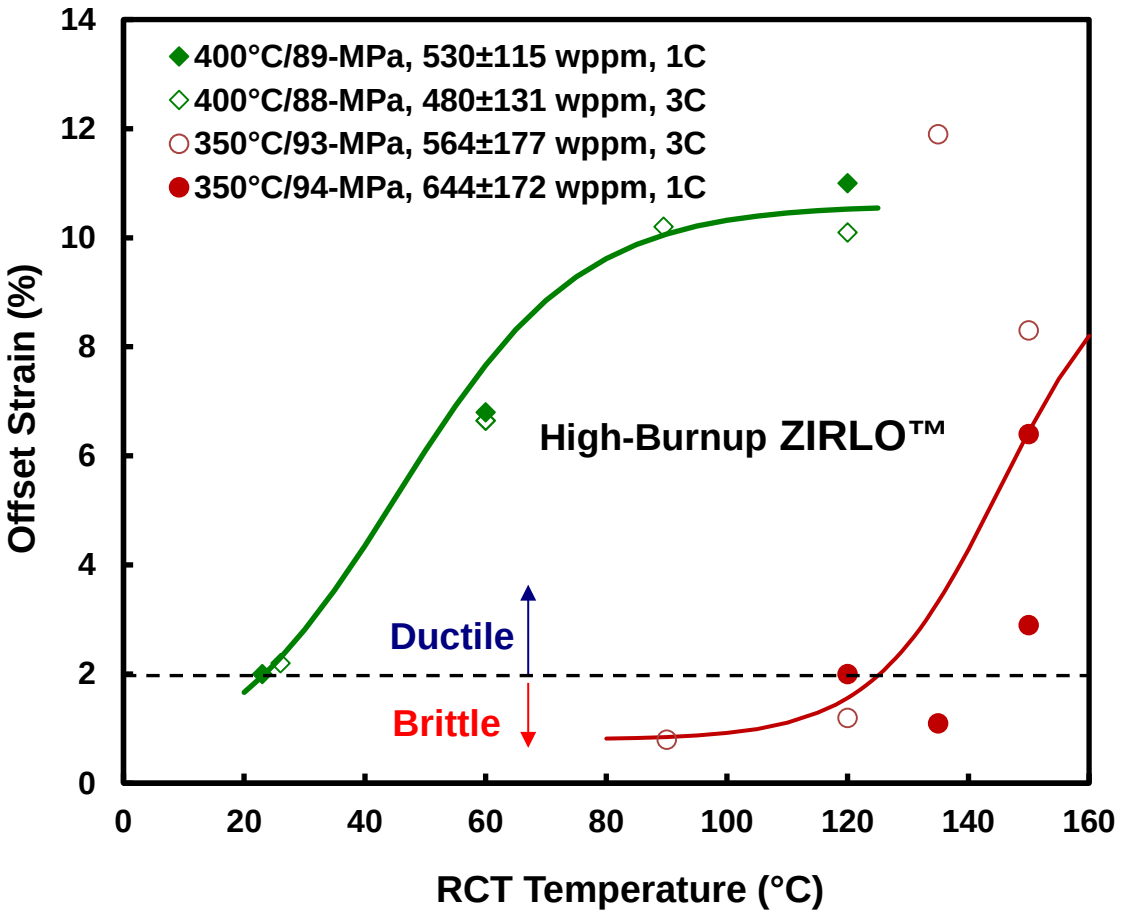

Figure 6: Summary of ductility data for HBU ZIRLO™ following RHT at 400°C and 350°C PCTs and peak hoop stresses in the narrow range of 88−94 MPa.

Three hypotheses were postulated in an attempt to explain the low ductility values and correspondingly high DBTT value measured for 350°C-PCT samples: (a) the DBTT for HBU ZIRLO™ could be highly sensitive to peak RHT hoop stress within a very narrow range of peak stresses (88–94 MPa) and precipitation-initiation stresses (80–84 MPa); (b) degradation due to high average and/or high local hydrogen contents could lower ductility and increase the DBTT for HBU ZIRLO™; and (c) the DBTT for HBU ZIRLO™ could be increased due to the potential decrease in irradiation-induced-hardening annealing for the decrease in PCT from 400°C to 350°C. However, without additional data, no definitive conclusions could be drawn [11].

4. RESULTS FROM CURRENT TESTS

4.1 HBU M5® FOLLOWING COOLING FROM 350°C PCT

The new HBU M5® test was designed to test the hypothesis that total hydrogen content within the range of 58–94 wppm has a significant effect on the DBTT following cooling from RHT conditions. The absolute value of fill pressure at RT (23°C) was chosen to be 5.90 MPa to give a target hoop stress of about 90 MPa at the PCT (350°C). A schematic of the rodlet selected for this test is shown in Fig. 7.

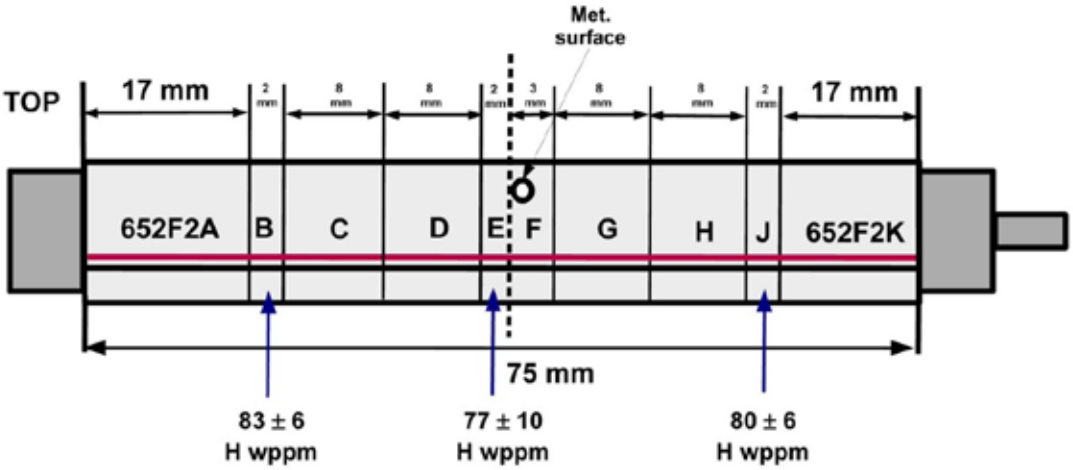

Figure 7: Sectioning diagram for HBU M5® rodlet 652F2 following RHT at 350°C PCT.

Hydrogen-content measurements are displayed in Fig. 7 at three axial locations (4 measurements of quarter-arc samples per axial location). The average and 1-sigma variation for the rodlet were calculated to be 80±7 wppm based on mass-averaging of the samples. This value is slightly lower than expected based on the hydrogen content (92±9 wppm) measured for another rod in the assembly at the same axial elevation. The difference could easily be due to rod-to-rod variation in hydrogen pickup and/or to the loss of about 10 wppm to the Zicadyne end fixtures during RHT. However, 80 wppm proved to be sufficient to test the hypothesis regarding the effects of hydrogen content on the DBTT.

The segment D_o, h_{ox}, D_{mo}, h_m, and D_{mi} were measured to be 9.53 mm, 11±1 μm, 9.51 mm, 0.57 mm, and 8.36 mm, respectively. The geometrical factor (R_{mi}/h_m) used in Eq.1 to convert pressure difference across the cladding wall to wall-averaged hoop stress (89 MPa) was 7.28.

Three sets of metallographic images were generated for sample 652F2F to determine the effective lengths and degree of axial connectivity of radial hydrides: (a) at the indicated surface (0-mm axial location) following grinding, polishing, and etching; (b) after grinding off about 0.5 mm followed by polishing and etching (-0.5-mm axial location); and after grinding off an additional 0.1 mm using fine grit paper followed by polishing and etching (-0.6-mm axial location). The circumferential orientations (45 for the 0-mm location) for the 100X images were selected to cover the whole cross section with some overlapping regions from image to image. Images at 200X were also taken to better determine continuity of hydrides in the radial direction. Figures 8a and 8b show images at 100X and 200X, respectively, of the longest radial hydride (95% RHCF), which occurred near the 1:00 o'clock orientation.

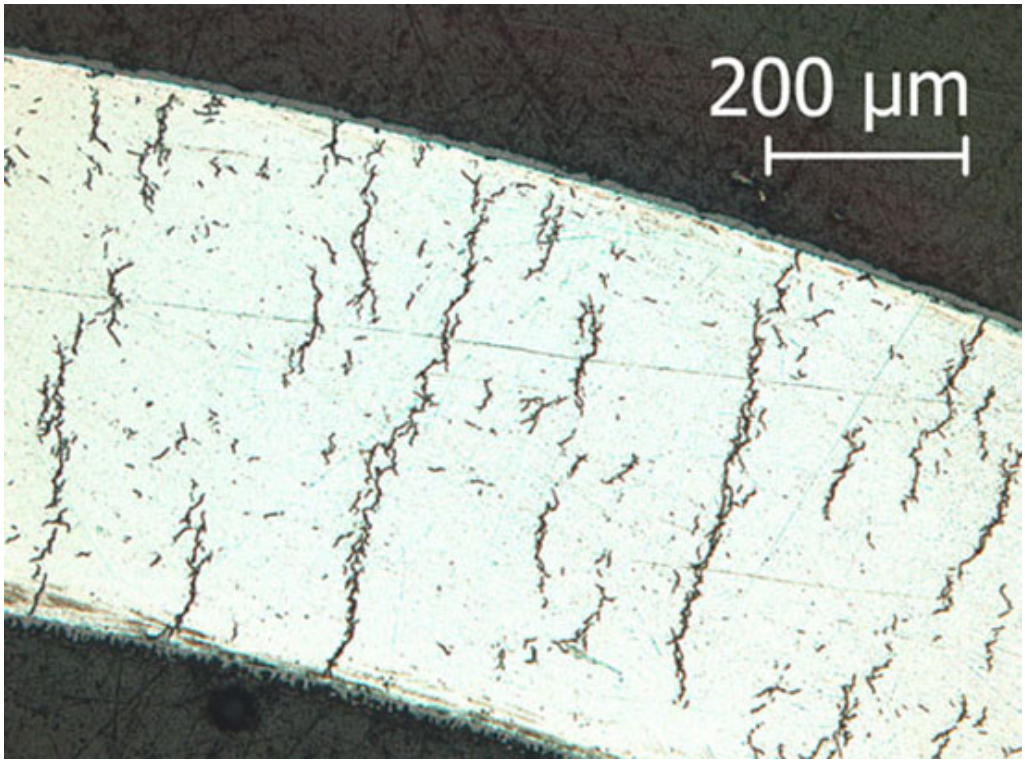

(a) 100X

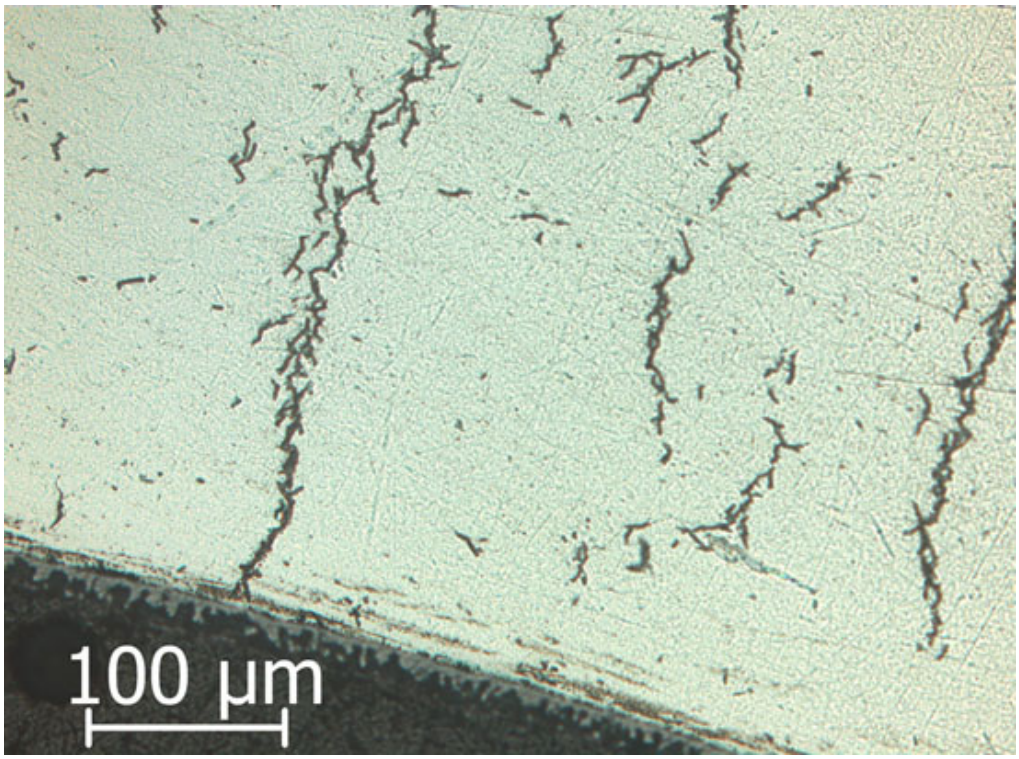

(b) 200X

Figure 8: Longest radial hydride observed for the 652F2F cross section at the reference axial location: (a) 100X and (b) 200X.

The average and 1-sigma variation in the effective radial hydride length (i.e., radial hydride continuity factor, RHCF) were determined to be 49±14% of the cladding wall thickness. These values are the lengths of the longest radial hydrides per 100X image. Figure 9 shows the longest radial hydride (95% RHCF) observed after grinding off about 0.5 mm. It is interesting to note that it occurred at a different circumferential orientation (3:00 vs. 1:00 o'clock) than shown in the Fig. 8a, and it had a different shape. On the basis of 37 100X images taken at this location (-0.5 mm), not a single radial hydride from the second set of images could be correlated with radial hydrides in the first set of images in terms of shape, length, and location across the cladding wall. These results suggest that if there was continuity of radial hydride platelets in the axial direction for the 80-wppm sample, it occurred along an axial length less than ≈500 μm. However, the average length (58±18% RHCF) of radial hydrides was higher than, but comparable to, what was observed in the first set of images taken at the 0-mm axial location.

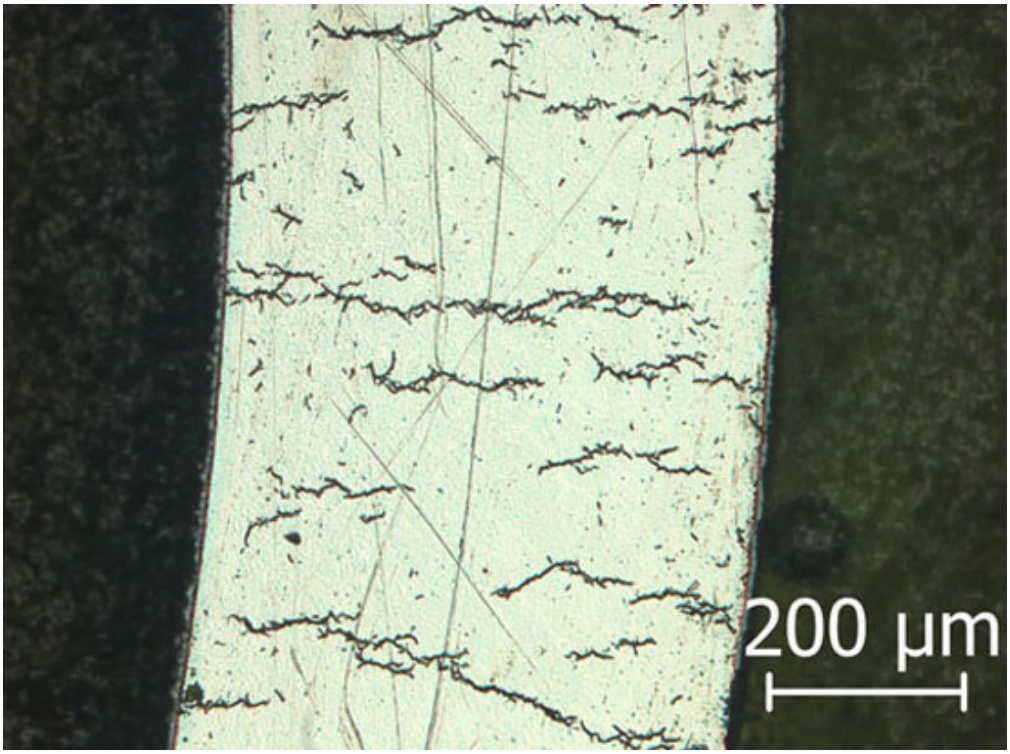

Figure 9: Longest radial hydride observed for the 652F2F cross section at the -0.5-mm axial location.

The image shown in Fig. 9 was not of high enough quality because of the scratches remaining on the surface even after polishing. In order to remove the scratches, additional grinding of about 0.1 mm was performed with fine-grit paper followed by re-polishing and re-etching. Forty three 100X images were taken of this cross section labeled as -0.6 mm relative to the reference surface. The longest radial hydride (95% RHCF) occurred between the 12:00 and 12:30 o'clock orientations for this surface, as shown in Fig. 10a. Although this hydride had about the same length as observed at the 0-mm and -0.5-mm axial locations, it occurred at a different circumferential location and it had a different shape. As with the previous comparison, none of the radial hydrides at -0.6 mm appeared to correlate with those observed on the -0.5-mm surface in terms of length, shape, and location across the cladding wall. Thus, it appears that the axial extent of hydride platelets is <100 μm for the 80-wppm sample. However, the average and 1-sigma values for the RHFC were essentially the same: 58±14%. The combined average of all three data sets gave 55±16%. Figure 10b shows an image from the third data set with 55% RHCF.

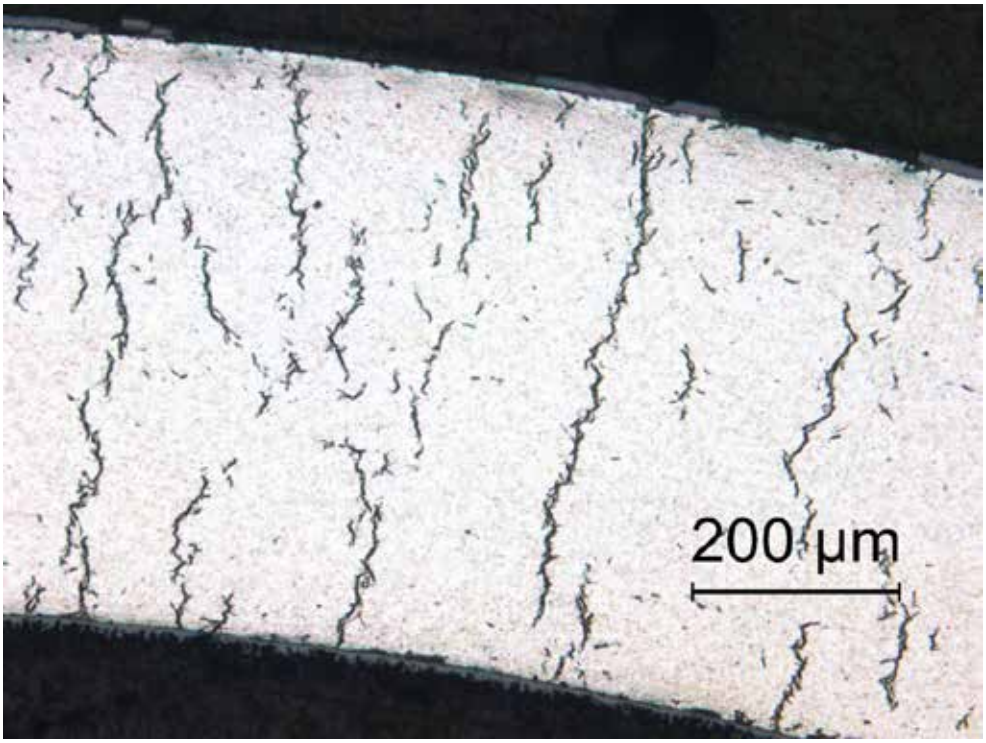

(a) Longest length (95% RHCF)

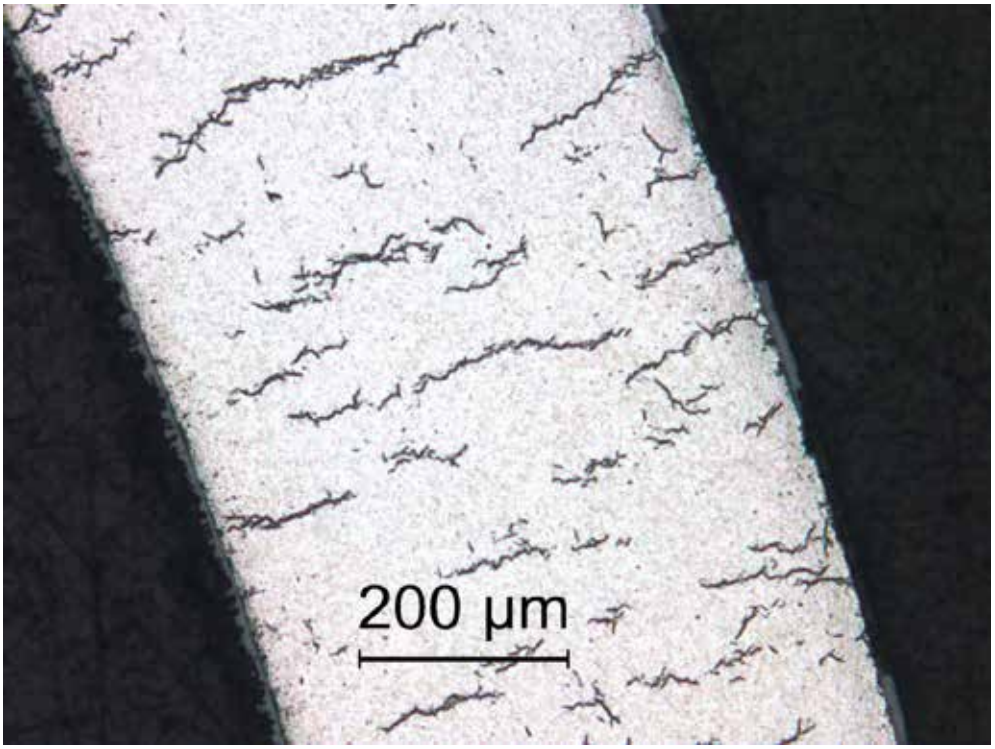

(b) Average length (55% RHCF)

Figure 10: Radial hydrides observed on the -0.6-mm 652F2F cross section: (a) longest length (95% RHCF) and (b) average length (55% RHCF).

RCTs were performed at 5 mm/s displacement rate to 1.7-mm maximum sample displacement using samples C, D, G, and H identified in Fig. 7. The RCTs were performed at 23°C (H), 60°C (D), 90°C (C), and 120°C (G). Load-displacement curves for these four tests are shown in Figs. 11–14, respectively. Corrected offset strains were measured to be 0.3% at 23°C, 1.7% at 60°C, 3.8% at 90°C, and >10.4% at 120°C (no cracking observed). As shown in Fig. 11, cracking initiated in the 23°C sample at 310 N during the rise in load and propagated during a series of three small load drops. At the end of the second load drop, the combined decrease in load was 27%, which is sufficient to generate a crack >50% of the wall thickness. However, based on subsequent tests, the expected peak load was about 450 N. This suggested that cracking was more extensive than indicated by the load drops starting at 310 N. Thus, the offset strain (0.3%) was determined using the data point at 310 N, the measured loading stiffness, and the unloading-stiffness factor given in Eq. 2a. The load-displacement curve shown in Fig. 12 for the 60°C sample was easier to interpret. Cracking initiated at 425 N and propagated rapidly to >50% of the wall thickness as indicated by the 39% drop in load. The corrected offset strain corresponding to the data point at 425 N was 1.7%. The load-displacement curve shown in Fig. 13 for the 90°C sample indicates a very steep load drop of 36% starting with the peak load of 453 N. The corresponding corrected offset strain was 3.8%. The load-displacement curve shown in Fig. 14 for the 120°C-RCT sample exhibited no significant load drop. Minor ripples in the curve are likely due to cracking of the thin oxide layer. The corrected offset strain was 10.4% at the end of the loading phase, which agreed quite well with the directly measured permanent strain of 9.9%. Thus the offset strain corresponding to >50% wall cracking was >10.4%.

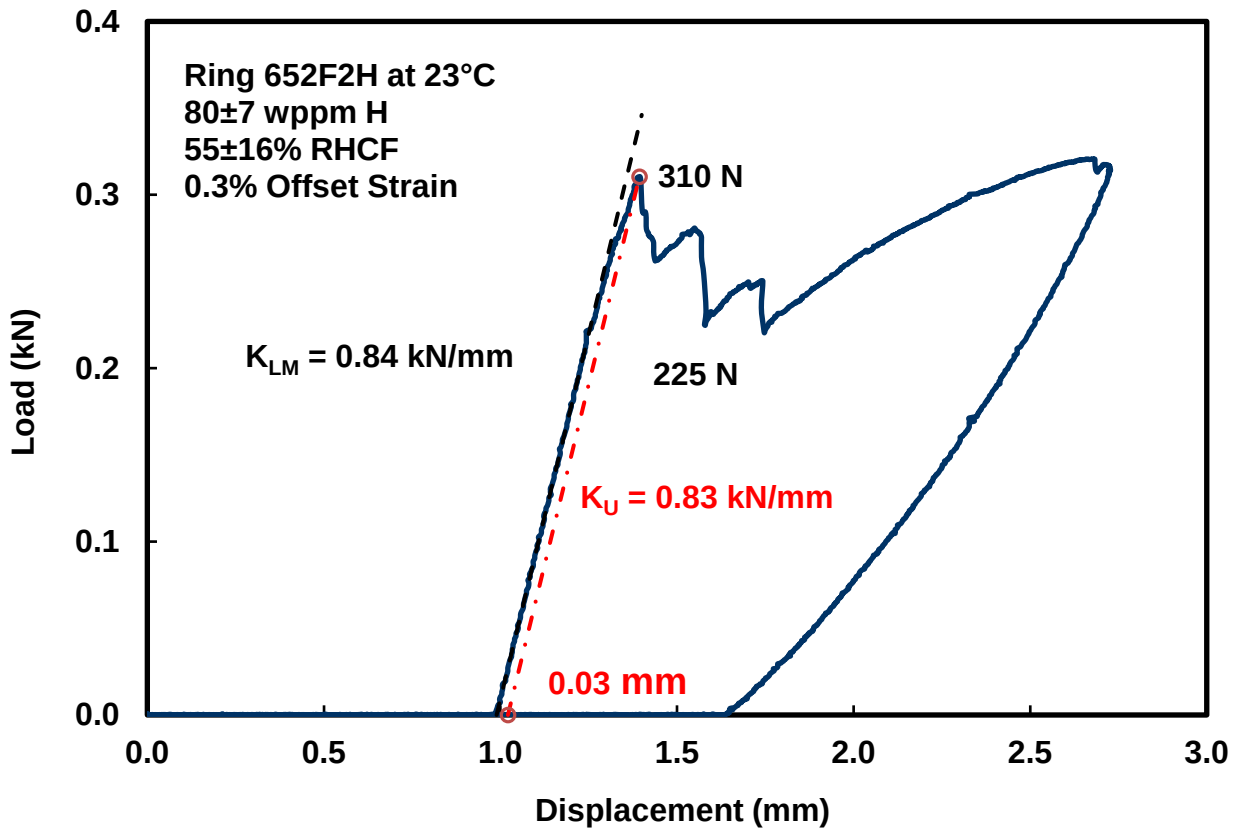

Figure 11: Load-displacement curve for the 652F2H sample tested at 23°C.

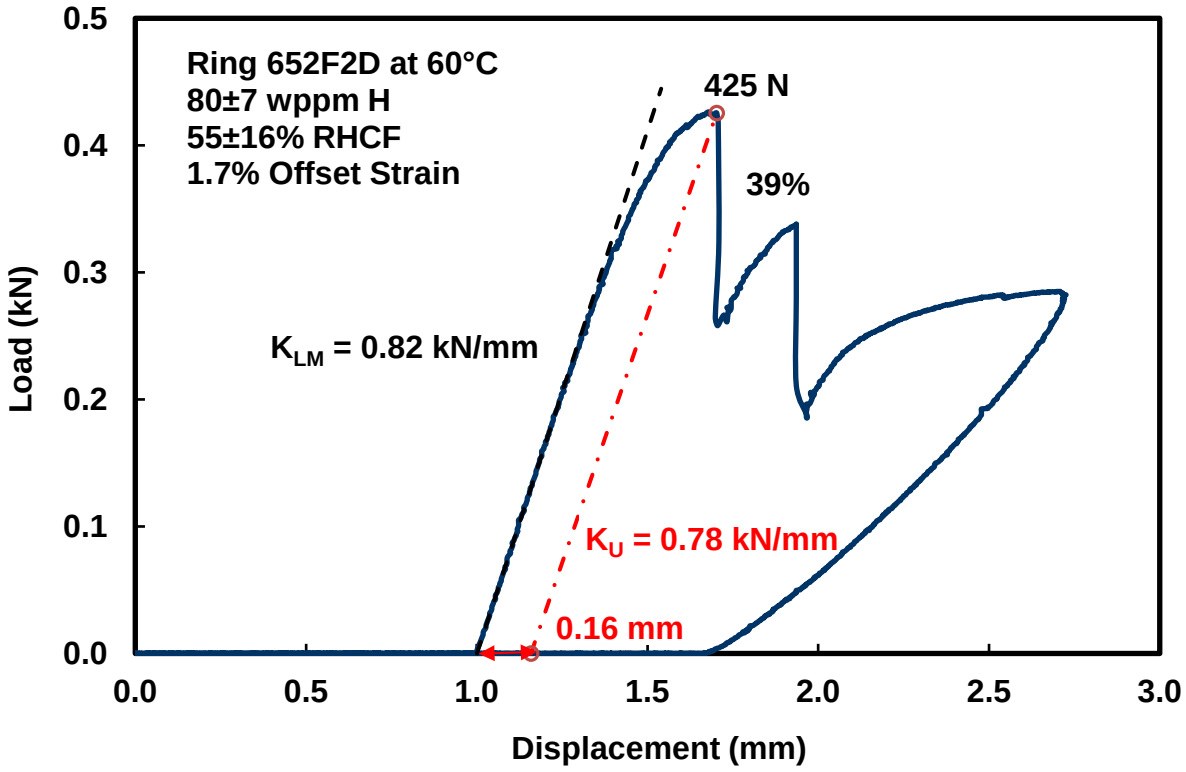

Figure 12: Load-displacement curve for the 652F2D sample tested at 60°C.

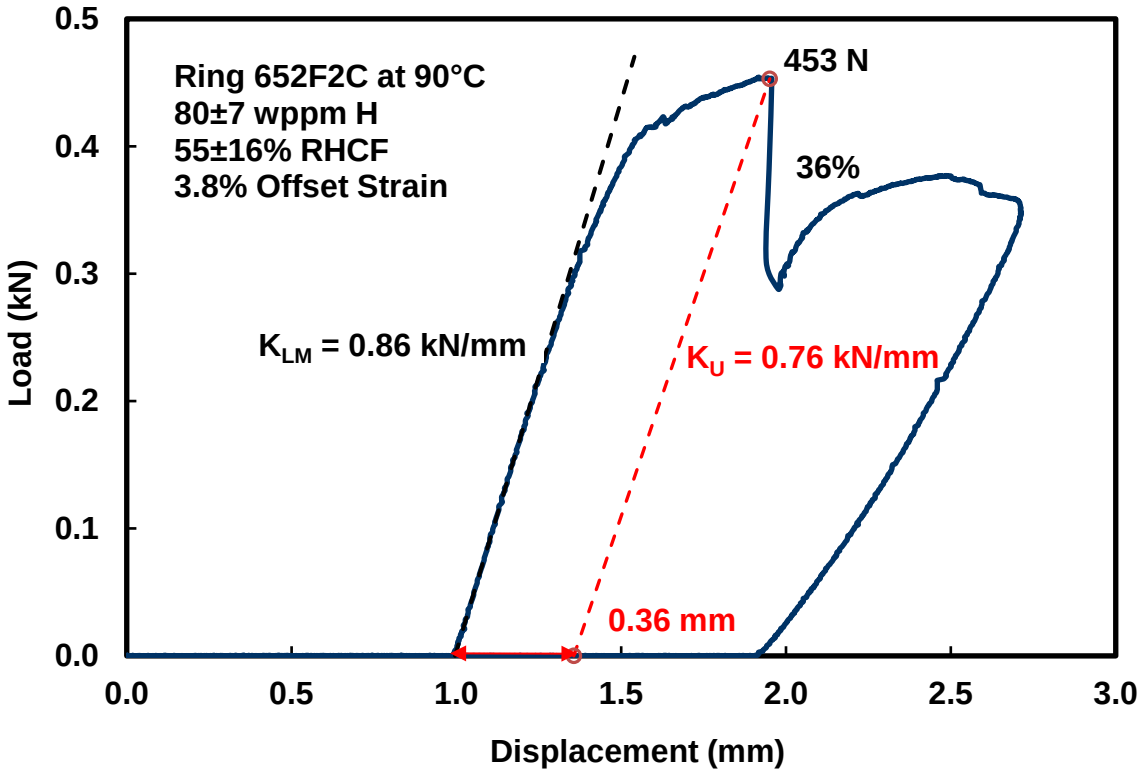

Figure 13: Load-displacement curve for the 652F2C sample tested at 90°C.

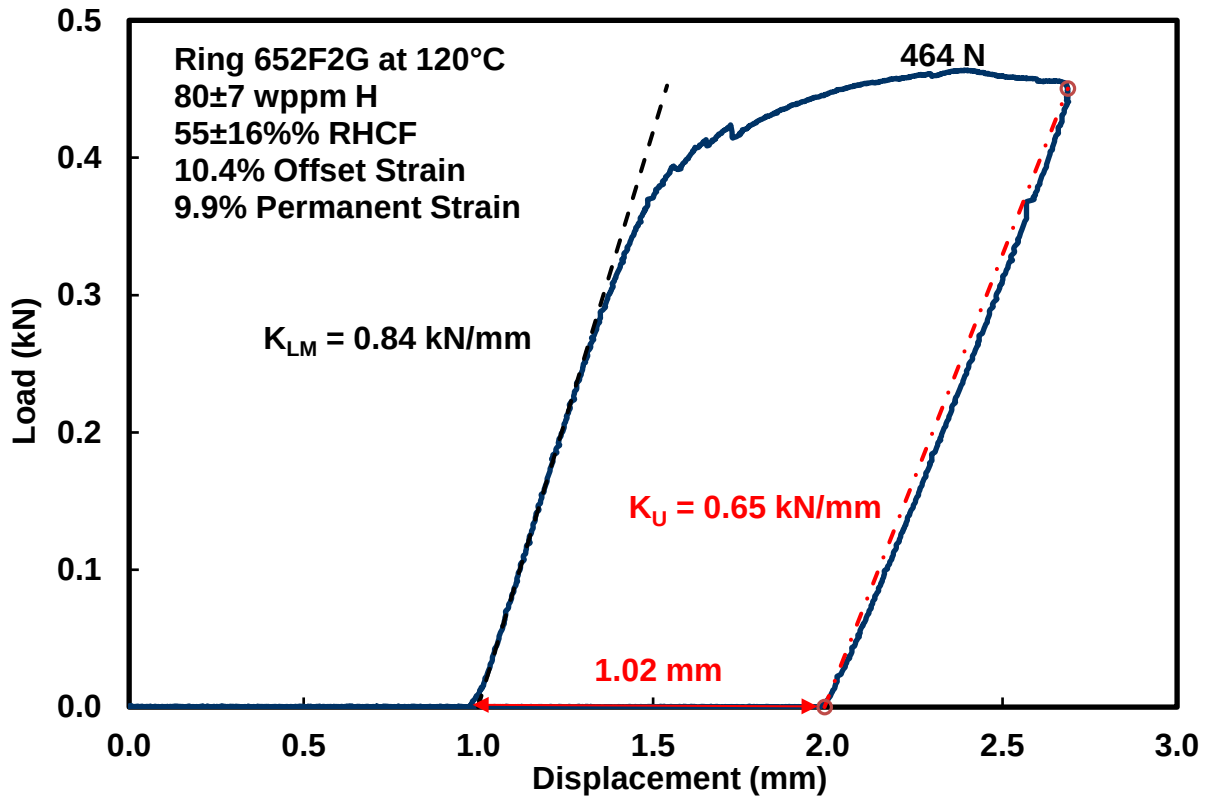

Figure 14: Load-displacement curve for the 652F2G sample tested at 120°C.

Table 2 shows the comparison between the new and previous results for HBU M5® following cooling from PCTs of 350°C and 400°C. The increase in peak stress (from 89 MPa to 142 MPa) and precipitation stress (from 74 MPa to 113 MPa) had very little effect on the DBTT (70–80°C) for hydrogen contents in the range of 72–94 wppm. Also, within this stress range, the RHCF exhibited a small increase from 54% to 61%. The low sensitivity of DBTT and RHCF to stress within this hydrogen-content range suggests that neither hydrogen content nor hoop stress has a significant effect on the DBTT for HBU M5®.

The drop of over 50°C in DBTT occurred with the concurrent decrease in hydrogen content (from 80 wppm to 58 wppm) and precipitation stress (from 74 MPa to 67 MPa) for tests conducted at the same peak hoop stress. Consistent with this result, the RHCF also decreased from 55% to 37%. The decrease in hydrogen content appears to have had a more significant effect on DBTT than the decrease in precipitation stress within this range (58–80 wppm). These results suggest that there is a critical hydrogen content (about 60 wppm) for HBU M5® below which radial hydrides are too short and discontinuous in the axial direction to cause embrittlement at temperatures greater than RT.

For the samples that exhibited DBTT values in the range of 70–80°C, there appears to be a secondary effect of reduced ductility due to reduced annealing at 350°C vs. 400°C for offset strains measured at 90°C RCT temperature. The 3.8% offset strain measured for the 350°C /89-MPa sample is lower than the corresponding offset strains measured for the 400°C /111-MPa sample (>10.8%) and for the 400°C /142-MPa sample (6.1%). However, for RCTs conducted at 120°C, no conclusions can be drawn about the effects of reduced irradiation-induced annealing because the 10.4% listed for the 350°C /89-MPa sample is a lower bound as the sample did not crack within the 1.7-mm displacement. Also, the other samples were not tested at 120°C.

Table 2 Characterization results for HBU M5® cladding following cooling from 350°C and 400°C.

Parameter	Rodlet 651E3	Rodlet 652F2	Rodlet 651E5	Rodlet 645D
C_H, wppm	58±15	80±7	72±10	94±6
PCT, °C	400	350	400	400
T_D, °C	291	315	307	329
T_P, °C	226	250	242	264
σ_θ(PCT), MPa	90	89	111	142
$\sigma_\theta(T_P)$, MPa	67	74	84	113
Average RHCF, %	37±17	55±16	54±20	61±18
Surface 1 RHCF, %	47±15	49±14	57±16	67±20
Surface 2 RHCF, %	36±14	58±18	64±20	67±13
Surface 3 RHCF, %	33±19	58±14	33±8	51±14
Surface 4 RHCF, %	24±9	–	–	–
Ductility @ RT, %	8.4, >10.5	0.3	1.1	0.7
Ductility @ 60°C	>9.6	1.7	0.9	0.0
Ductility @ 90°C	–	3.8	>10.8	6.1
Ductility @ 120°C	—	>10.4	–	–
Ductility @ 150°C	–	–	–	>11.6
DBTT, °C	<20	70	70	80

The RCT ductility values are plotted in Figure 15, along with trend curves, for the data given in Table 2, along with the data for as-irradiated cladding. Figure 16 shows the sharp decrease in DBTT with the decrease in hydrogen content from 72 wppm to 58 wppm. The total-hydrogen-content hypothesis could be supported further if additional tests were conducted at stresses >110 MPa with HBU M5® that contained only 60-wppm hydrogen. However, the peak hoop stress for standard M5®-clad fuel rods is anticipated to be <80 MPa. As such, it is more important to conduct a bounding test at 80 MPa with HBU M5® that contains about 100–120 wppm hydrogen.

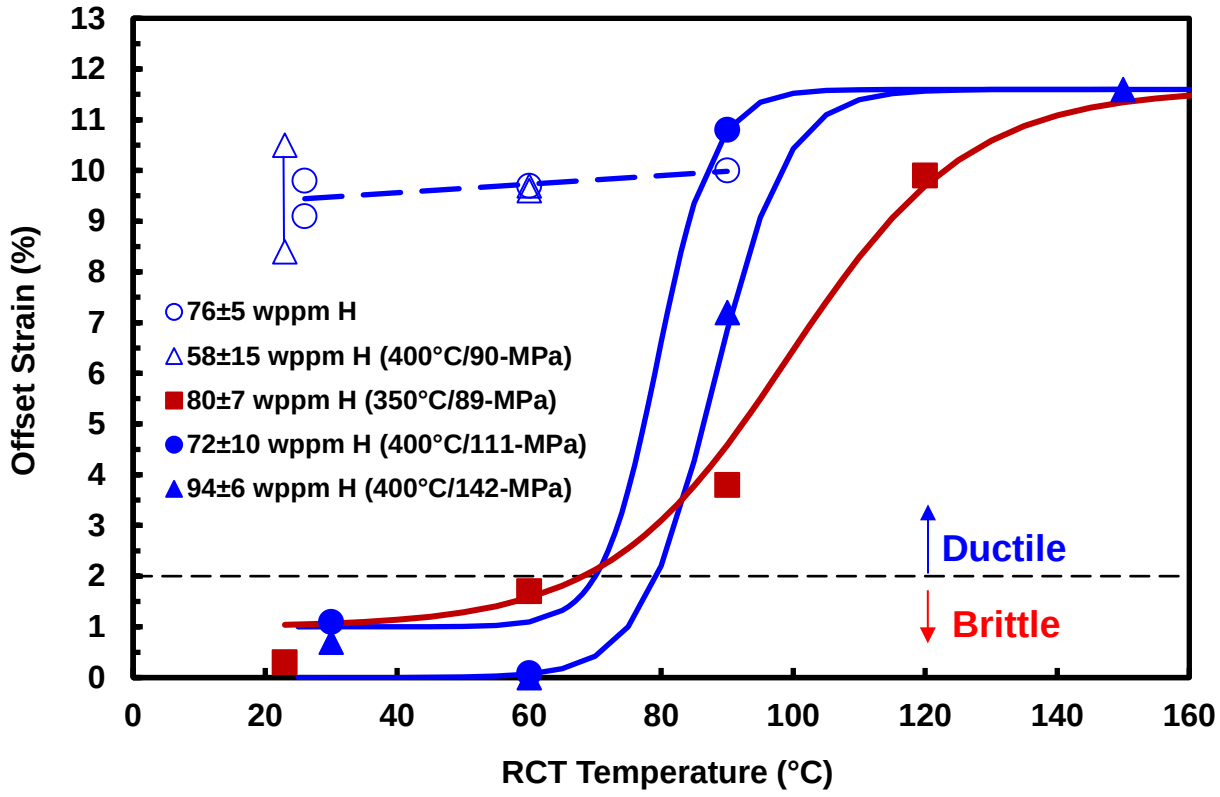

Figure 15: RCT ductility curves for HBU M5® in the as-irradiated condition and following RHT at 350°C and 400°C PCTs.

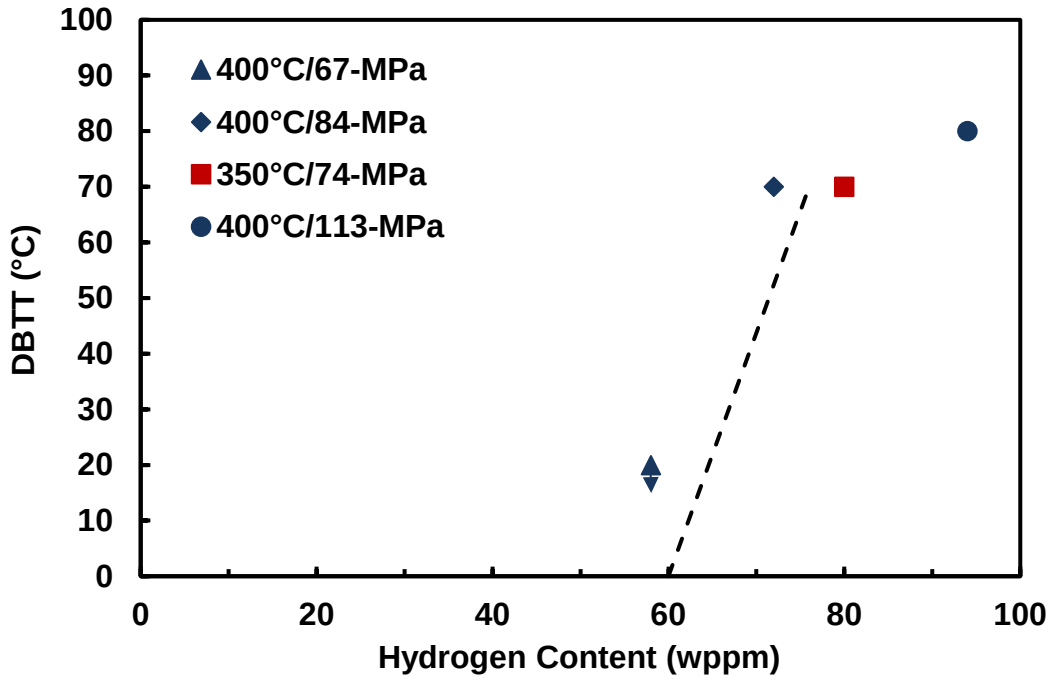

Figure 16: DBTT for HBU M5® vs. hydrogen content following RHT at 350°C and 400°C PCTs.

4.2 HBU ZIRLO™ FOLLOWING COOLING FROM 350°C PCT

The new HBU ZIRLO™ test was designed to test the hypothesis that the DBTT for this material is highly sensitive to peak RHT hoop stress and the corresponding stress at the initiation of precipitation. The absolute value of fill pressure at RT (23°C) was chosen to be 5.60 MPa to give a target hoop stress of about 90 MPa at the PCT (350°C). The hold time (24 h) and the estimated hydrogen content were chosen to be similar to the 648C rodlet test with 350±80 wppm subjected to higher PCT (400°C) and higher peak hoop stress (111 MPa). By keeping the hydrogen content approximately the same, the effects of both lower PCT (350°C) and lower target hoop stress could be assessed. A schematic of the rodlet selected for this test is shown in Fig. 17.

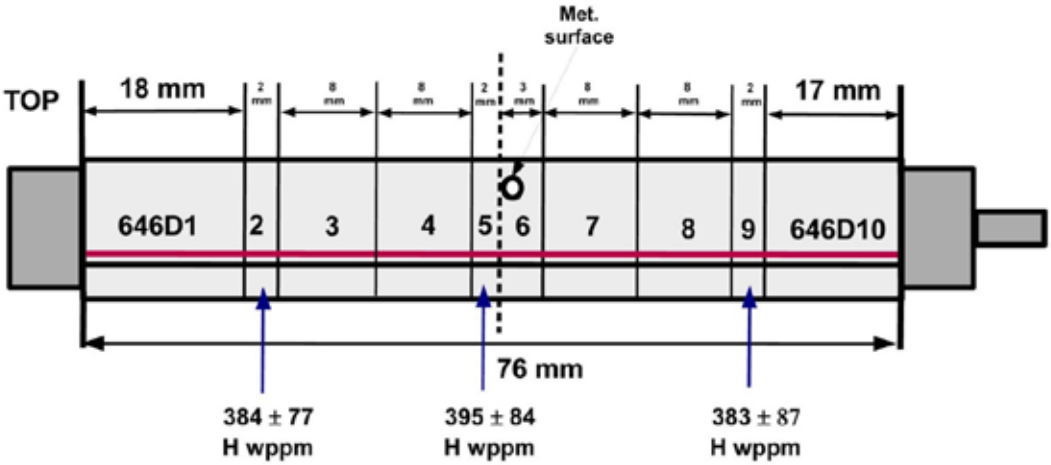

Figure 17: Sectioning diagram for the HBU ZIRLO™ rodlet 646D following RHT at 350°C PCT.

Hydrogen-content measurements are displayed in Fig. 17 at three axial locations (4 measurements of quarter-arc samples per axial location). The average and 1-sigma variation were calculated to be 387±72 wppm for the rodlet based on mass-averaging of the hydrogen contents shown in Fig. 17. These are close enough to the rodlet with 350±80 wppm to allow a direct comparison of results.

The geometrical parameters measured for this rodlet were 9.49-mm D_o, 30±1 µm h_{ox}, 9.43-mm D_{mo}, 0.56-mm h_m, and 8.31-mm D_{mi}. The geometrical factor (R_{mi}/h_m) used in Eq.1 to convert pressure difference across the cladding wall to wall-averaged hoop stress (87 MPa) was 7.46. The 87-MPa peak hoop stress was essentially the same as for two previous tests conducted at 400°C and peak hoop stresses of 88 MPa and 89 MPa and slightly lower than two previous tests conducted at 350°C PCT and peak hoop stresses of 93 MPa and 94 MPa.

Appendix A contains 100X images at 42 overlapping circumferential orientations. 200X images were also taken to assess radial-hydride continuity across the cladding wall. Selected 100X and 200X images are presented in this section. The average and 1-sigma variation in effective radial hydride length (RHCF) were determined to be 20±12%. These values are comparable to those measured for the 400°C/88-MPa (18±7%) and 400°C/89-MPa (19±9%) rodlets. Figure 18 shows 100X and 200X images of the circumferential orientation with the longest radial hydrides (50% RHCF). Figure 19 shows 100X and 200X images of the orientation at 12 o'clock with average-length radial hydrides (20% RHCF). Figure 20 shows an orientation with essentially no radial hydrides (≈5% RHCF).

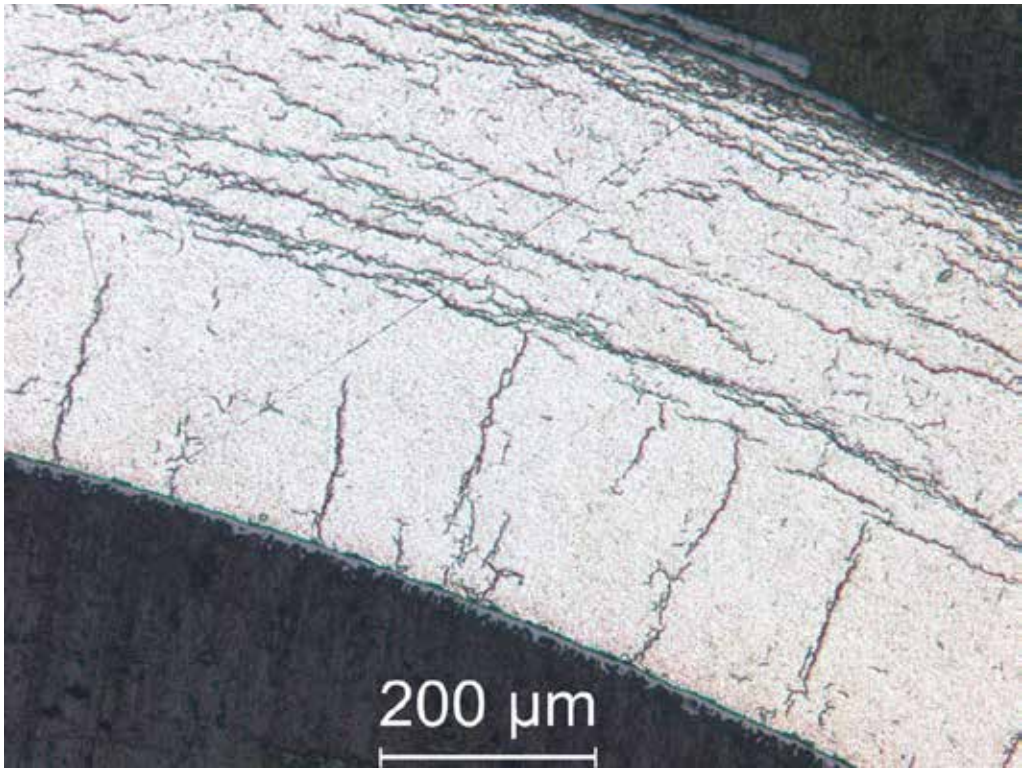

(a) 100X

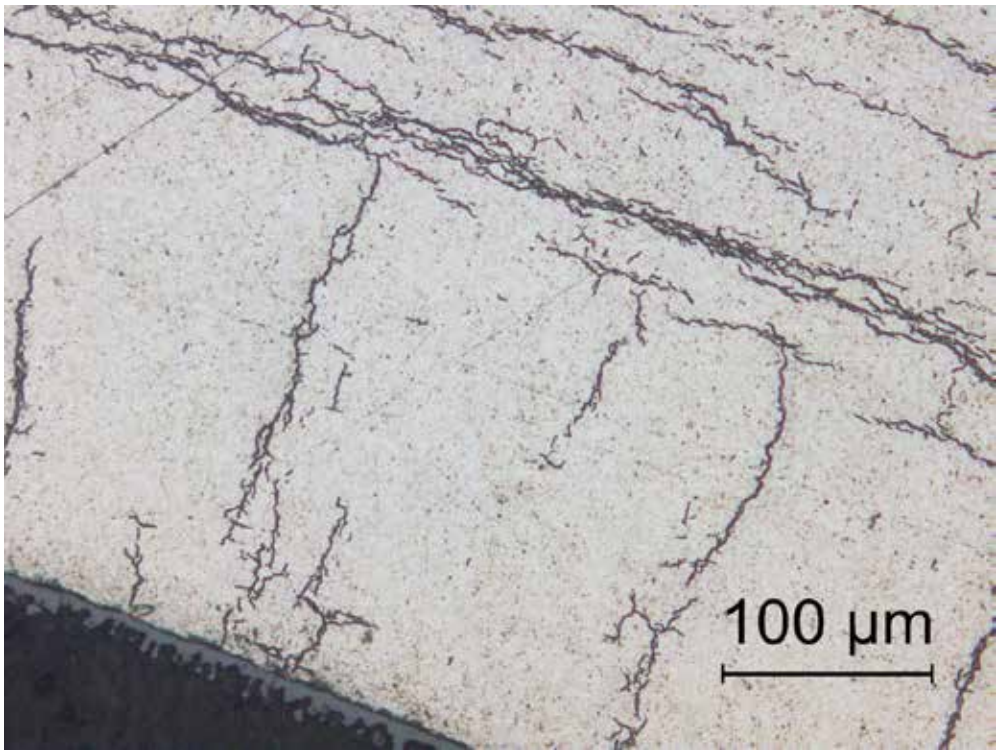

(b) 200X

Figure 18: Longest radial hydrides observed for the 646D6 cross section: (a) 100X and (b) 200X.

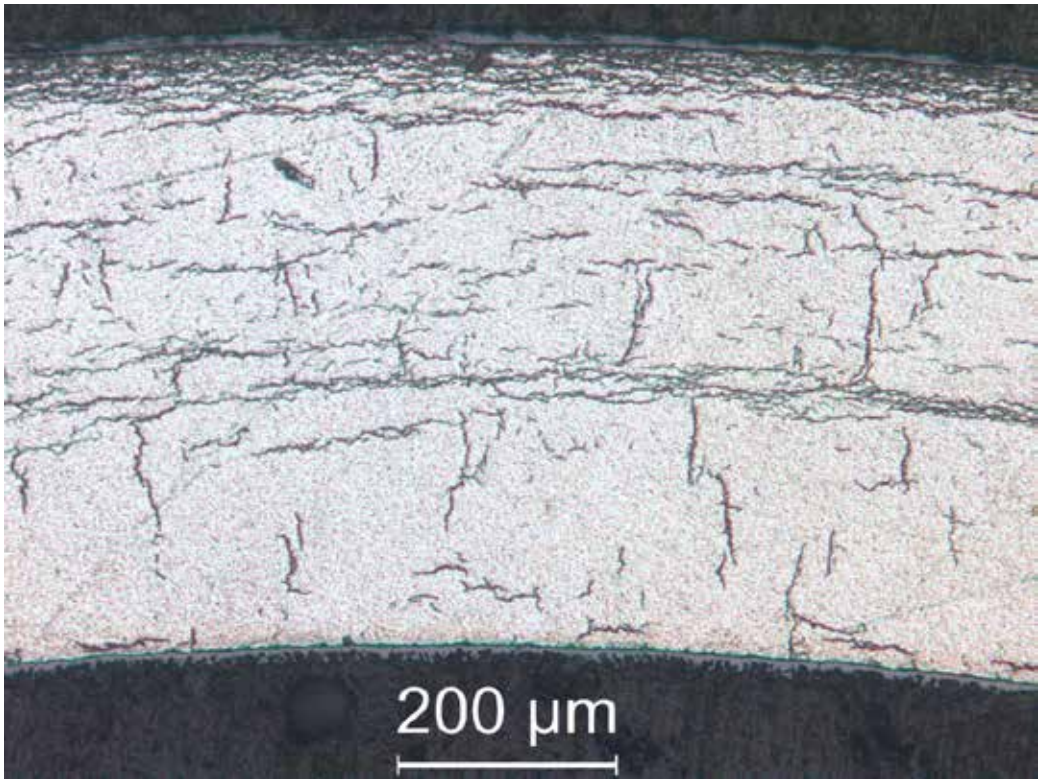

(a) 100X

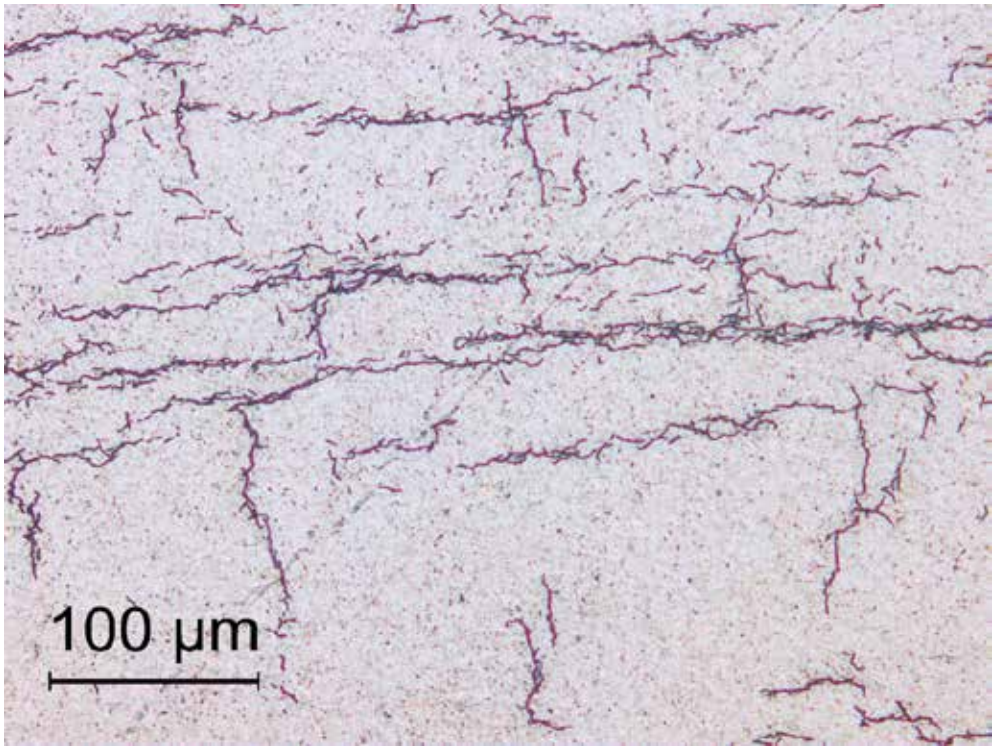

(b) 200X

Figure 19: Average-length radial hydrides observed for the 646D6 cross section: (a) 100X and (b) 200X.

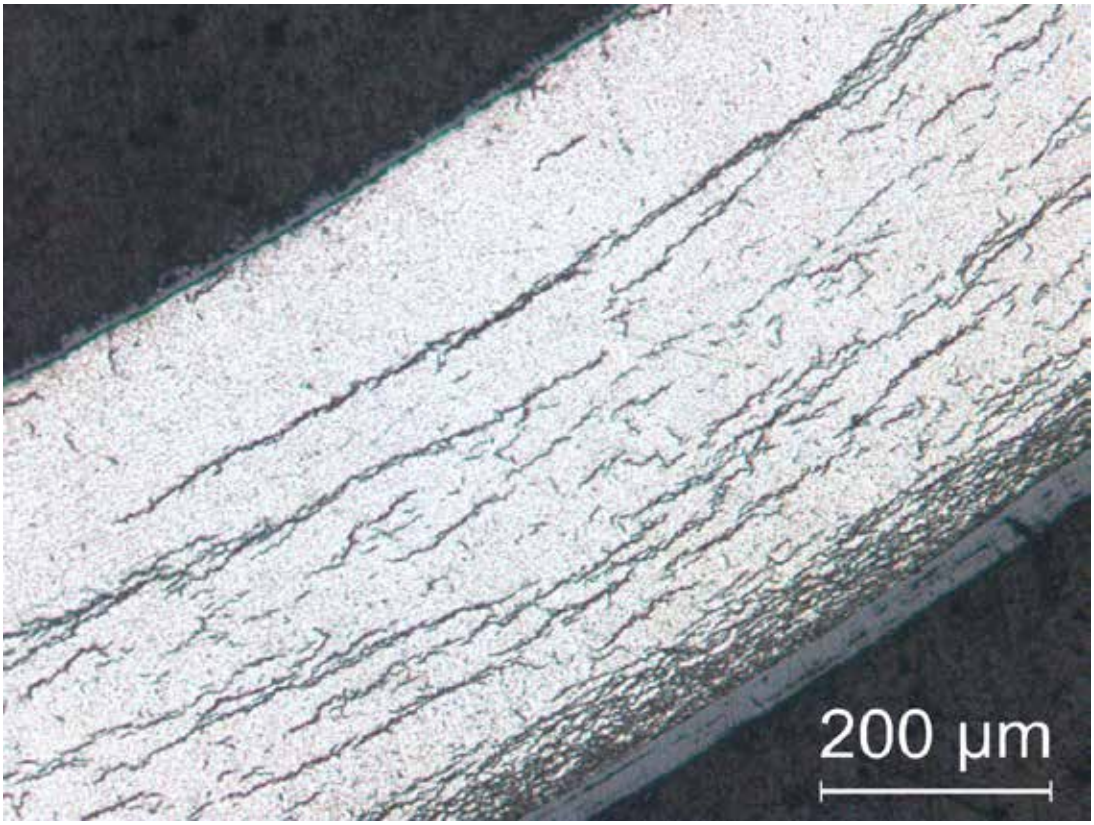

Figure 20: Circumferential orientation of the 652F2F cross section with essentially no radial hydrides.

RCTs were conducted at 5 mm/s to 1.7-mm sample displacement for samples 3, 4, 7, and 8 shown in Fig. 17 at: 27°C (sample 8), 60°C (sample 4), 90°C (sample 7), and 120°C (sample 3). Load-displacement curves for these four tests are shown in Figs. 21-24. The load-displacement curve in Fig. 21 for the 27°C sample exhibited a load drop of 23% at the peak load of 519 N followed by a load drop of 35% at a larger displacement. The 23% load drop is marginal compared to the criterion of >25% load drop required for a crack to grow to >50% of the wall thickness. °C RCT (see Fig. 22), the sample exhibited a mild 10% load drop at 560 N and 5.8% offset strain, which represents a lower bound on ductility. The load increased and decreased slightly to 500 N just prior to the 44% load drop. The sample was severely cracked at the end of the 44% load drop. The 10.2% offset strain calculated just prior to the 44% load drop represents an upper bound on the ductility because the actual unloading stiffness of the partially cracked sample would be less than the one calculated using Eq. 2b. The load and unloading slope shown in Fig. 22 correspond to a displacement midway between the 10% and 44% load drops. The calculated ductility for this point was 8.0%, which is halfway between the lower and upper bounds. For the 90°C- and 120°C-RCT results shown in Figs. 23–24, the samples survived the full 1.7-mm displacement with no significant load drops and no cracking. Thus, the corresponding offset strain values of 9.9% and 9.6% were lower bounds on ductility. Measured permanent strains were 8.4% and 8.9%, respectively.

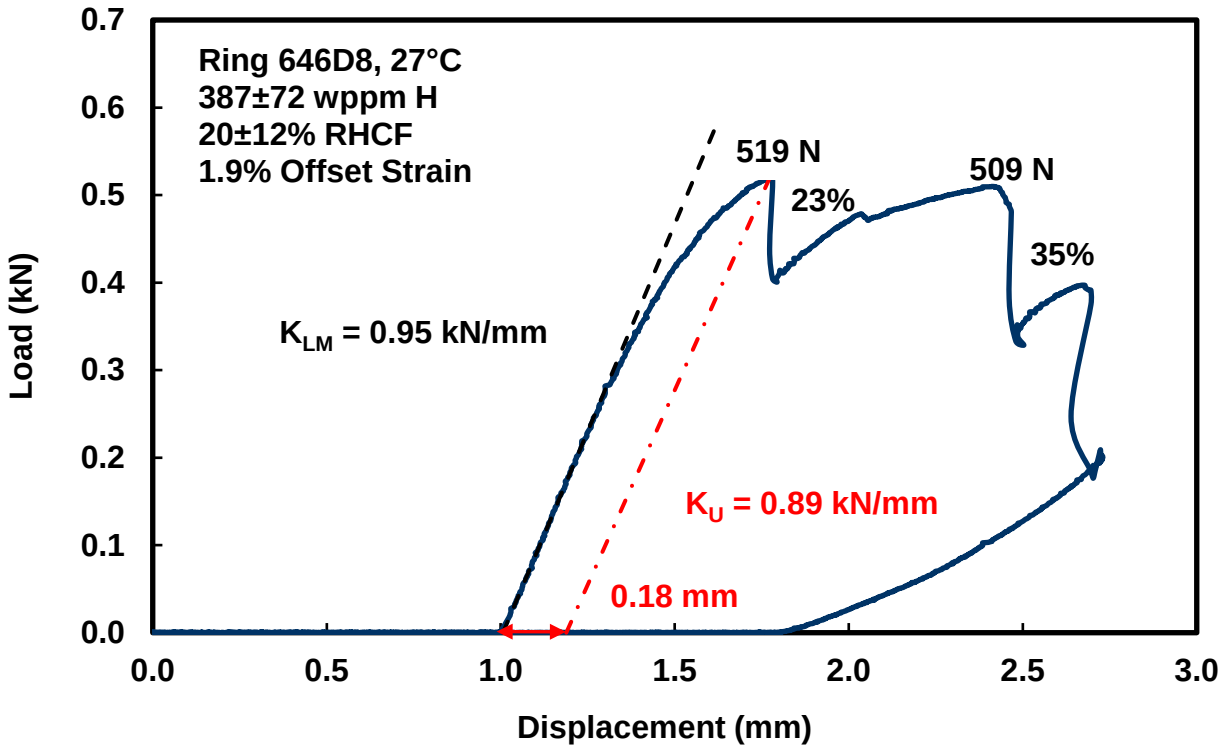

Figure 21: Load-displacement curve for the 646D8 sample tested at 27°C.

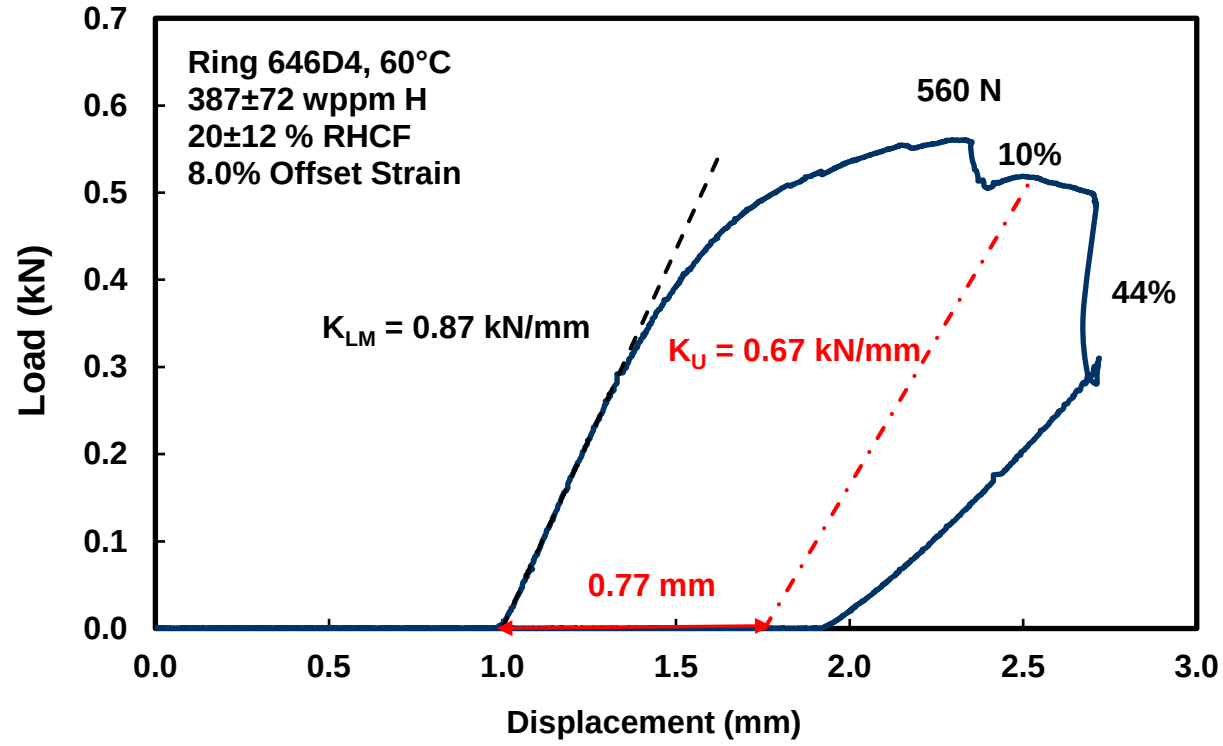

Figure 22: Load-displacement curve for the 646D4 sample tested at 60°C.

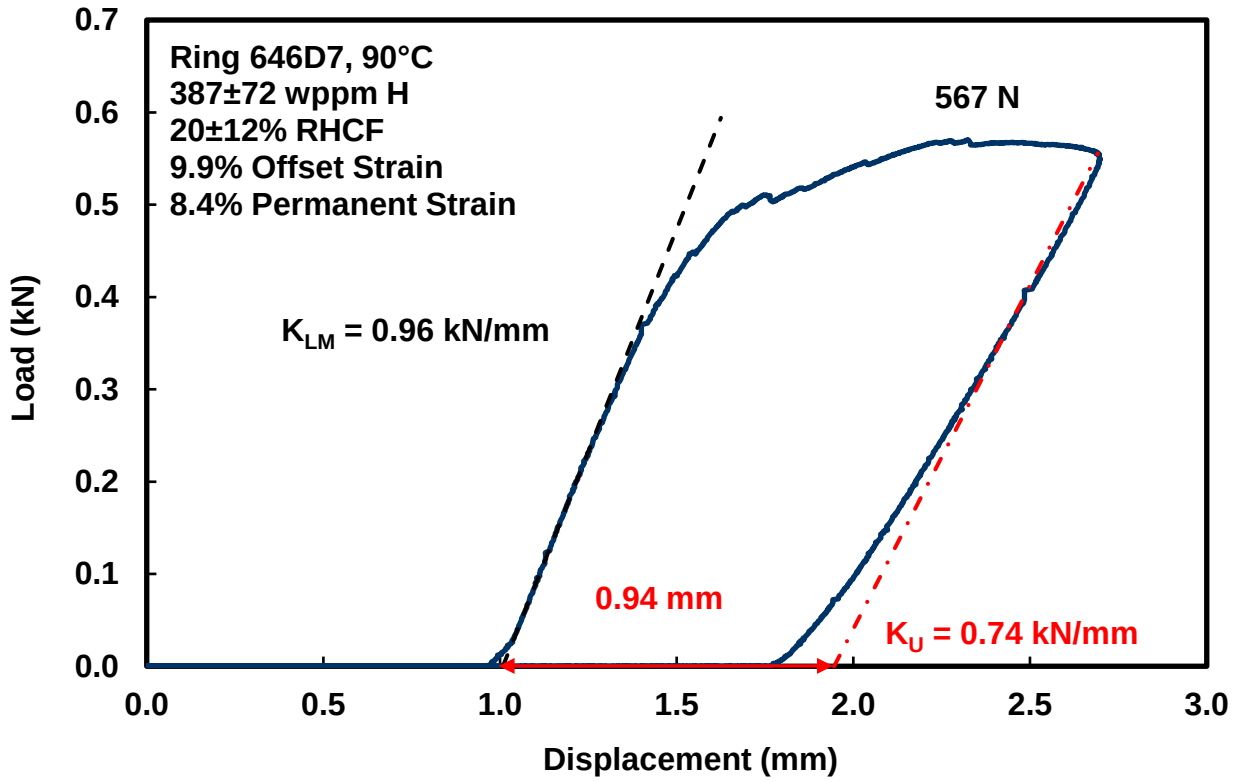

Figure 23: Load-displacement curve for the 646D7 sample tested at 90°C.

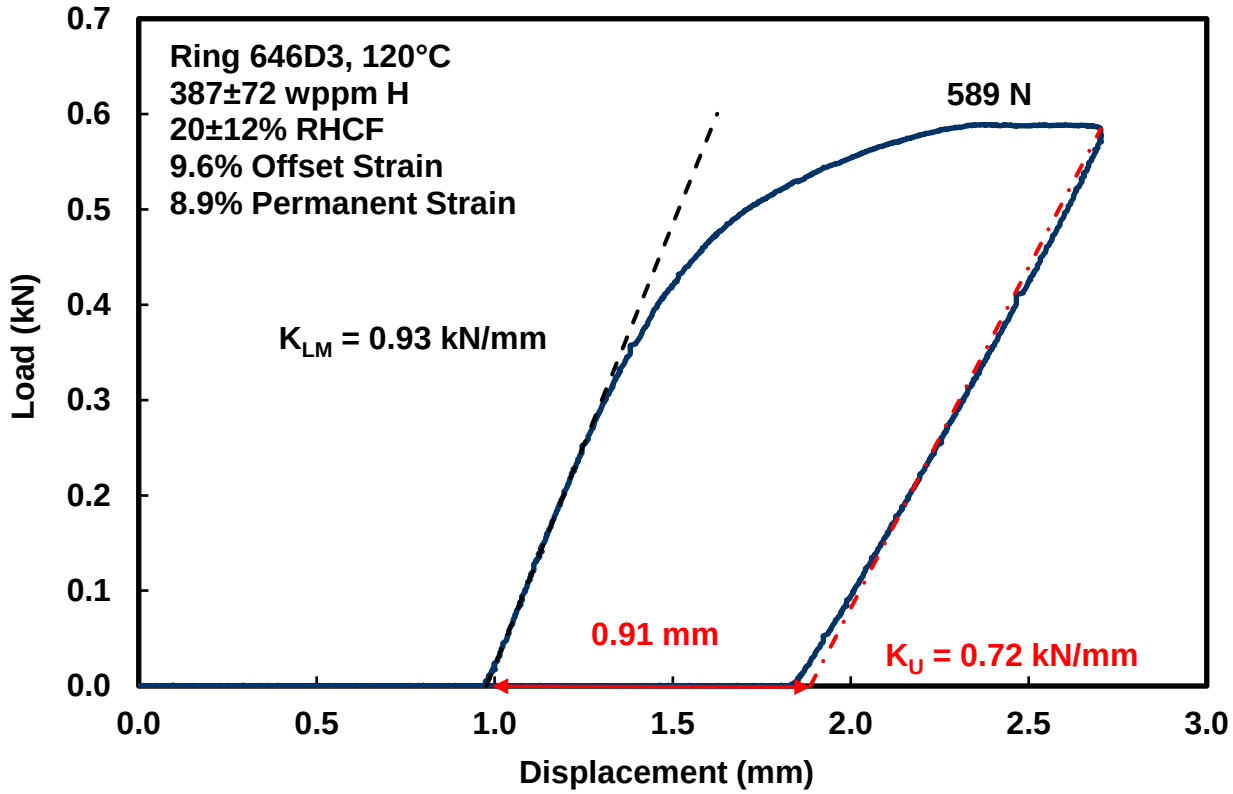

Figure 24: Load-displacement curve for the 646D3 sample tested at 120°C.

Characterization and RCT results for the 646D rodlet sample are listed in Table 3, along with results for other relevant rodlets subjected to RHT at 350°C and 400°C.

Table 3 Characterization results for HBU ZIRLO™ cladding following cooling from 350°C and 400°C.

Parameter	Rodlet 105C	Rodlet 105D	Rodlet 646D	Rodlet 105E	Rodlet 648D
C_H, wppm	530±115	480±131	387±72	564±177	350±80
PCT, °C	400	400	350	350	400
C_{HD}, wppm	206±5	206±5	126±6	126±6	206±5
T_P, °C	335	335	285	285	335
σ_θ(PCT), MPa	89	88	87	93	111
$\sigma_\theta(T_P)$, MPa	80	80	78	83	100
Average RHCF, %	19±9	18±7	20±12	30±11	32±13
Surface 1 RHCF, %	17±9	20±9	20±12	32±12	32±13
Surface 2 RHCF, %	20±9	17±6	–	37±8	–
Surface 3 RHCF, %	21±9	–	–	26±10	–
Ductility @ RT, %	2.0 (23°C)	2.3 (26°C)	1.9 (27°C)	–	0.3 (30°C)
Ductility @ 60°C	6.8	6.6	8.0	–	–
Ductility @ 90°C	>10.8	>10.2	>9.9	0.8	0.4
Ductility @ 120°C	>11.0	>10.1	>9.6	1.2	1.4
Ductility @ 135°C	–	–	–	>11.0	–
Ductility @ 150°C	–	–	–	8.3	>10.2
DBTT, °C	23	23	28	127	122

Offset strain is plotted vs. RCT temperature in Fig. 25 for the test results shown in Table 3, along with the results for rodlet 105F (350°C/94-MPa with 644±172-wppm hydrogen) and the results of rodlet 648D (400°C/111-MPa with 425±63-wppm hydrogen). Trend curves are also shown for individual data sets and for combinations of data sets. Although the data for very high-hydrogen-content rodlet 105F are shown in Fig. 25, they were not used to generate the trend curve for the samples subjected to RHT at 350°C PCT and 93-94 MPa. The new data for rodlet 646D (350°C/87-MPa) support the hypothesis that the DBTT for HBU ZIRLO™ is very sensitive to the peak RHT hoop stress within the narrow range of 90±3 MPa, which corresponds to a narrow range of precipitation stresses (78–83 MPa). Within this stress range, the DBTT increases rapidly by ≈100°C. Figure 26 shows the sharp increase in DBTT during the narrow increase in peak and precipitation hoop stresses. In further support of this hypothesis, the RHCF increased rather abruptly from about 20% to ≥30% in this narrow stress range (Fig. 27). There does not appear to be an effect of total hydrogen content on DBTT within the range of 350–550 wppm. However excessive hydrogen content (>600 wppm average) with relatively large circumferential variation leading to >850 wppm local maximum hydrogen content) can degrade ductility, increase data scatter, and possibly increase the DBTT. Such data are not relevant to ZIRLO™-clad fuel rods irradiated to less than the licensing limit. If irradiation-hardening annealing occurred at 400°C, it appears to be a tertiary factor.

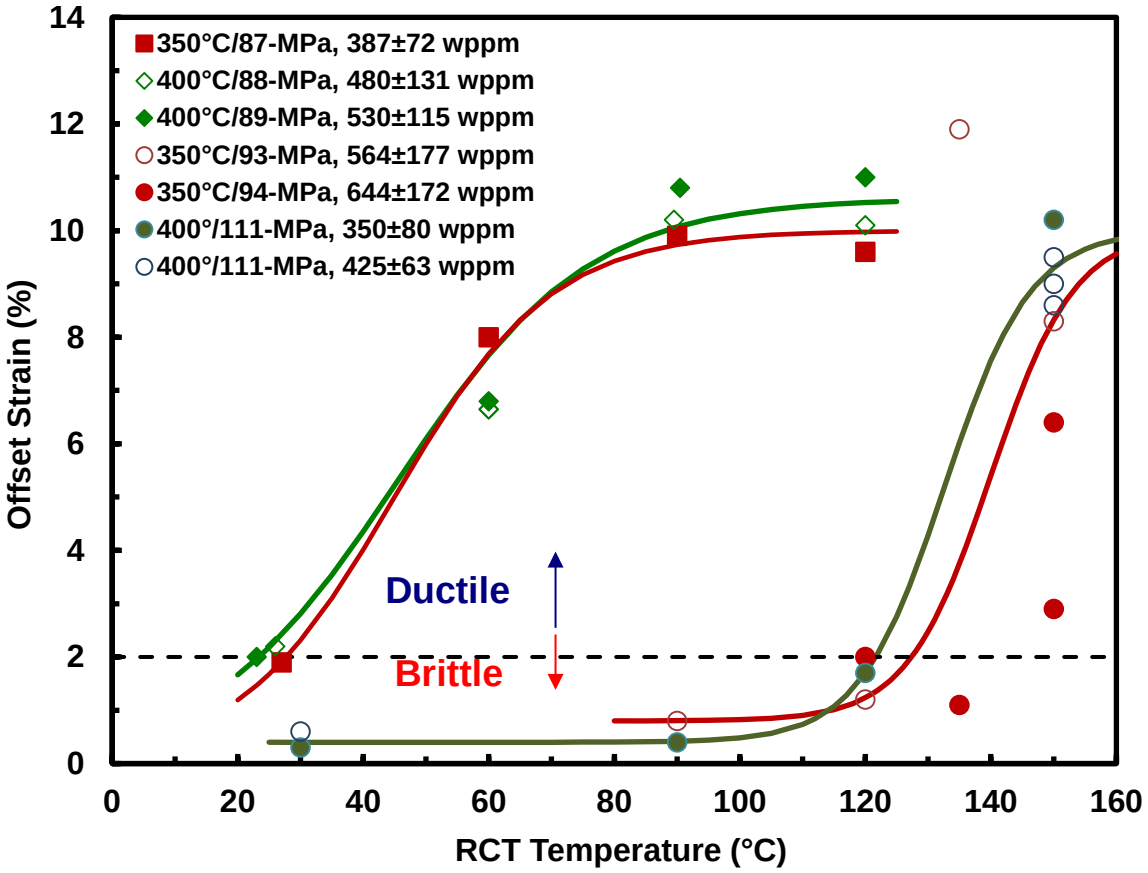

Figure 25: Summary of ductility data for HBU ZIRLO™ following RHT at 400°C and 350°C PCTs.

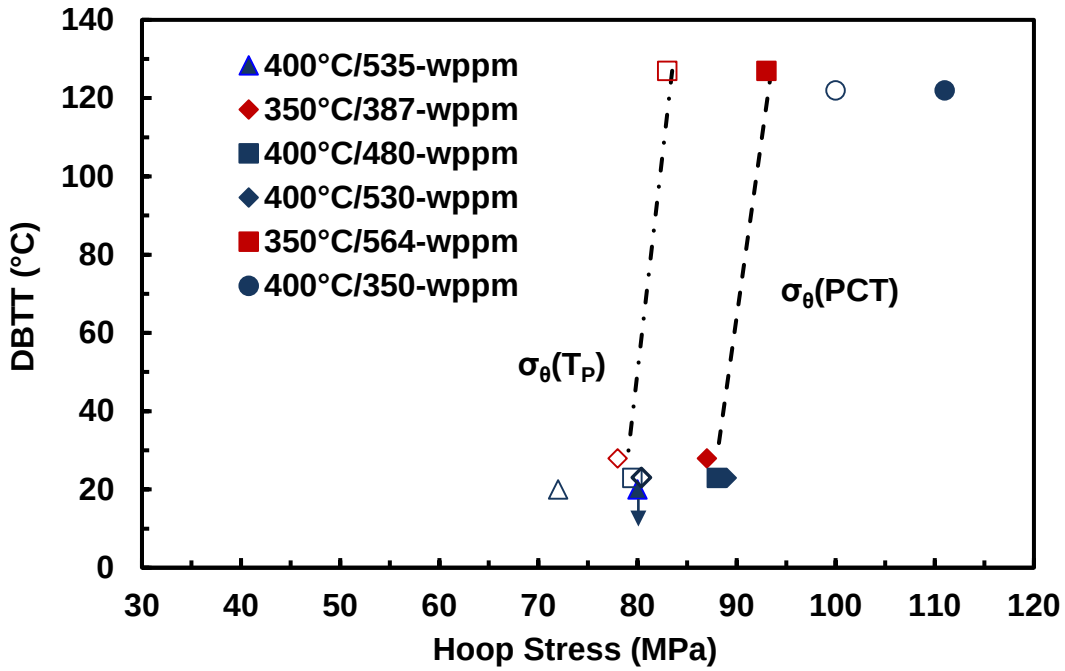

Figure 26: DBTT vs. hoop stress for HBU ZIRLO™ following RHT at 400°C and 350°C PCTs.

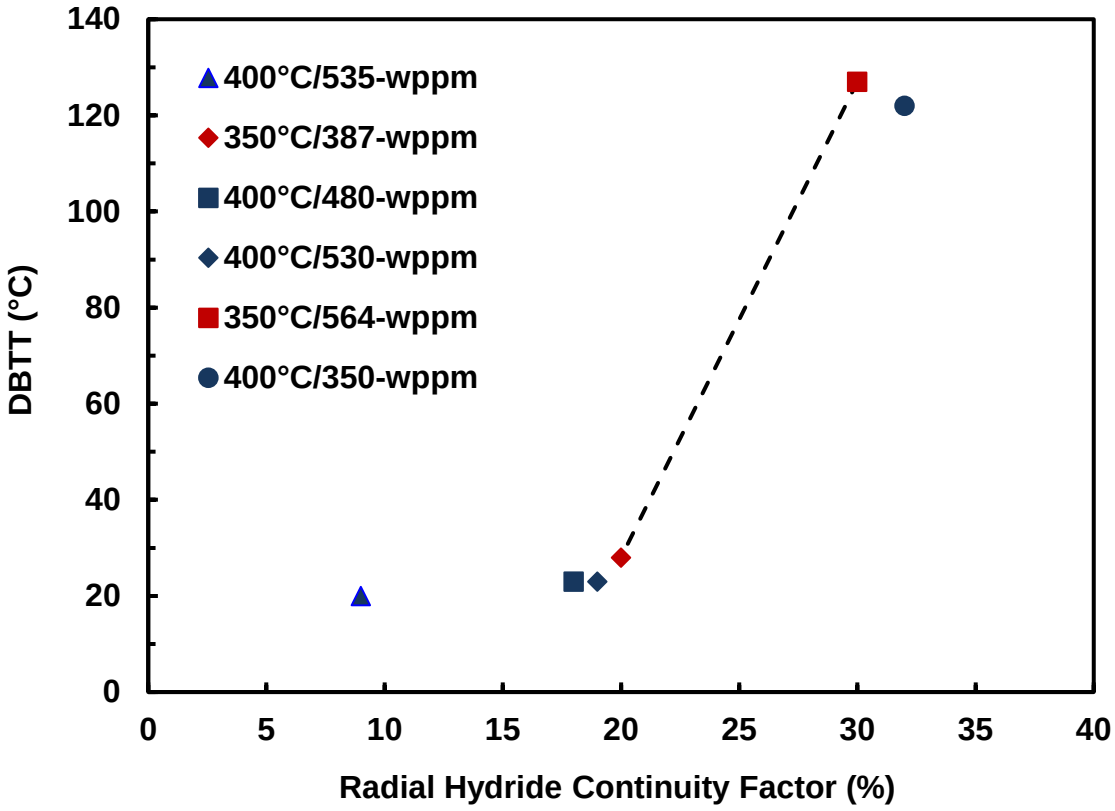

Figure 27: DBTT vs. the effective lengths of radial hydrides (RHCF) for HBU ZIRLO™ following RHT at 400°C and 350°C PCTs.

Page intentionally blank

5. DISCUSSION AND SUMMARY

Hydrogen Dissolution and Precipitation

The hydrogen dissolution and precipitation curves shown in Fig. 1 indicate a mild discontinuity in dissolution temperature (T_D) and a more significant discontinuity in precipitation temperature (T_P) for low hydrogen-content levels. The effects of these uncertainties are discussed below for the new HBU M5® rodlet, which contained 80±7 wppm hydrogen (local values of 66–90 wppm). With regard to dissolution, the predicted T_D values for 80-wppm hydrogen range from 303°C (Kammenzind et al. [15] for Zry-2 and Zry-4) to 310°C (Kearns [14] for Zry-2 and Zry-4) to 315°C (Kearns [14] for Zr, Zry-2 and Zry-4) to 329°C (McMinn et al. [16] for Zry-2 and Zry-4). It should be noted that McMinn et al. measured lower T_D values (closer to those determined in Refs. 14 and 15 for Zry-2 and Zry-4) for lightly irradiated Zry-2. Given that the RHT test was conducted at 350°C, all four correlations predict full dissolution of hydrides at this PCT, even for the local maximum value of 90 wppm. The correlation chosen for the M5® studied in this program was the Kearns correlation for Zr, Zry-2, and Zry-4. Although these researchers did not include Nb-bearing alloys in their studies, the absence of tin in M5® suggests a dissolution temperature between Zr and Zry-2/Zry-4.

The effects of the uncertainty in precipitation temperature are perhaps more significant. To minimize bias due to the experimental differences, the differences in precipitation-dissolution temperatures (ΔT_{PD}) are compared. The Kammenzind et al. correlations predict 66°C ΔT_{PD}, while the McMinn et al. correlations predict 46°C ΔT_{PD}. Using 315°C as T_D, T_P could be in the range of 249°C to 269°C. This variation in T_P causes a variation in the calculated internal pressure (p_i) and corresponding hoop stress at the initiation of precipitation. The precipitation-initiation pressure is calculated by the ratio of absolute temperatures times the RT fill pressure (5.90 MPa at 23°C): $[(T_P + 273\ K)/296\ K] \times 5.90$ MPa. For the 66°C and 46°C temperature drops, calculated p_i would be 10.62 MPa and 10.40 MPa, respectively. Thus, the 20°C uncertainty in ΔT_{PD} results in an uncertainty of only about ±1% in internal pressure at precipitation initiation.

Effects of Hydrogen Content on Ductility and DBTT

There appears to be several ranges of hydrogen contents that should be considered in assessing the effects of C_H on ductility and DBTT. At very low hydrogen contents, radial hydrides are shorter and lack enough connectivity or continuity in the axial direction to cause embrittlement regardless of how high the hoop stress level is at precipitation initiation. At very high hydrogen contents, the presence of a thick hydride rim and radial hydrides within and below that rim can cause significant degradation as reflected by the decrease in ductility and increase in DBTT. Within these two hydrogen levels, there are two cases to consider: hydrogen contents close to the solubility limit at the PCT such that no or relatively few circumferential hydrides are present at the PCT and hydrogen contents well above the solubility limit at the PCT, such that a significant fraction of the total hydrogen remains precipitated as circumferential hydrides at the PCT. Not all of these ranges were included in the Argonne samples. The M5® samples included the low hydrogen-content range of about 60–100 wppm. Test results indicated an increase of >50°C in DBTT concurrent with the increase in average hydrogen content from 58 wppm to 72 wppm for the precipitation stress range of 67 MPa to 84 MPa. Within a more narrow precipitation-stress range (67–74 MPa), the transition occurred with the hydrogen-content increase from 58 wppm to 80 wppm. Although definitive conclusions cannot be drawn from such a limited database, it does appear that the primary reason for the >50°C increase in M5® DBTT was due to the increase in hydrogen content. The modest increase in precipitation stress is considered to be secondary within the range of 67 MPa to 74 MPa. This preliminary conclusion is based on measured lengths of radial hydrides for the

two cases and speculation regarding the decrease in spacing of radial hydrides in the axial direction. A test could be conducted to confirm these preliminary conclusions: HBU M5® with 60-wppm hydrogen subjected to a high hoop stress (110–140 MPa) at either 350°C or 400°C PCT. If the DBTT remained below 20°C, then it could be concluded that hydrogen contents <60 wppm would not cause radial hydride embrittlement. However, such a test would be of more scientific than engineering value because peak hoop stresses are expected to be <80 MPa for standard M5®-clad fuel rods irradiated to burnups less than the licensing limit (62 GWd/MTU).

None of the samples tested by Argonne contained hydrogen contents close to the solubility limit at the PCT. It is speculated that such samples subjected to RHT at high enough peak hoop stress would experience the growth of long radial hydrides with enough effective continuity in the axial direction to degrade cladding mechanical properties in response to hoop stress loading.

The ZIRLO™ samples tested by Argonne fell into two categories: samples with average hydrogen content in the range of 350–550 wppm and samples with >640 wppm. Measured DBTT values appeared to be insensitive to total hydrogen content within the 350–550 wppm range. However, for an average hydrogen content of 644 wppm (>960-wppm maximum local value), a reduction in ductility, along with increased data scatter, was observed. As the peak hydrogen content for both standard and IFBA ZIRLO™ fuel rods irradiated to less than the license limit is expected to be bounded by the 350–550 wppm range, no effect of peak hydrogen content on the DBTT is anticipated.

Although not included in the Argonne test program due to unavailability, Optimized ZIRLO™ with reduced tin content behaves better during normal reactor operation than standard ZIRLO™ (now ZIRLO®) due to the decrease in oxide layer growth and the corresponding decrease in hydrogen pickup. Future studies should include this alloy as peak hydrogen contents could be close to the solubility limit for drying and early storage temperatures. Also, the texture of this alloy is between the texture of RXA M5® and CWSRA ZIRLO™. Both of these factors would make Optimized ZIRLO™ more susceptible to radial-hydride precipitation.

Effects of Drying and Storage Hoop Stress on the DBTT

The sensitivities of HBU M5® and HBU ZIRLO™ to peak and precipitation-initiation hoop stresses were quite different. For M5® with 72–94 wppm hydrogen content, DBTT values were in the range of 70–80°C for peak hoop stresses of 89–142 MPa and precipitation-initiation hoop stresses of 74–113 MPa. These results do make sense if precipitation-initiation hoop stresses as low as 74 MPa are sufficient to precipitate essentially all the hydrogen in the radial direction. Metallographic examinations confirm that this was the case. For the sample with only 58-wppm hydrogen, the precipitation stress was 67 MPa and most of the hydrides precipitated in the radial direction (>80% by number density and much higher if the longer lengths of radial hydrides were included as a weighting factor).

The DBTT for HBU ZIRLO™ with 350–550 wppm hydrogen exhibited a very high sensitivity to hoop stress within the peak hoop stress range of 90±3 MPa and precipitation hoop stresses within the range of about 80±2 MPa. Within these stress ranges, the DBTT increased by about 100°C independent of the 350°C and 400°C PCTs. This peak stress range is above the upper bound stress estimated for standard ZIRLO™-clad rods, but it is lower than estimated peak stresses for IFBA rods. These ranges may not be as sharp as indicated by the data collected to date. Additional tests conducted at 350°C and peak hoop stresses of 90–100 MPa with samples containing 300–400 wppm hydrogen would be needed to better quantify this critical stress range. Such tests would be important for assessing the DBTT for IFBA fuel rods.

Relevant Ranges of Internal Pressures and Hoop Stresses

Members of the UFD Campaign have been working with the Electric Power Research Institute (EPRI), fuel vendors, cask vendors, and the international community to determine relevant ranges of end-of-life (EOL) PWR rod-internal pressures (RIPs), as well as PCTs and rod-averaged gas temperatures. EPRI documented results for publicly available PWR EOL RIPs at 25°C [17]. In addition, ORNL used the FRAPCON code to predict the gas pressures for over 68,000 fuel rods irradiated during Cycles 1–12 in the Watts Bar Nuclear Unit 1 (WBN1) reactor [18]. The data presented in Ref. 17, as well as the predictions documented in Ref. 18, were for Zry-4-clad and ZIRLO™-clad fuel rods. The data set did not include any M5®-clad fuel rods or ZIRLO™-clad IFBA fuel rods. Also, for burnups <60 GWd/MTU, most of the database rods were clad in Zry-4 and all of the rods were irradiated prior to the increases in rod power and burnup that occurred during the 1990s. As such, results from these older fuel-rod designs irradiated under less aggressive conditions are referred to as legacy results.

Figure 28 summarizes the measured and calculated results. For IFBA rods, results are presented separately for rods with hollow blanket pellets (HBP, increased void volume) and solid blanket pellets (SBP).

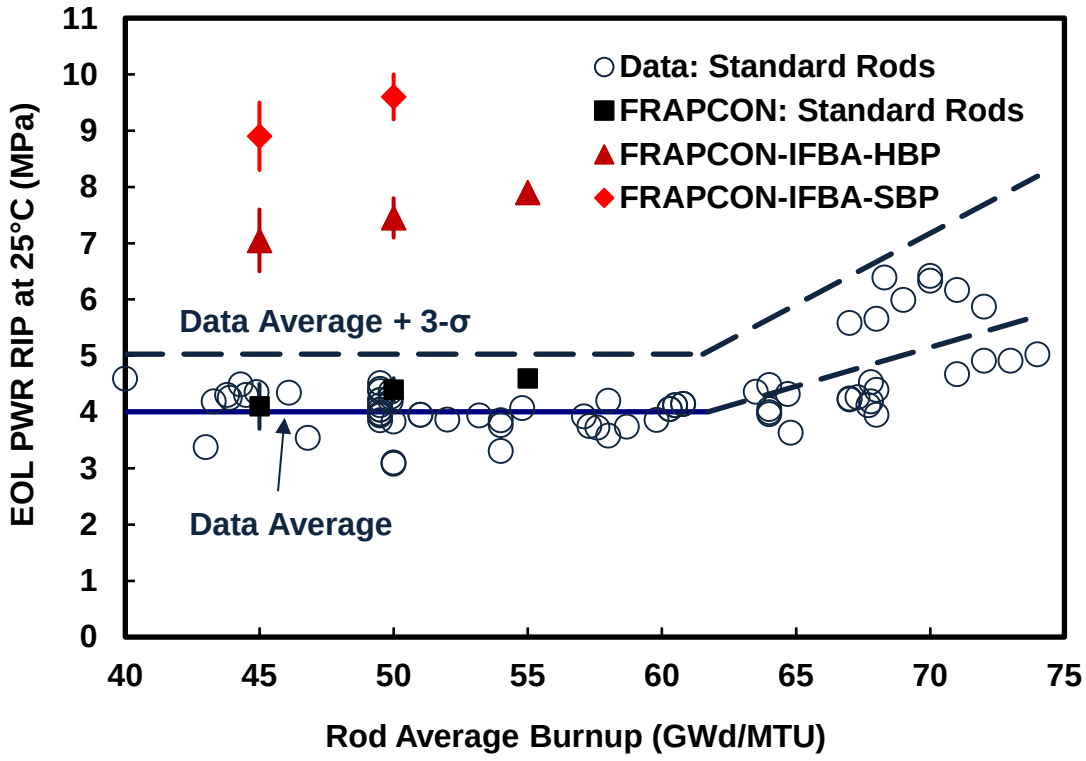

Figure 28: Data and FRAPCON predictions for end-of-life (EOL) PWR rod-internal pressures (RIPs) at 25°C as a function of burnup.

For burnups within the licensing limit, the average of the data is 4 MPa at 25°C and the 3-sigma upper bound is 5 MPa. This upper bound also bounds the FRAPCON-predicted results for standard PWR fuel

rods irradiated in WBN1, most of which were ZIRLO™-clad fuel rods. The data and predicted values for EOL RIP are remarkable "flat" within the burnup range of 40–62 GWd/MTU.

In order to calculate upper-bound gas pressures during drying and storage, the range of temperatures estimated at the top of the fuel column were used. It is expected that most of the gas is in the plenum region, which is at a lower average temperature than the top of the fuel column. For vacuum drying and for casks filled with atmospheric helium – both horizontal and vertical – the upper-bound temperatures used were 180–200°C. For vertical casks with pressurized helium, which induces natural circulation and higher temperatures at the top of the fuel column, an upper bound temperature of 340°C was assumed. Thus, calculations were performed for the temperature range of 180–340°C. These upper-bound gas pressures were used in Eq. 1 to calculate upper bound hoop stresses for standard and IFBA PWR rods. In determining the geometrical factor (R_{mi}/h_m), the inner radius of the cladding metal was assumed to be the same as the as-fabricated value (i.e., creep out was equal to creep down) and the thickness was reduced consistent with oxide layer thicknesses of 10 μm (for M5®), 40 μm (for ZIRLO™) and 80 μm (for Zry-4). The results of these calculations were: (a) <80 MPa peak hoop stress for standard PWR fuel rods during drying and storage and (b) <120 MPa for ZIRLO™-clad IFBA rods with hollow blanket pellets.

The PWR database will be greatly enhanced after ORNL measures the EOL RIP values for the 25 standard "sister" rods irradiated under more modern operating conditions in the reactors at the North Anna plant: four Zry-4-clad rods, nine M5®-clad rods, and 12 ZIRLO™-clad rods.

Recommended Additional Testing

Throughout Sections 4 and 5, recommendations have been made for additional tests that "should' be conducted and for tests that "could" be conducted. The "should" refers to tests with engineering value conducted within the relevant range of hydrogen contents and hoop stresses. The "could" refers to tests with scientific value outside the relevant ranges for hydrogen-content and/or stresses.

For standard PWR M5®-clad fuel rods, the peak hoop stress is expected to be <80 MPa and the peak hydrogen content is anticipated to be <120 wppm. A confirmatory test that should be conducted is one with 350°C PCT and 80 MPa hoop stress. The target hydrogen content for this sample is in the range of 100–120 wppm. If the first ring subjected to the RCT is ductile at RT, then the remaining rings should also be tested at RT to obtain statistical significance. An additional test could be conducted with a sample containing about 60-wppm hydrogen subjected to 350°C PCT and high peak hoop stress (110–140 MPa). If the sample proves to have moderate-to-high ductility at RT, these results would confirm the speculation that no cladding degradation occurs for hydrogen contents <60 wppm.

Similar to the recommended test with HBU M5® cladding, a test should be conducted with HBU ZIRLO™ with RHT conditions of 350°C and a peak hoop stress of 80 MPa. The hydrogen content should be in the range of 250–350 wppm. Such samples are available at Argonne. Assuming the first RCT ring is ductile at RT, the remaining rings should also be tested at RT. The results of this test would hopefully rule out radial-hydride-induced embrittlement for standard PWR fuel rods clad in ZIRLO™. Additional tests should be conducted at 350°C PCT and peak hoop stresses of 90–120 MPa to address the radial hydride issue for IFBA PWR rods clad in ZIRLO™. The hydrogen contents should also be in the range of 250–350 wppm.

REFERENCES

[1] Geelhood, K.J., W.G. Lusher, and C.E. Beyer, *PNNL Stress/Strain Correlation for Zircaloy*, Pacific Northwest National Laboratory Report PNNL-17700, July 2008.

[2] Nuclear Regulatory Commission, Interim Staff Guidance (ISG)-11, Revision 3, "Cladding Considerations for the Transportation and Storage of Spent Fuel," November 2003. ML033230335 at http://www.nrc.gov/reading-rm/adams.html

[3] Billone, M.C., T.A. Burtseva, and Y. Yan, *Ductile-to-Brittle Transition Temperature for High-Burnup Zircaloy-4 and ZIRLO™ Cladding Alloys Exposed to Simulated Drying-Storage Conditions*, Argonne National Laboratory Report ANL-13/13, NRC ADAMS ML12181A238, Sept. 2012.

[4] Billone, M.C., T.A. Burtseva, and R.E. Einziger, "Ductile-to-Brittle Transition Temperature for High-Burnup Cladding Alloys Exposed to Simulated Drying-Storage Conditions," J. Nucl. Mater. **433**, 431–448 (2013).

[5] Billone, M.C., T.A. Burtseva, J.P. Dobrzynski, D.P. McGann, K. Byrne, Z. Han, and Y.Y. Liu, *Phase I Ring Compression Testing of High-Burnup Cladding*, FCRD-USED-2012-000039, Dec. 31, 2011.

[6] Billone, M.C., T.A. Burtseva, and Y.Y. Liu, *Baseline Studies for Ring Compression Testing of High-Burnup Fuel Cladding*, Argonne National Laboratory Report ANL-12/58, FCRD-USED-2013-000040, Nov. 23, 2012.

[7] Billone, M.C., T.A. Burtseva, and Y.Y. Liu, "Effects of Drying and Storage on High-Burnup Cladding Ductility," Proc. IHLRWMC, Albuquerque, NM, April 28–May 2, 2013, Paper 6973, 1106–1113 (2013).

[8] Billone, M.C., T.A. Burtseva, and Y.Y. Liu, "Baseline Properties and DBTT of High-Burnup PWR Cladding Alloys," Proc. PATRAM 2013, San Francisco, CA, August 18–23, 2013.

[9] Billone, M.C., T.A. Burtseva, Z. Han, and Y.Y. Liu, *Embrittlement and DBTT of High-Burnup PWR Fuel Cladding Alloys*, Argonne National Laboratory Report ANL-13/16, FCRD-UFD-2013-000401, Sept. 30, 2013.

[10] Billone, M.C., T.A. Burtseva, Z. Han, and Y.Y. Liu, *Effects of Multiple Drying Cycles on High-Burnup PWR Cladding Alloys*, Argonne National Laboratory Report ANL-14/11, FCRD-UFD-2014-000052, Sept. 26, 2014.

[11] Billone, M.C., T.A. Burtseva, and M.A. Martin-Rengel, *Effects of Lower Drying-Storage Temperatures on the DBTT of High-Burnup PWR Cladding*, Argonne National Laboratory Report ANL-15/21, FCRD-UFD-2015-000008, Aug. 28, 2015.

[12] Aomi, M., T. Baba, T. Miyashita, K. Kaminura, T. Yasuda, Y. Shinohara, and T. Takeda, "Evaluation of Hydride Reorientation and Mechanical Properties for High-Burnup Fuel-Cladding Tubes in Interim Dry Storage," J. ASTM Intl., JAI101262 (2008). www.astm.org

[13] Cuta, J.M., S.R. Suffield, J.A. Fort, and H.E. Adkins, *Thermal Performance Sensitivity Studies in Support of Material Modeling for Extended Storage of Used Nuclear Fuel*, Pacific Northwest National Laboratory Report PNNL-22646, FCRD-UFD-2013-000257, Sept. 27, 2013.

[14] Kearns, J.J., "Terminal Solubility and Partitioning of Hydrogen in the Alpha Phase of Zirconium, Zircaloy-2 and Zircaloy-4," J. Nucl. Mater. **22**, 292–303, 1967.

[15] Kammenzind, B.F., D.G. Franklin, H.R. Peters, and W.J. Duffin, "Hydrogen Pickup and Redistribution in Alpha-Annealed Zircaloy-4," *Zirconium in the Nuclear Industry: 11th Intl. Symp.*, ASTM STP 1295, E.R. Bradley and G.P. Sabol, Eds., ASTM, pp. 338–370, 1996.

[16] McMinn, A., E.C. Darby, and J.S. Schofield, "The Terminal Solid Solubility of Hydrogen in Zirconium Alloys, *Zirconium in the Nuclear Industry: 12th Intl. Symp.*, ASTM STP 1354, G.P. Sabol and G.D. Moan, Eds., ASTM, pp. 173–195, 2000.

[17] Machiels, A., *End-of-Life Rod Internal Pressures in Spent Pressurized Water Reactor Fuel*, EPRI Report 3002001949, Dec. 2013.

[18] Bratton, R.N., M.A. Jessee, and W.A. Wieselquist, *Rod Internal Pressure Quantification and Distribution Analysis Using FRAPCON*, DOE Report FCRD-UFD-2015-000636, ORNL Report ORNL/TM-2015/557, Sept. 30, 2015.

APPENDIX A METALLOGRAPHIC IMAGES OF ZIRLO™ CROSS SECTION 646D6 FROM 350°C/87-MPA RODLET 646D

Page intentionally blank

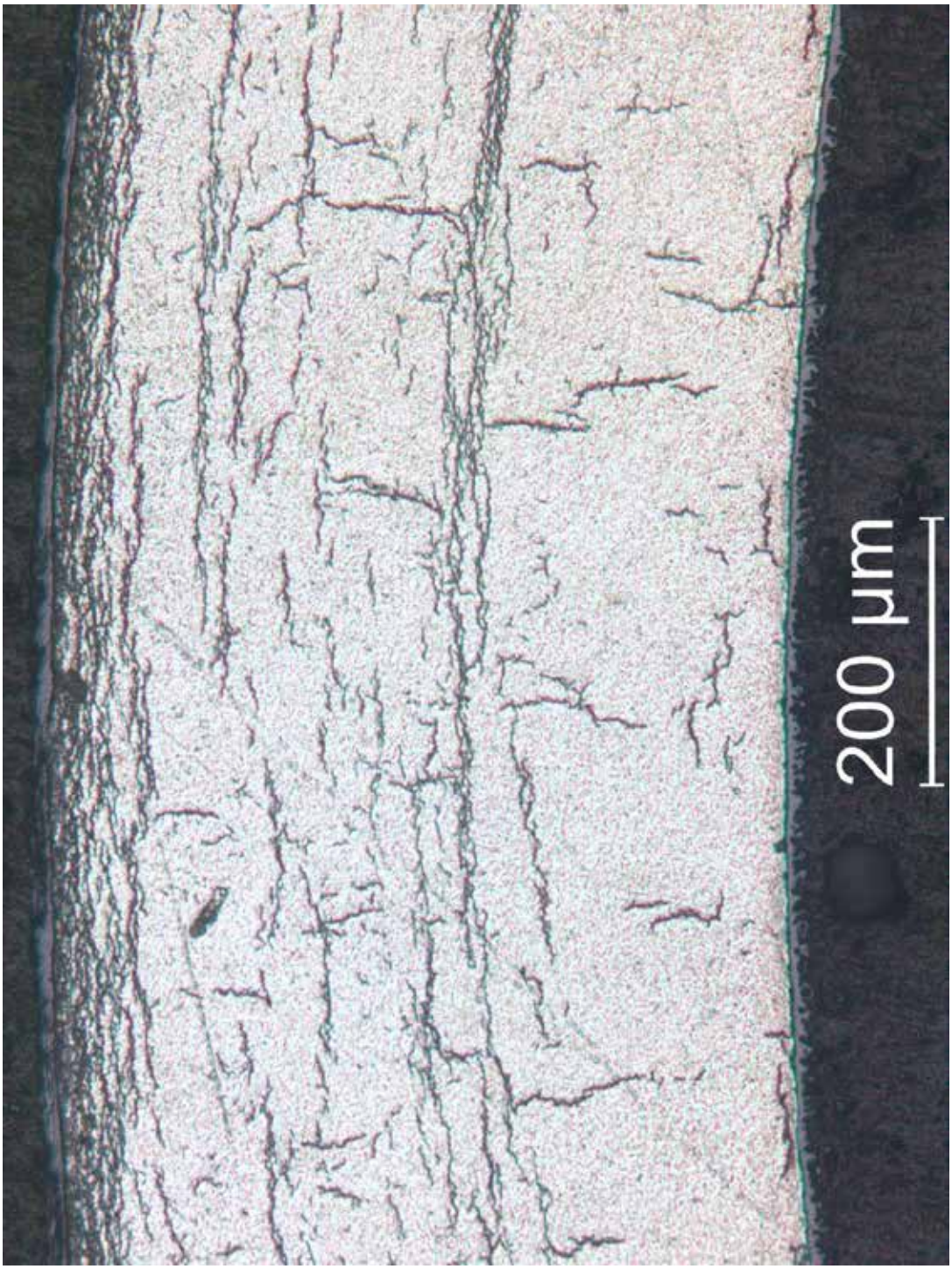

Figure A.1: Image (100X) of ZIRLO™ sample 646D6 in Area 1 (12:00 o'clock orientation) from 1-cycle 350°C/87-MPa rodlet 646D.

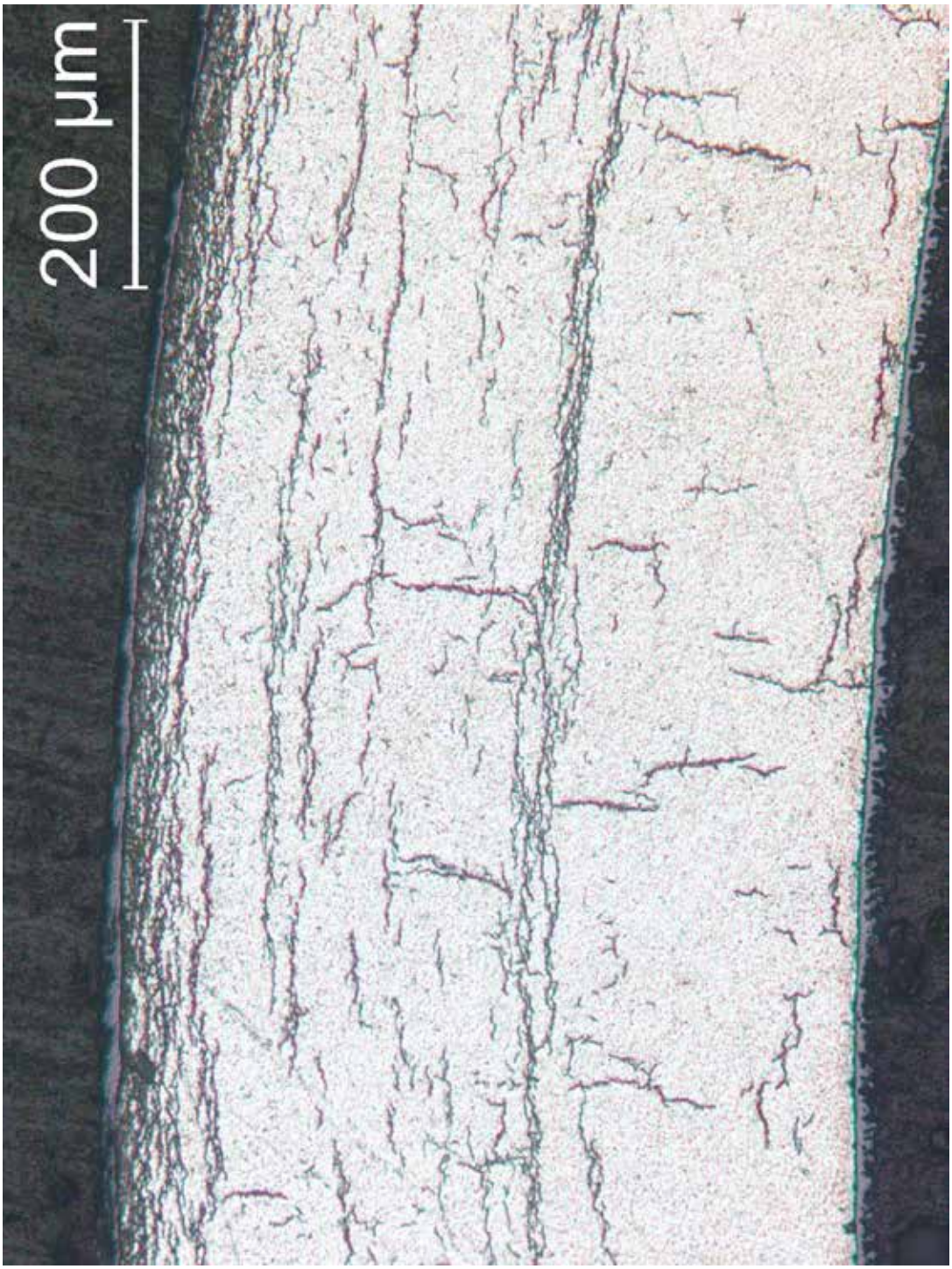

Figure A.2: Image (100X) of ZIRLO™ sample 646D6 in Area 2 from 1-cycle 350°C/87-MPa rodlet 646D.

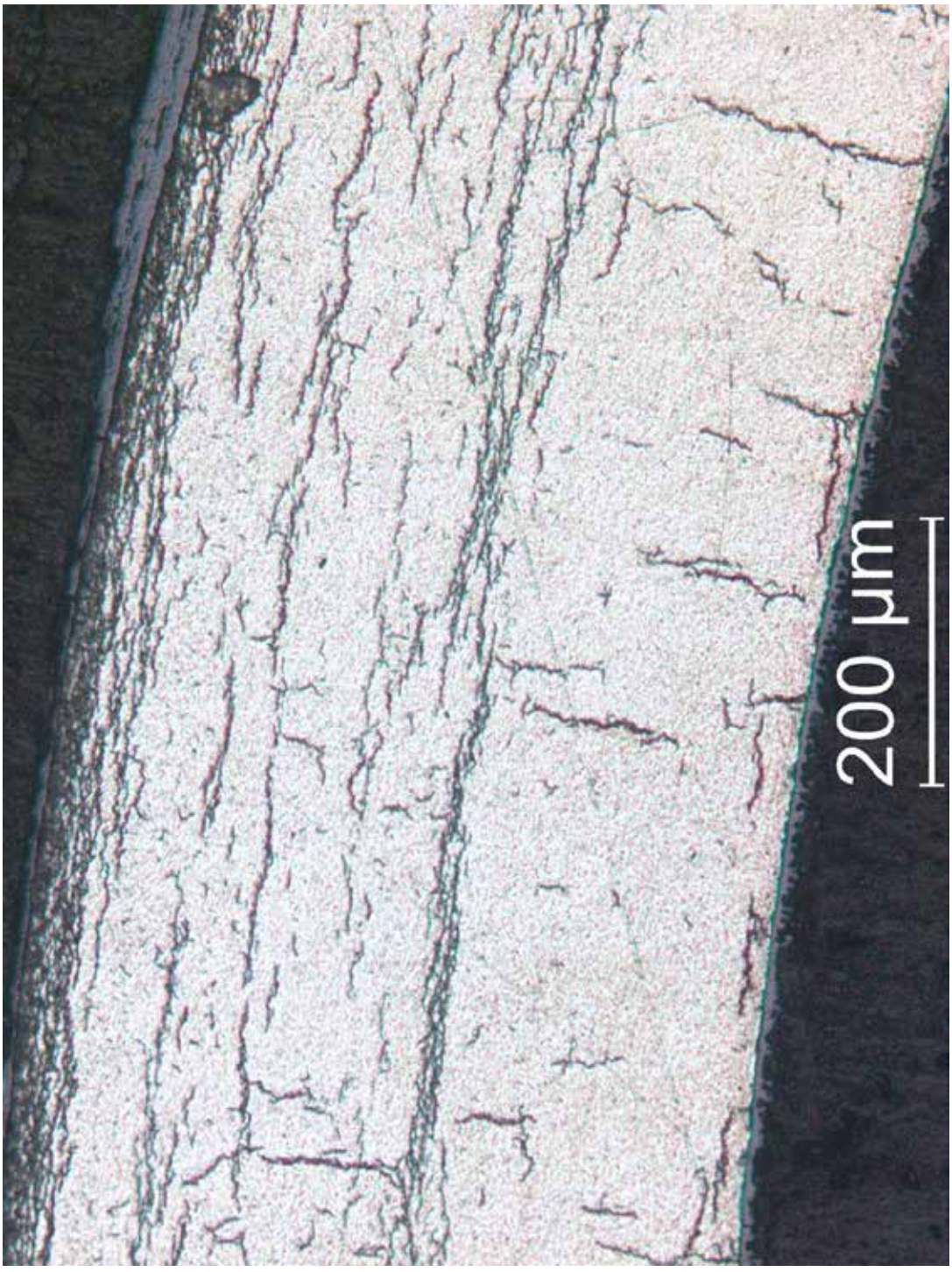

Figure A.3: Image (100X) of ZIRLO™ sample 646D6 in Area 3 from 1-cycle 350°C/87-MPa rodlet 646D.

Figure A.4: Image (100X) of ZIRLO™ sample 646D6 in Area 4 from 1-cycle 350°C/87-MPa rodlet 646D.

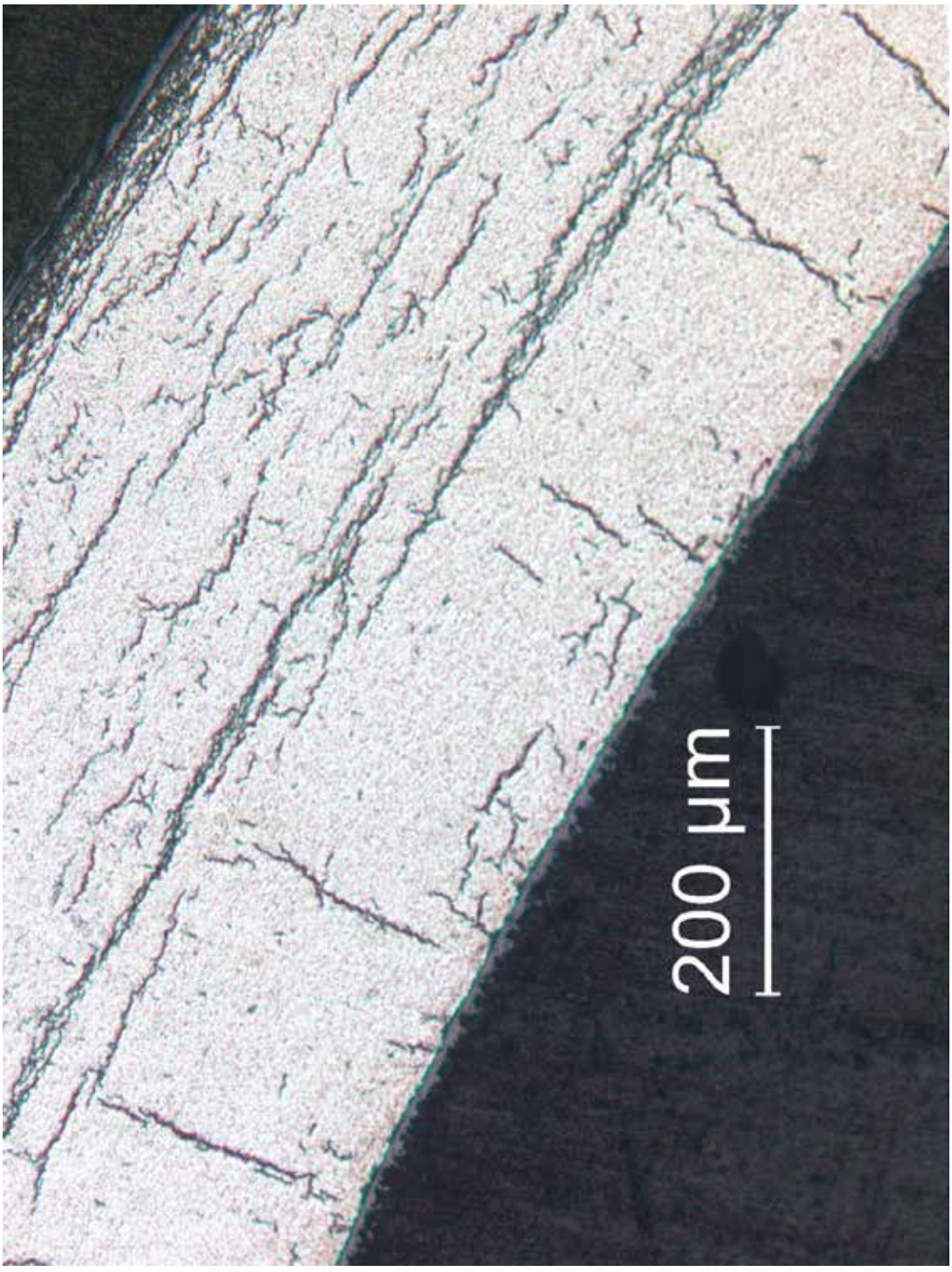

Figure A.5: Image (100X) of ZIRLO™ sample 646D6 in Area 5 from 1-cycle 350°C/87-MPa rodlet 646D.

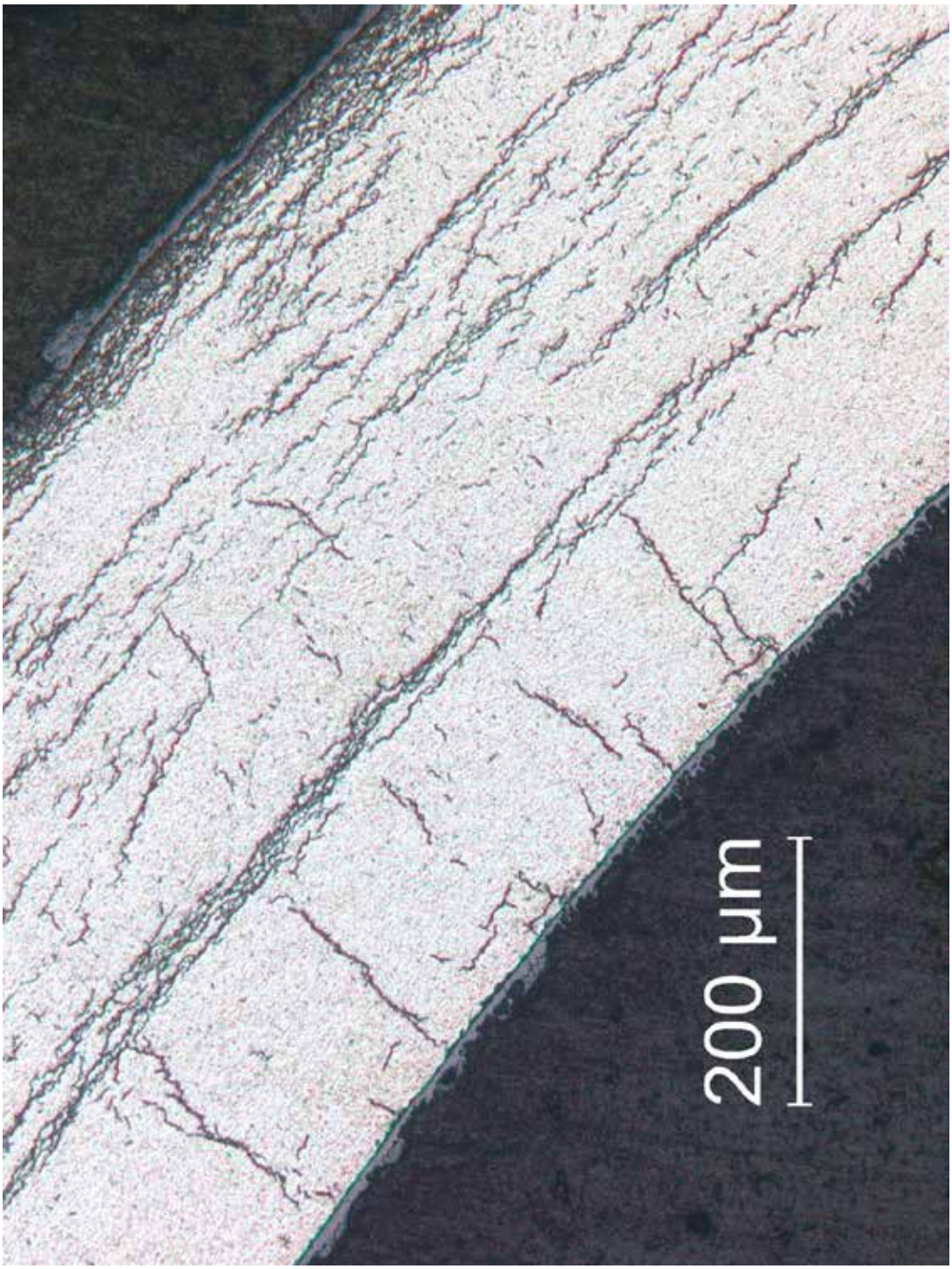

Figure A.6: Image (100X) of ZIRLO™ sample 646D6 in Area 6 from 1-cycle 350°C/87-MPa rodlet 646D.

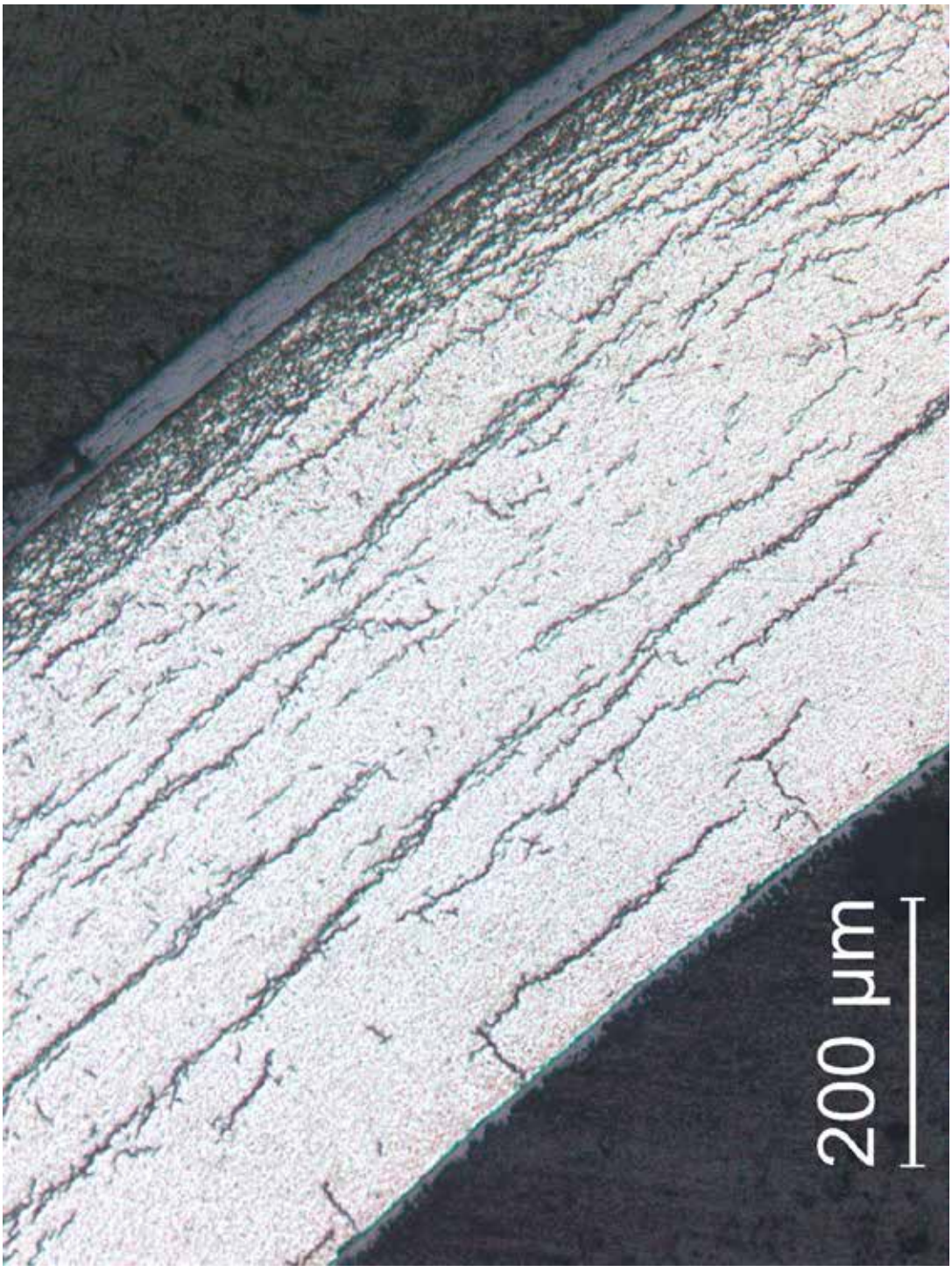

Figure A.7: Image (100X) of ZIRLO™ sample 646D6 in Area 7 from 1-cycle 350°C/87-MPa rodlet 646D.

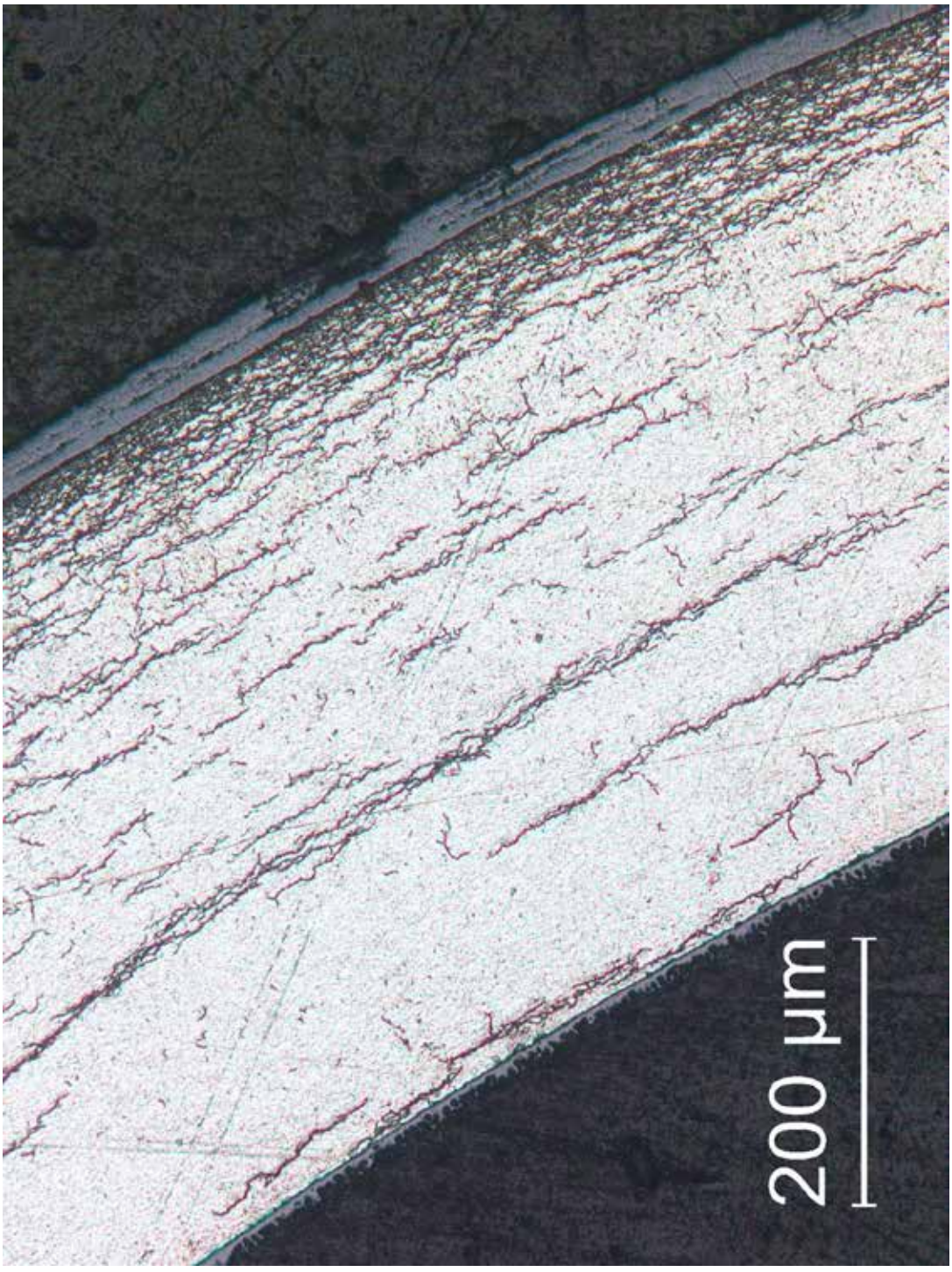

Figure A.8: Image (100X) of ZIRLO™ sample 646D6 in Area 8 from 1-cycle 350°C/87-MPa rodlet 646D.

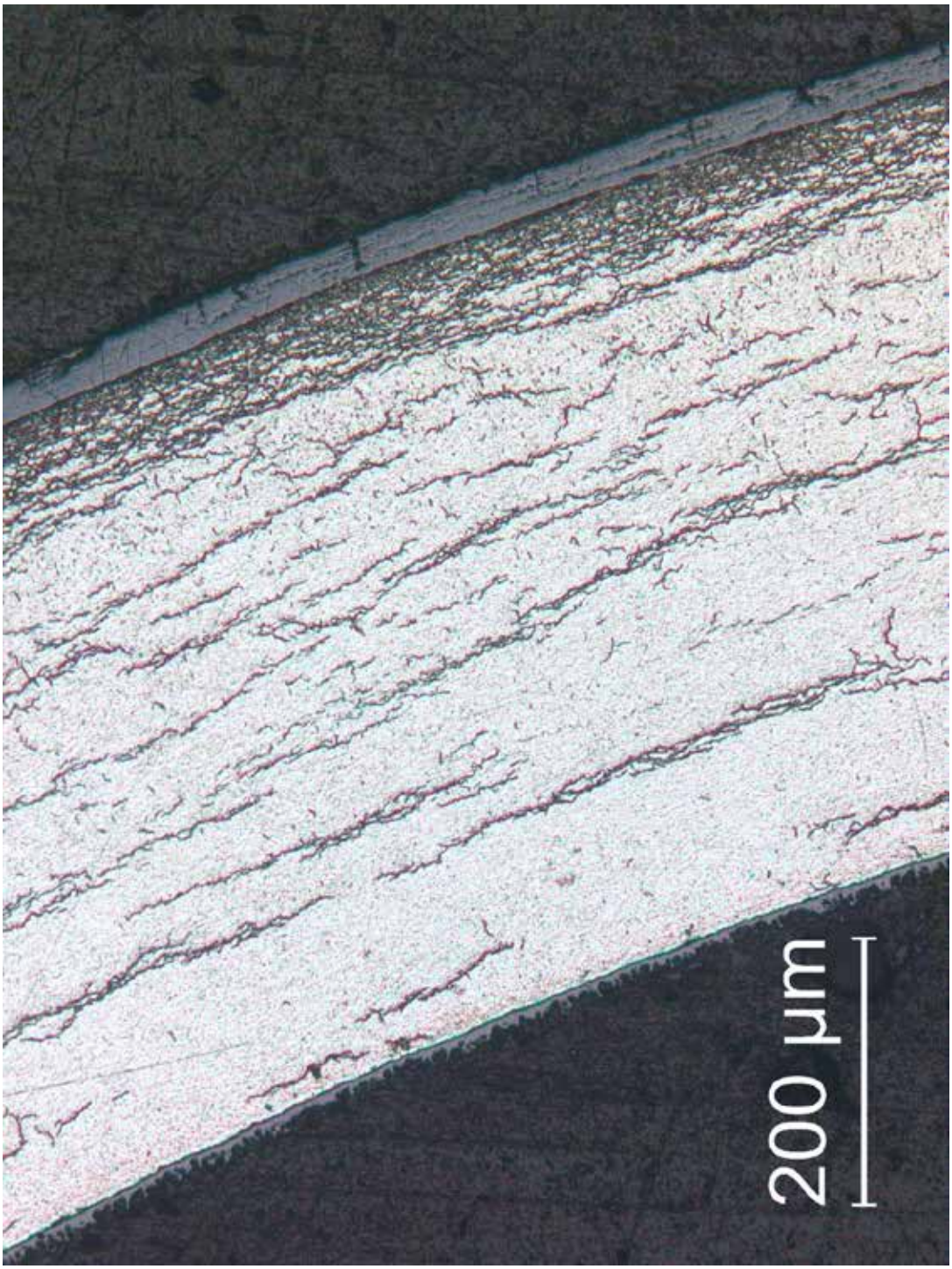

Figure A.9: Image (100X) of ZIRLO™ sample 646D6 in Area 9 from 1-cycle 350°C/87-MPa rodlet 646D.

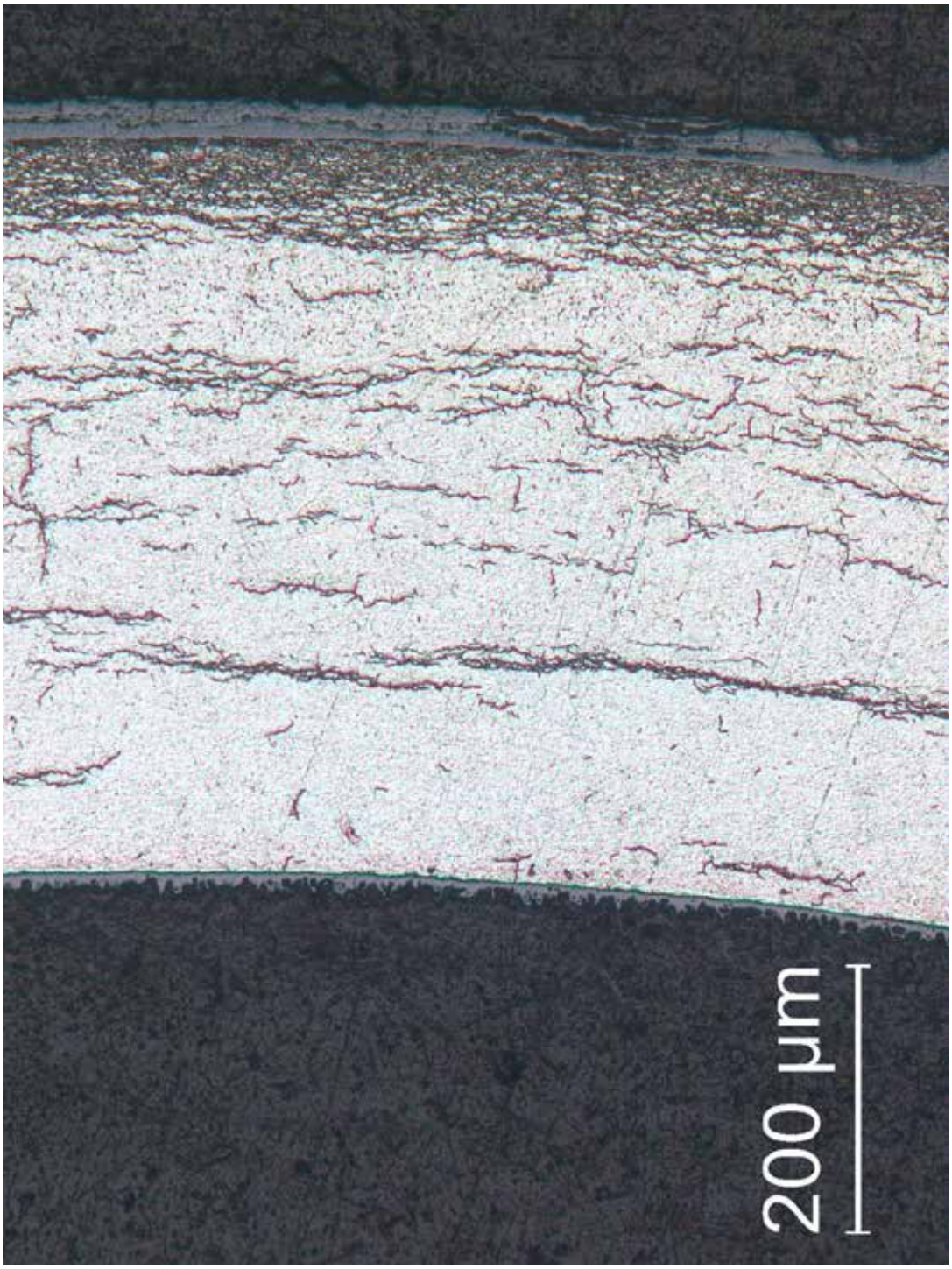

Figure A.10: Image (100X) of ZIRLO™ sample 646D6 in Area 10 from 1-cycle 350°C/87-MPa rodlet 646D.

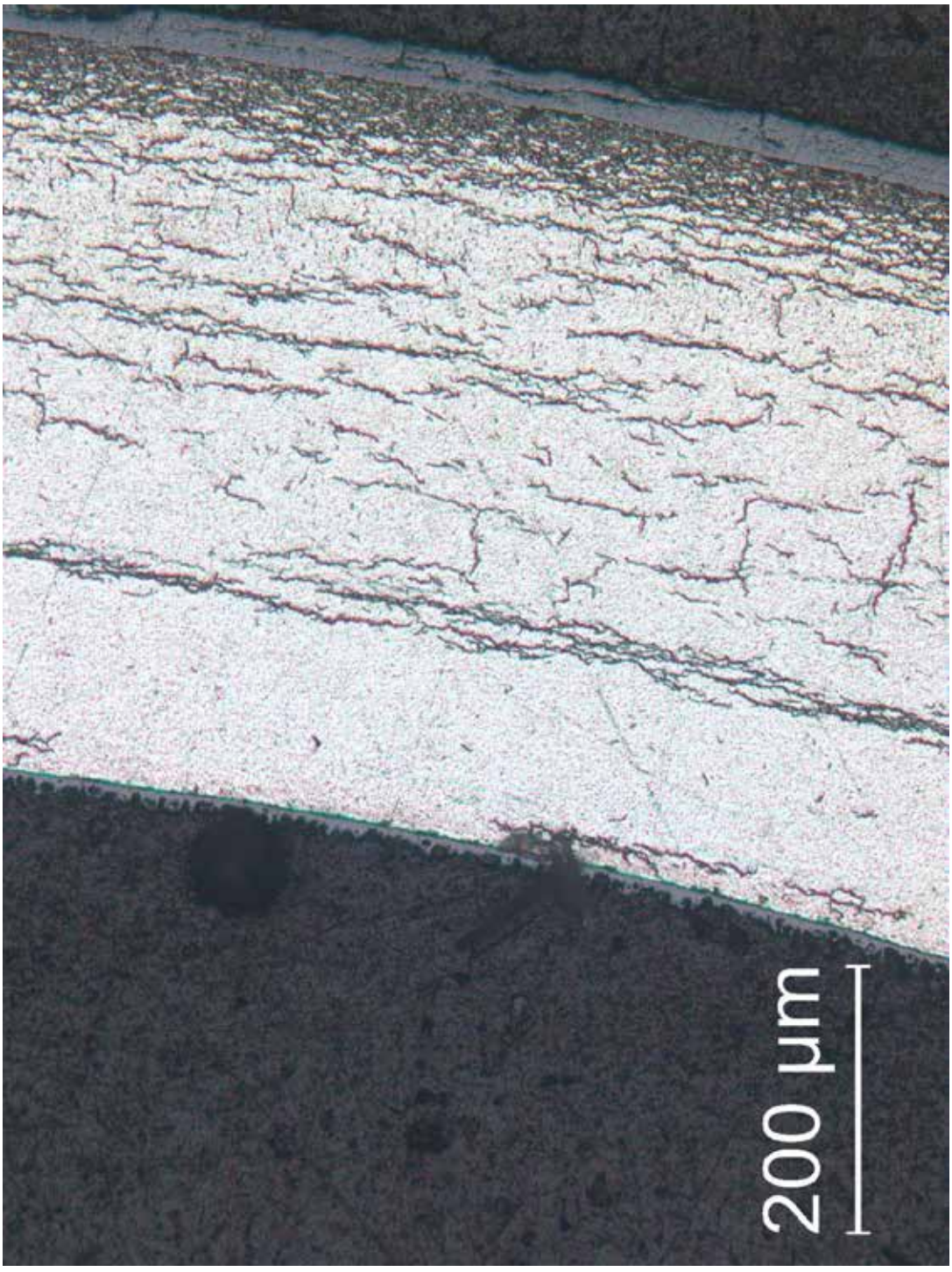

Figure A.11: Image (100X) of ZIRLO™ sample 646D6 in Area 11 from 1-cycle 350°C/87-MPa rodlet 646D.

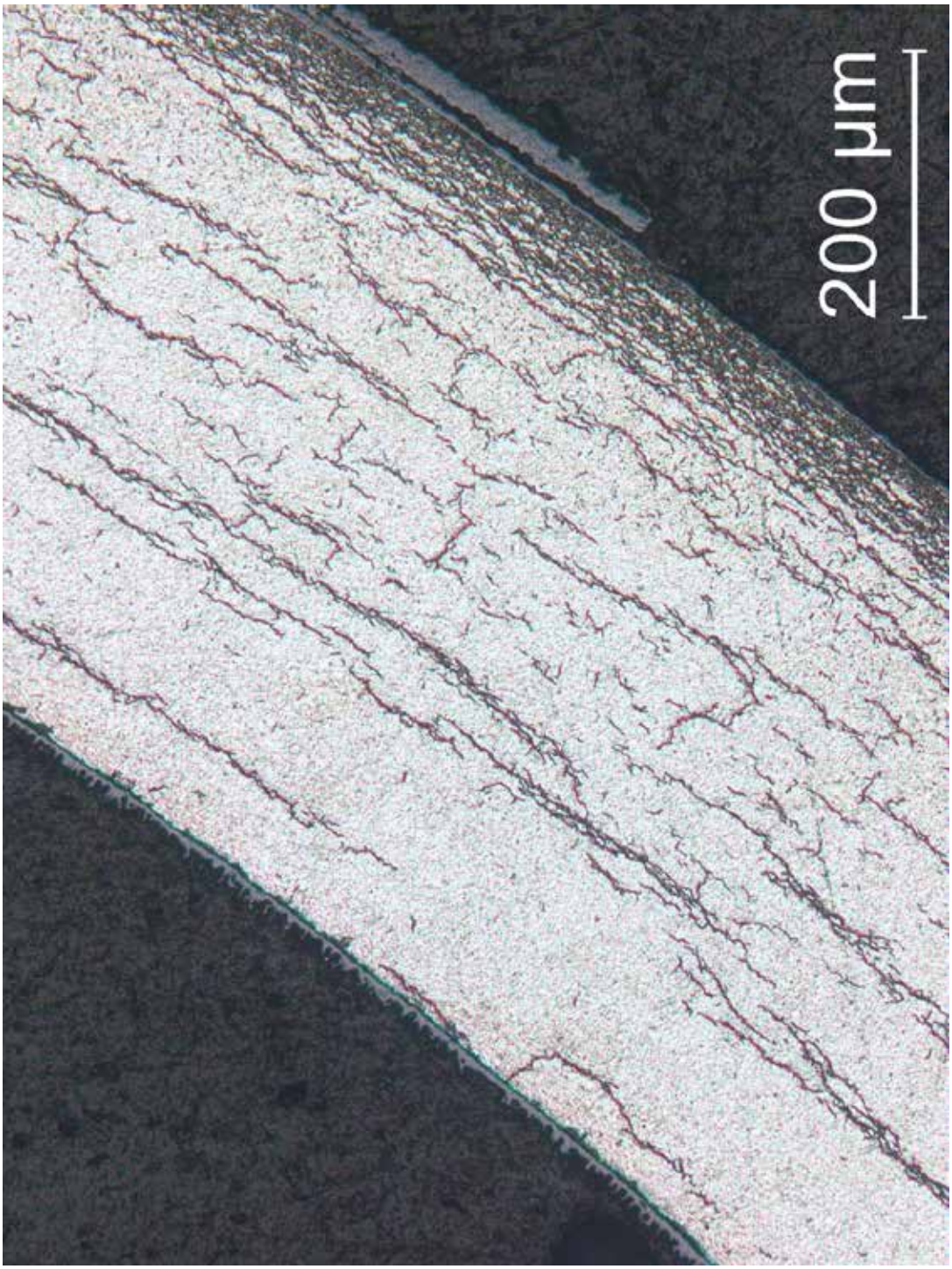

Figure A.12: Image (100X) of ZIRLO™ sample 646D6 in Area 12 from 1-cycle 350°C/87-MPa rodlet 646D.

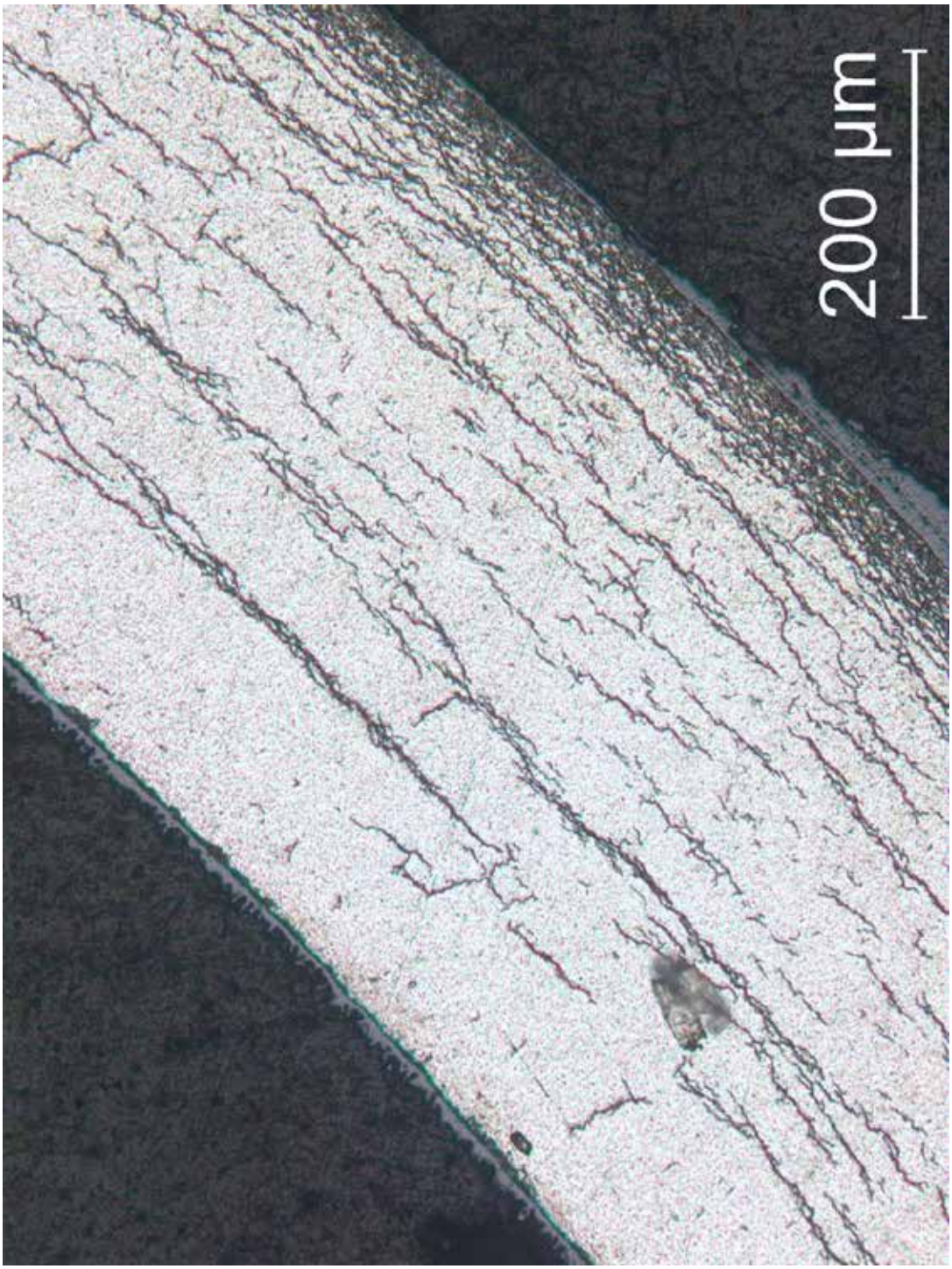

Figure A.13: Image (100X) of ZIRLO™ sample 646D6 in Area 13 from 1-cycle 350°C/87-MPa rodlet 646D.

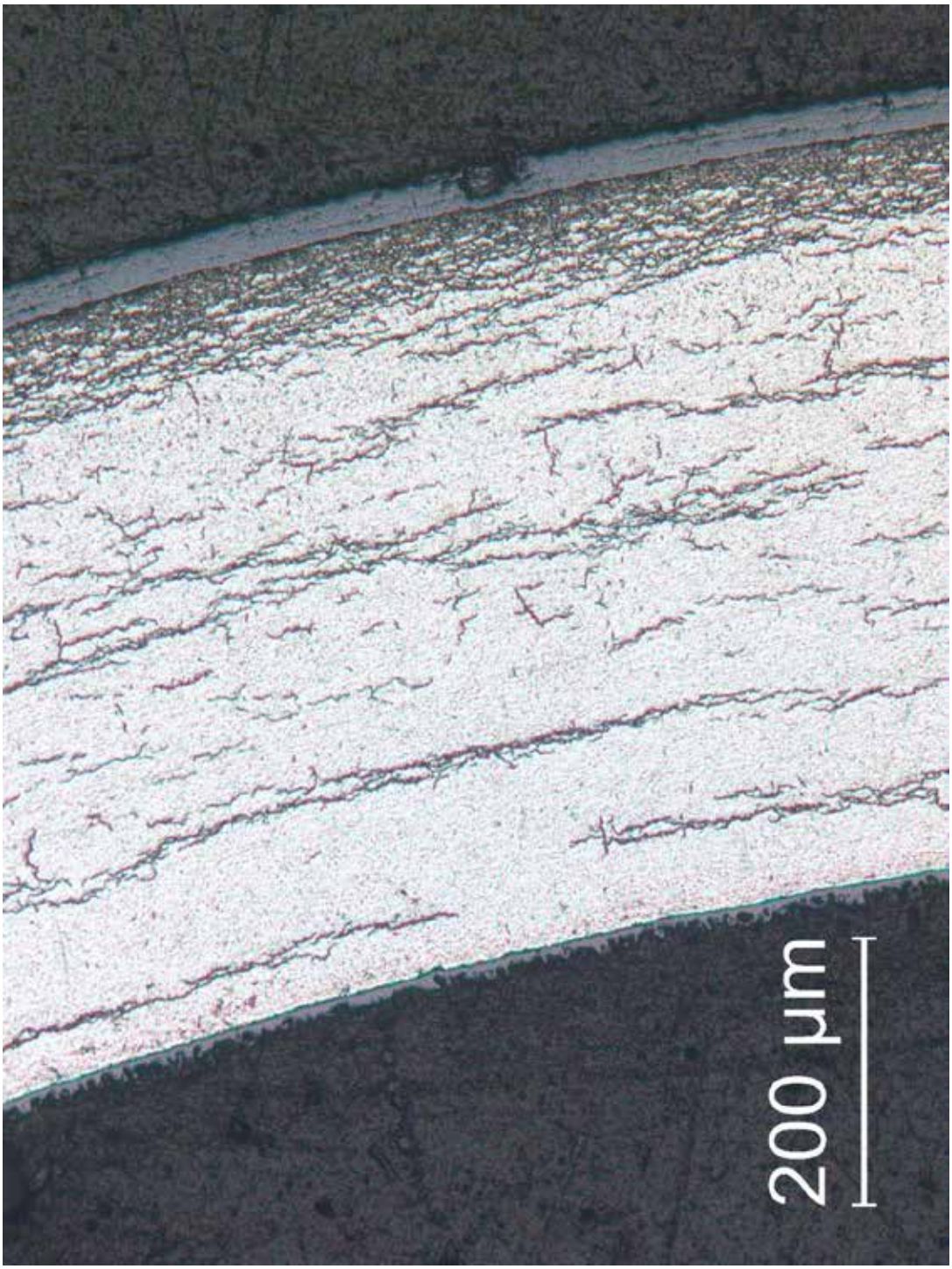

Figure A.14: Image (100X) of ZIRLO™ sample 646D6 in Area 14 from 1-cycle 350°C/87-MPa rodlet 646D..

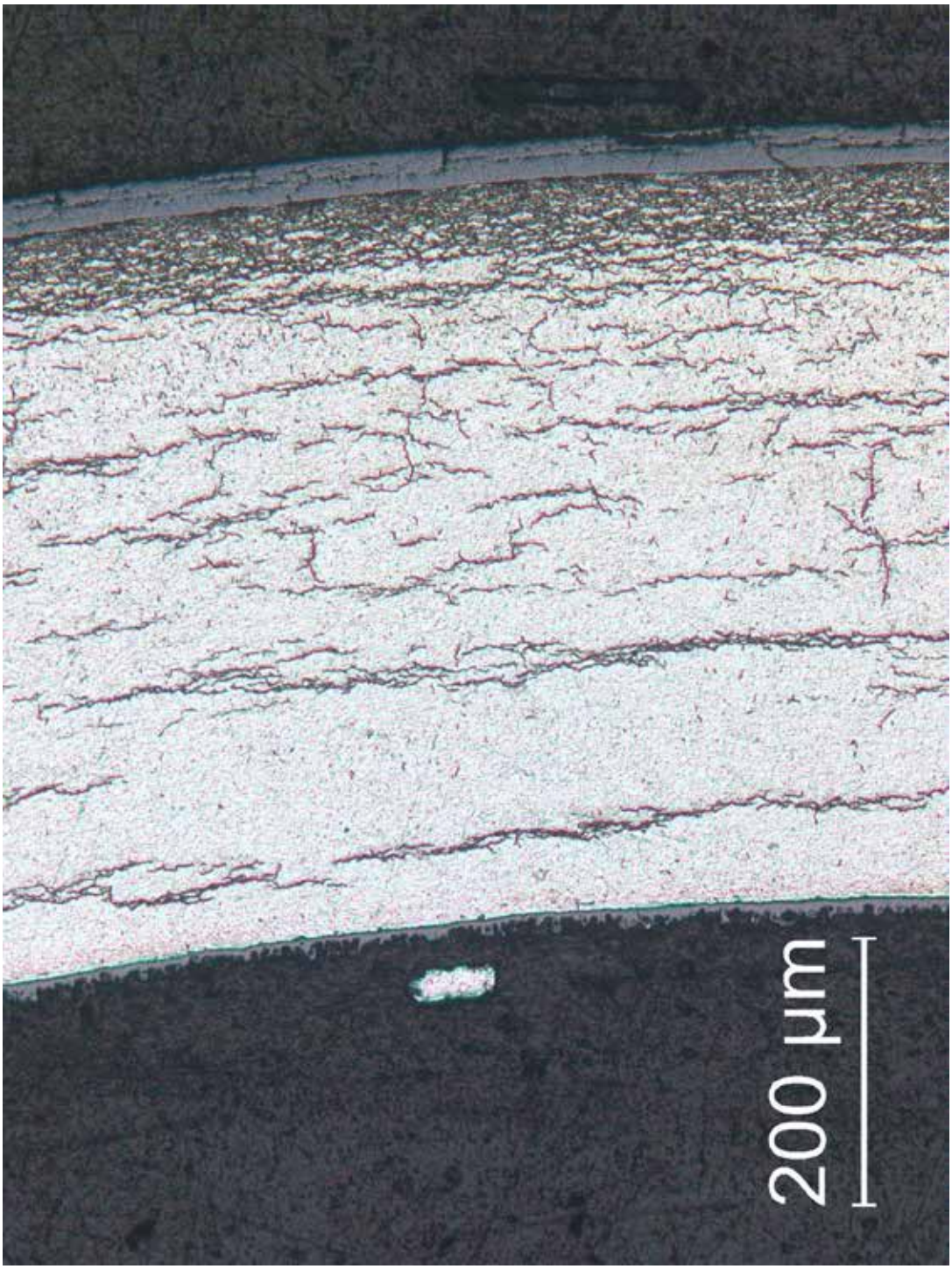

Figure A.15: Image (100X) of ZIRLO™ sample 646D6 in Area 15 from 1-cycle 350°C/87-MPa rodlet 646D..

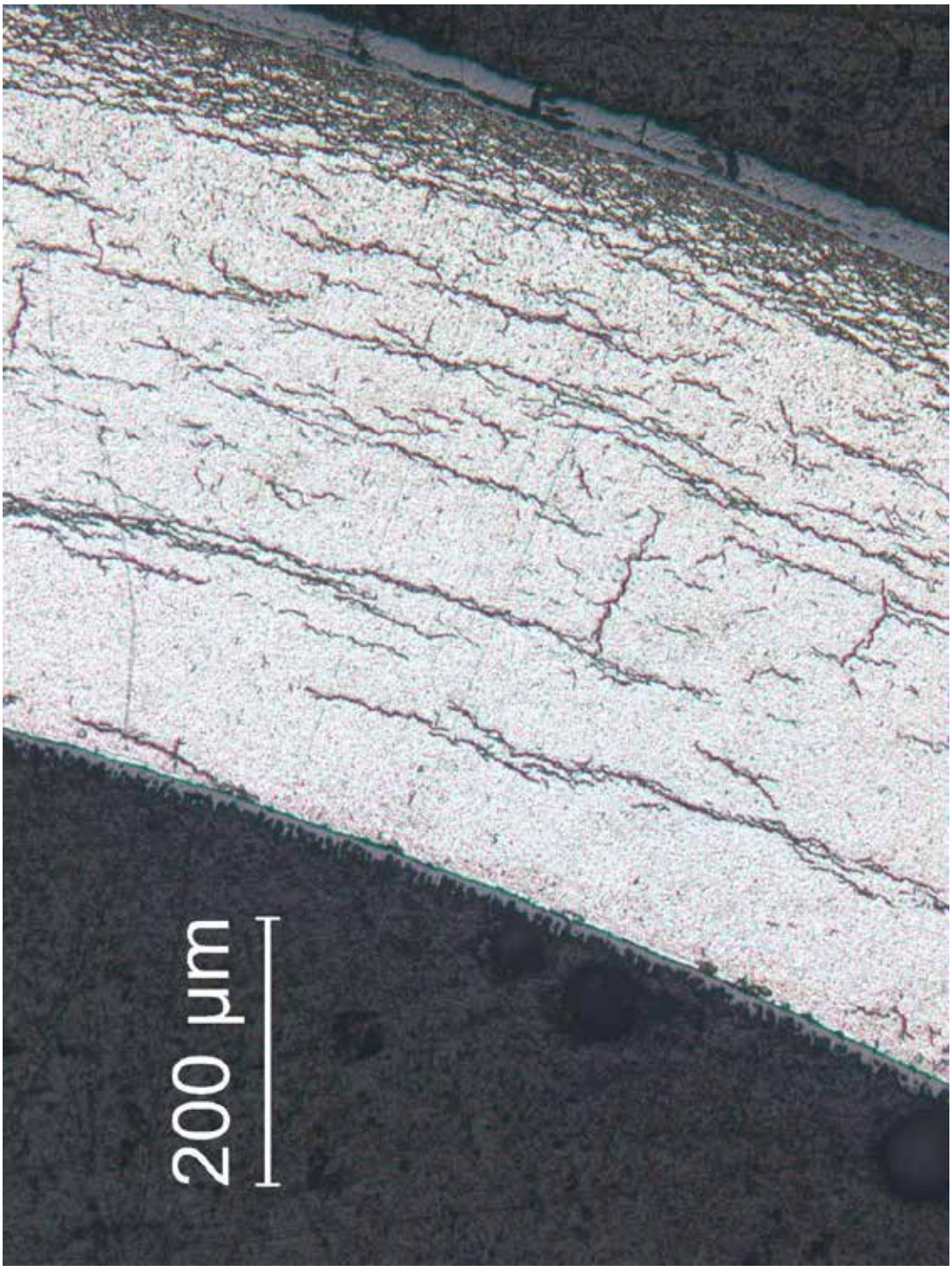

Figure A.16: Image (100X) of ZIRLO™ sample 646D6 in Area 16 from 1-cycle 350°C/87-MPa rodlet 646D.

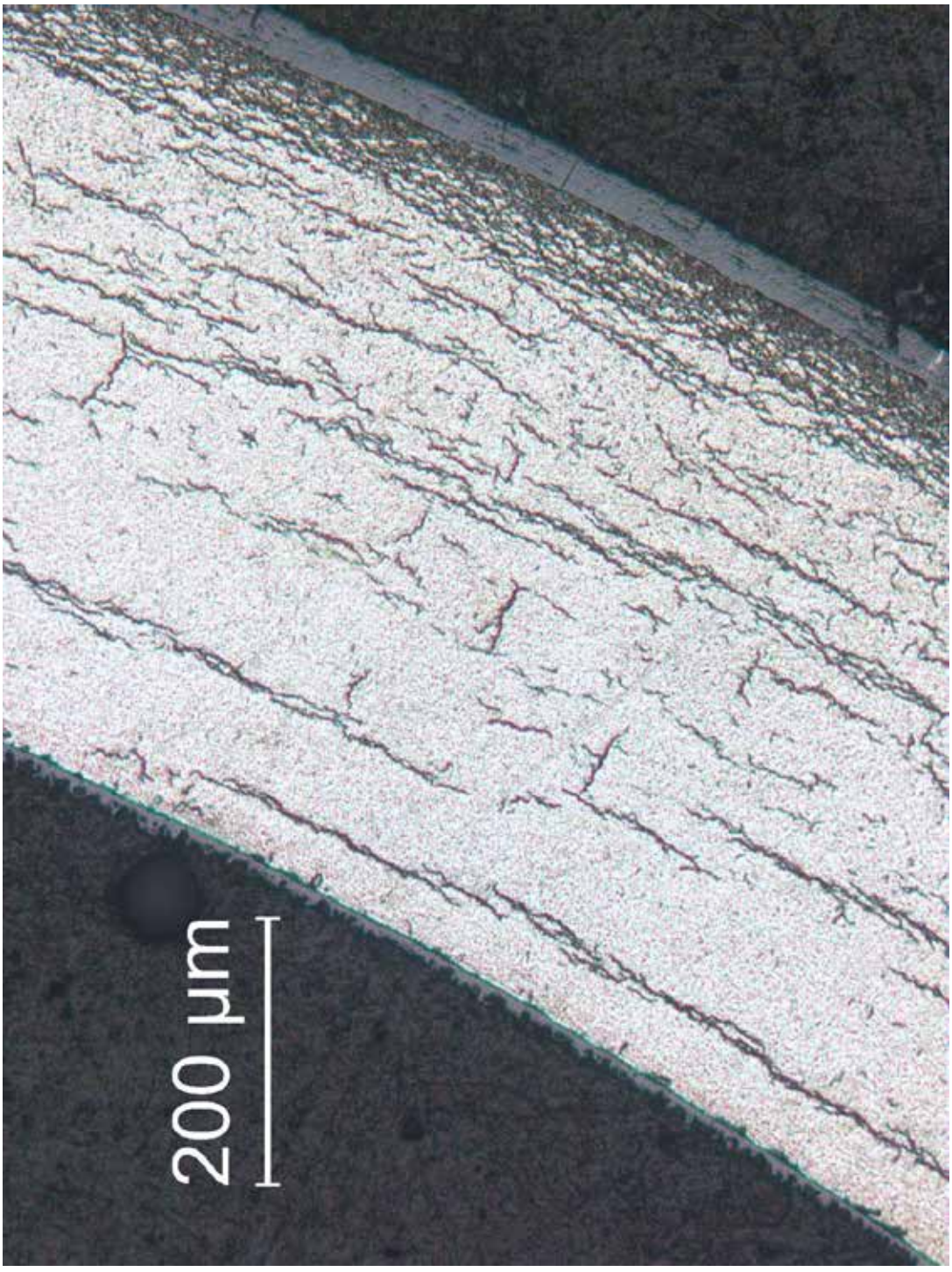

Figure A.17: Image (100X) of ZIRLO™ sample 646D6 in Area 17 from 1-cycle 350°C/87-MPa rodlet 646D.

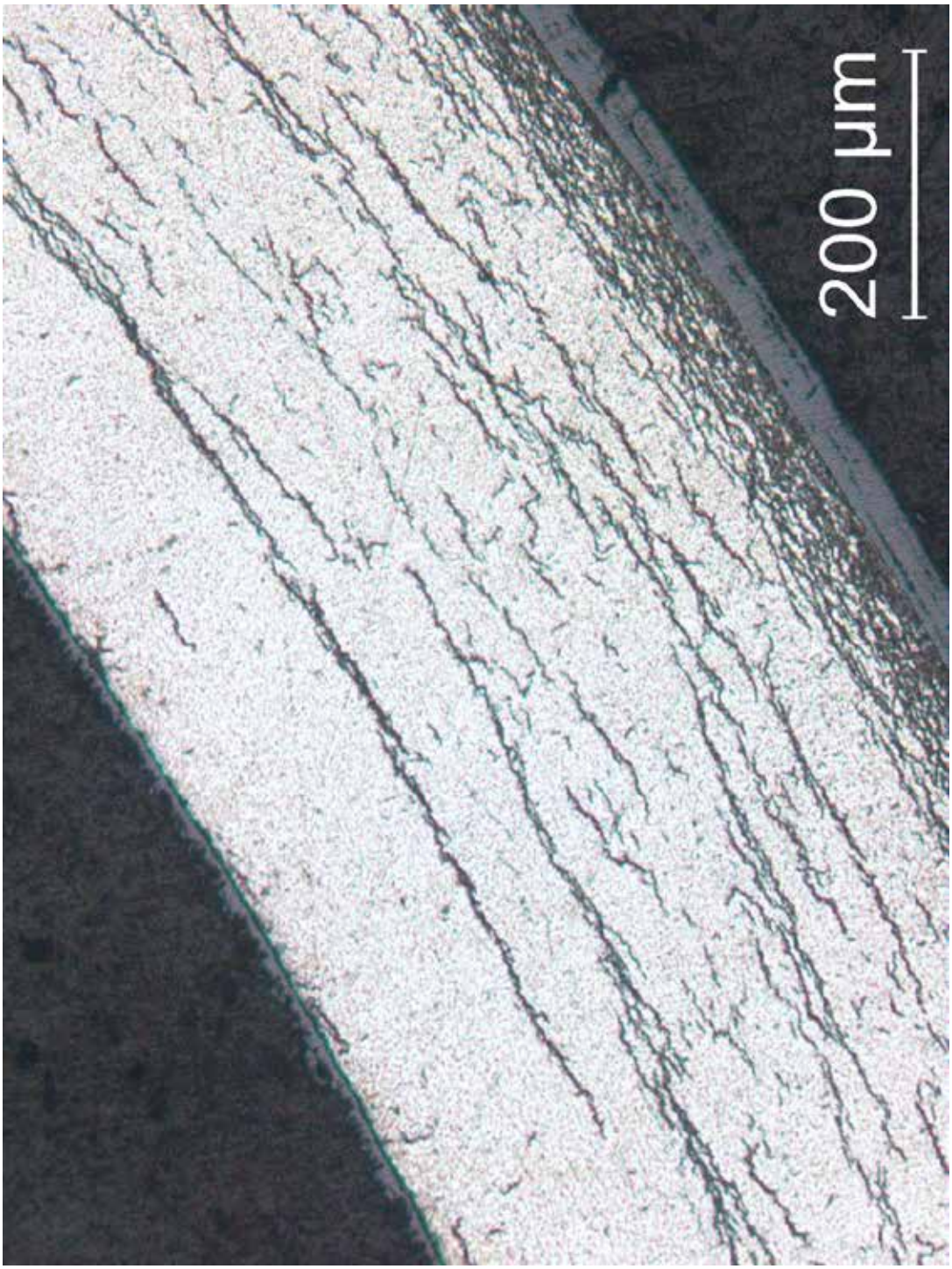

Figure A.18: Image (100X) of ZIRLO™ sample 646D6 in Area 18 from 1-cycle 350°C/87-MPa rodlet 646D.

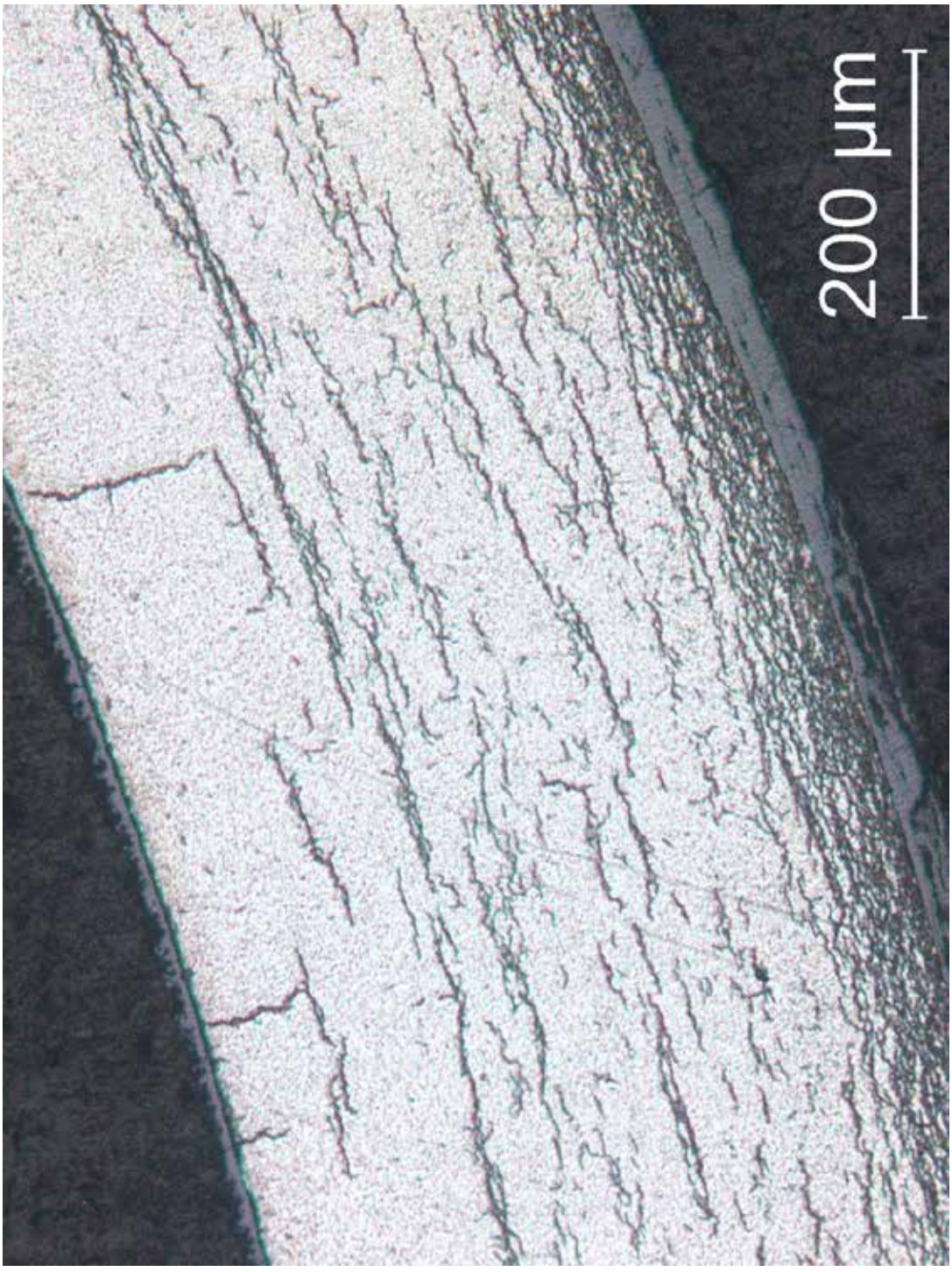

Figure A.19: Image (100X) of ZIRLO™ sample 646D6 in Area 19 from 1-cycle 350°C/87-MPa rodlet 646D.

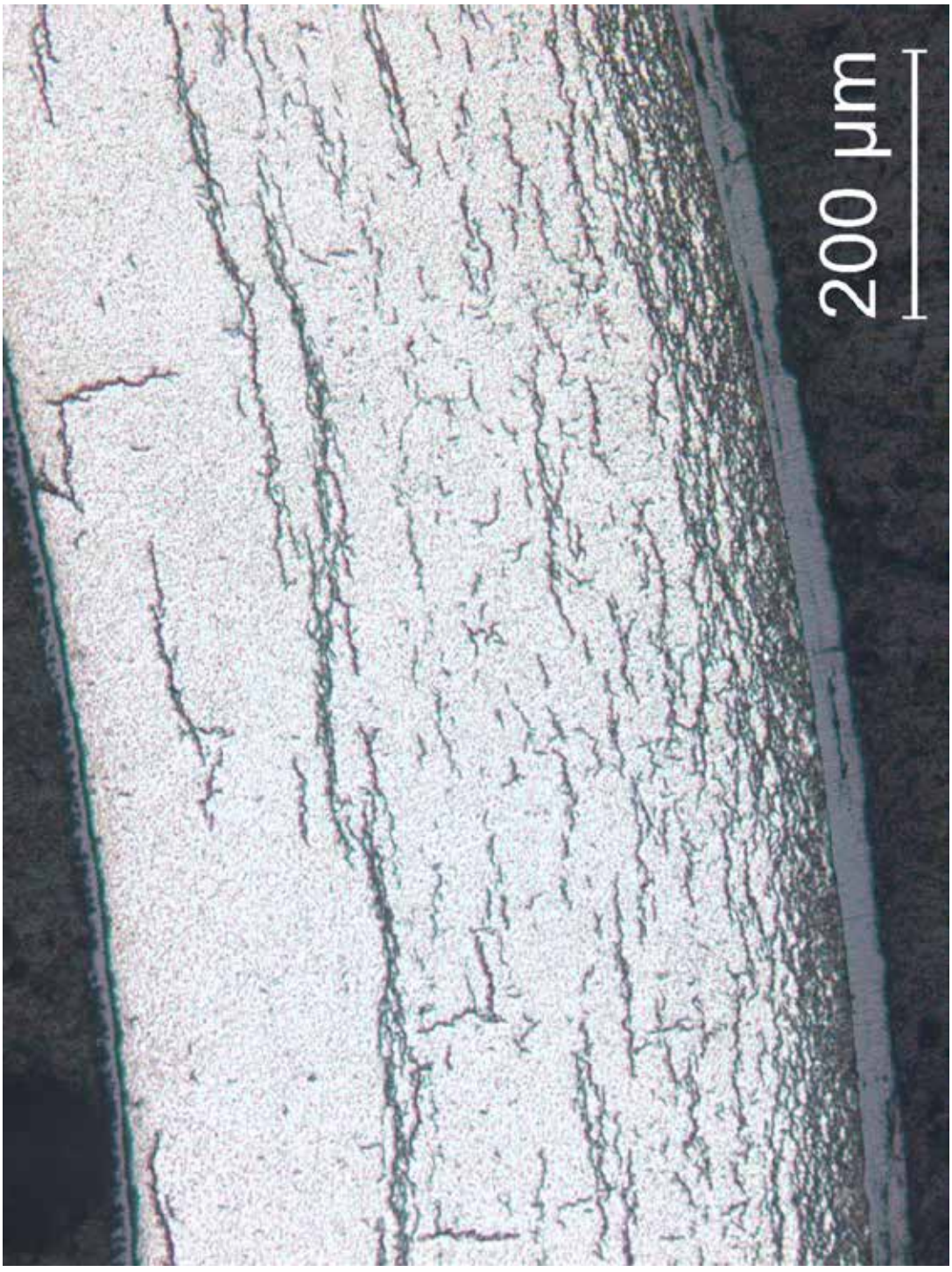

Figure A.20: Image (100X) of ZIRLO™ sample 646D6 in Area 20 from 1-cycle 350°C/87-MPa rodlet 646D.

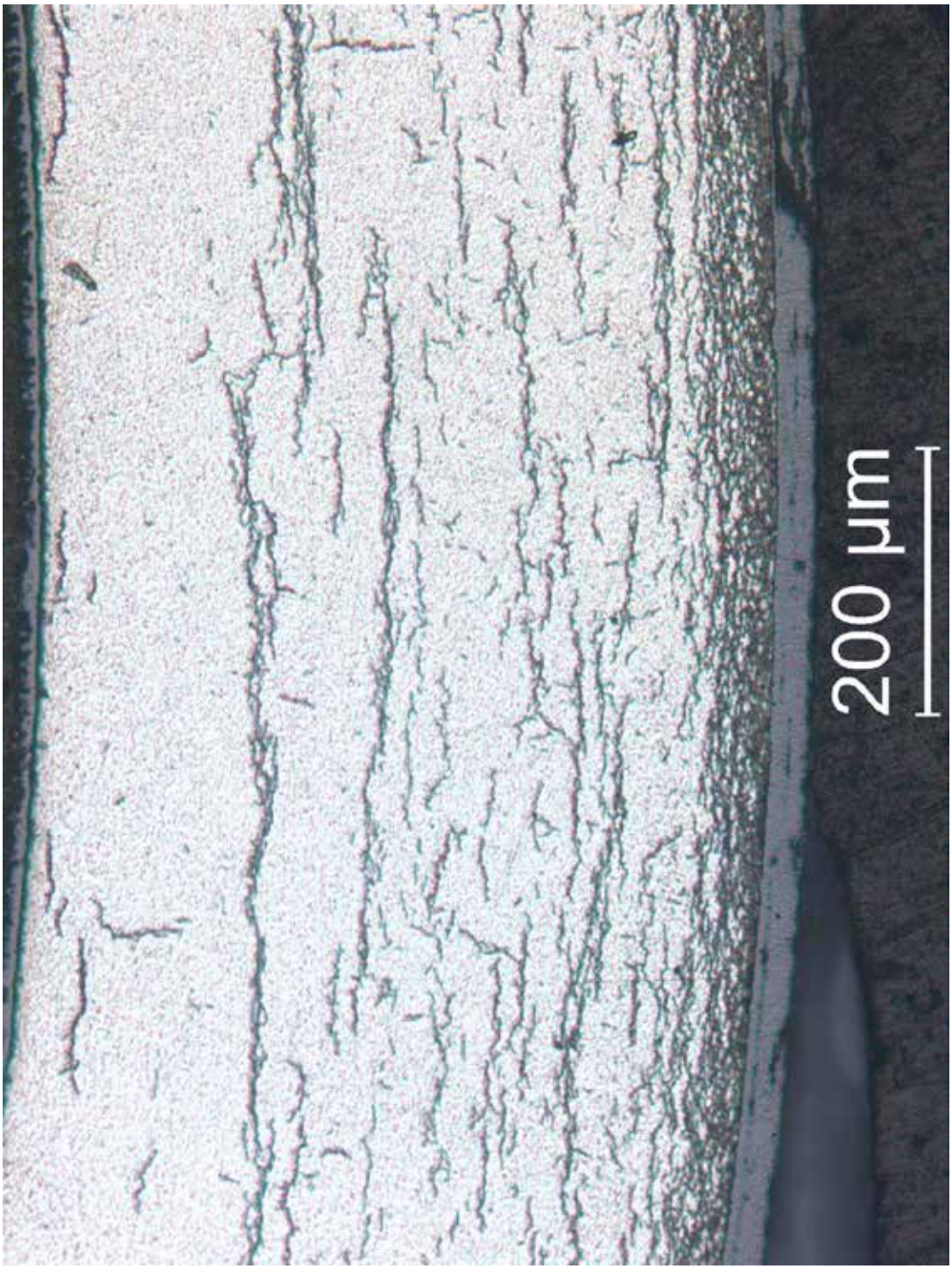

Figure A.21: Image (100X) of ZIRLO™ sample 646D6 in Area 21 from 1-cycle 350°C/87-MPa rodlet 646D.

Figure A.22: Image (100X) of ZIRLO™ sample 646D6 in Area 22 from 1-cycle 350°C/87-MPa rodlet 646D.

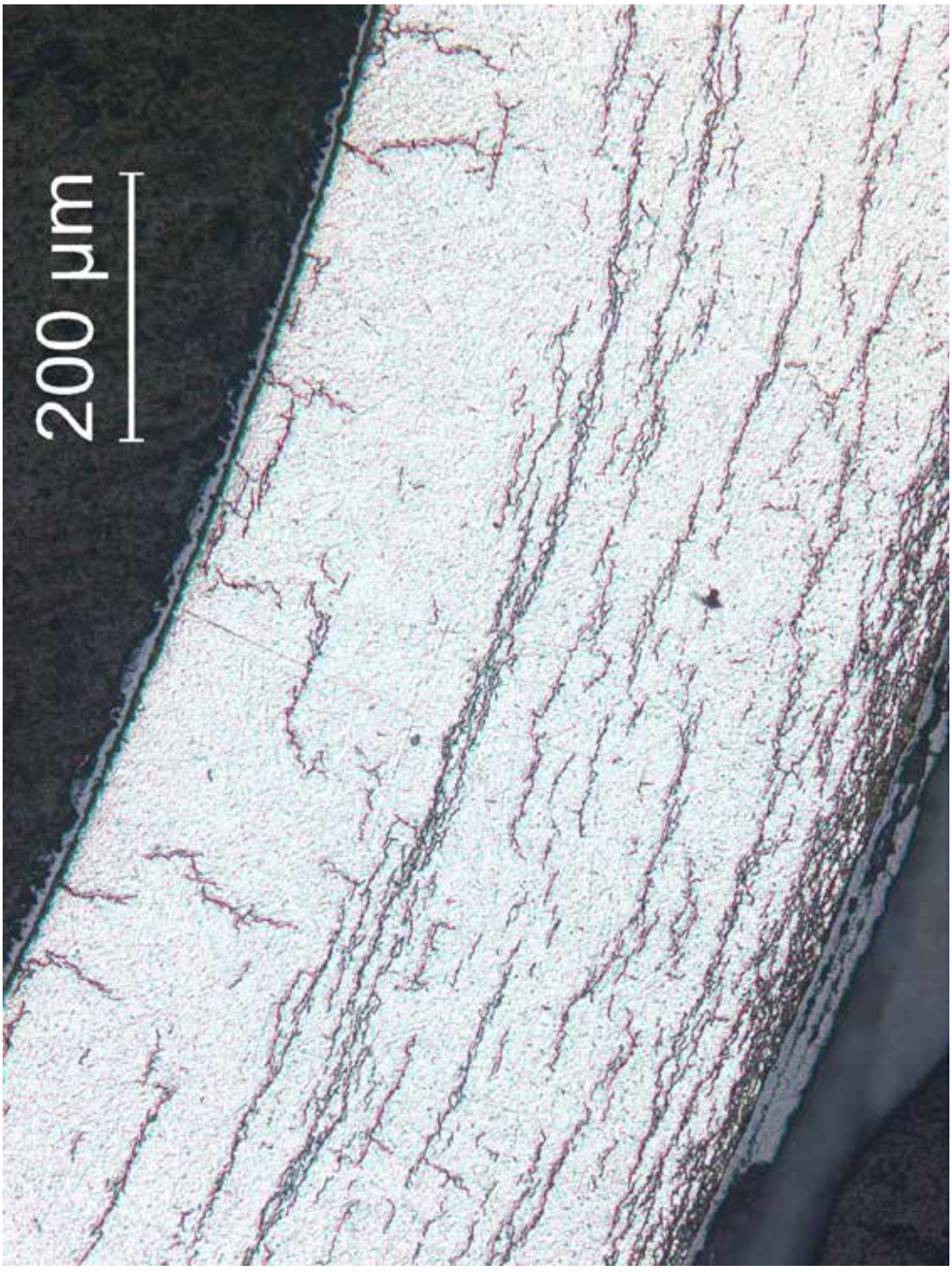

Figure A.23: Image (100X) of ZIRLO™ sample 646D6 in Area 23 from 1-cycle 350°C/87-MPa rodlet 646D.

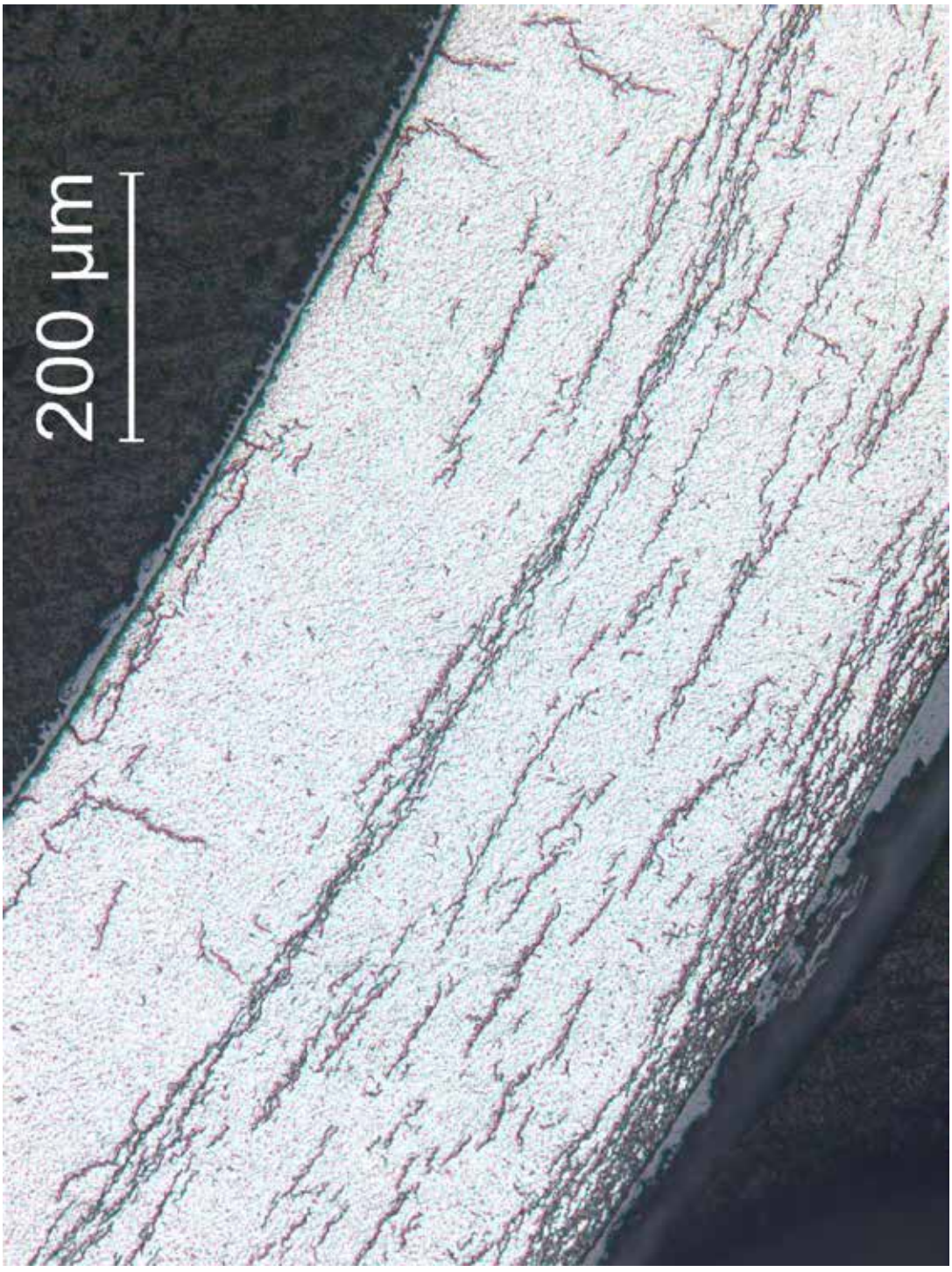

Figure A.24: Image (100X) of ZIRLO™ sample 646D6 in Area 24 from 1-cycle 350°C/87-MPa rodlet 646D..

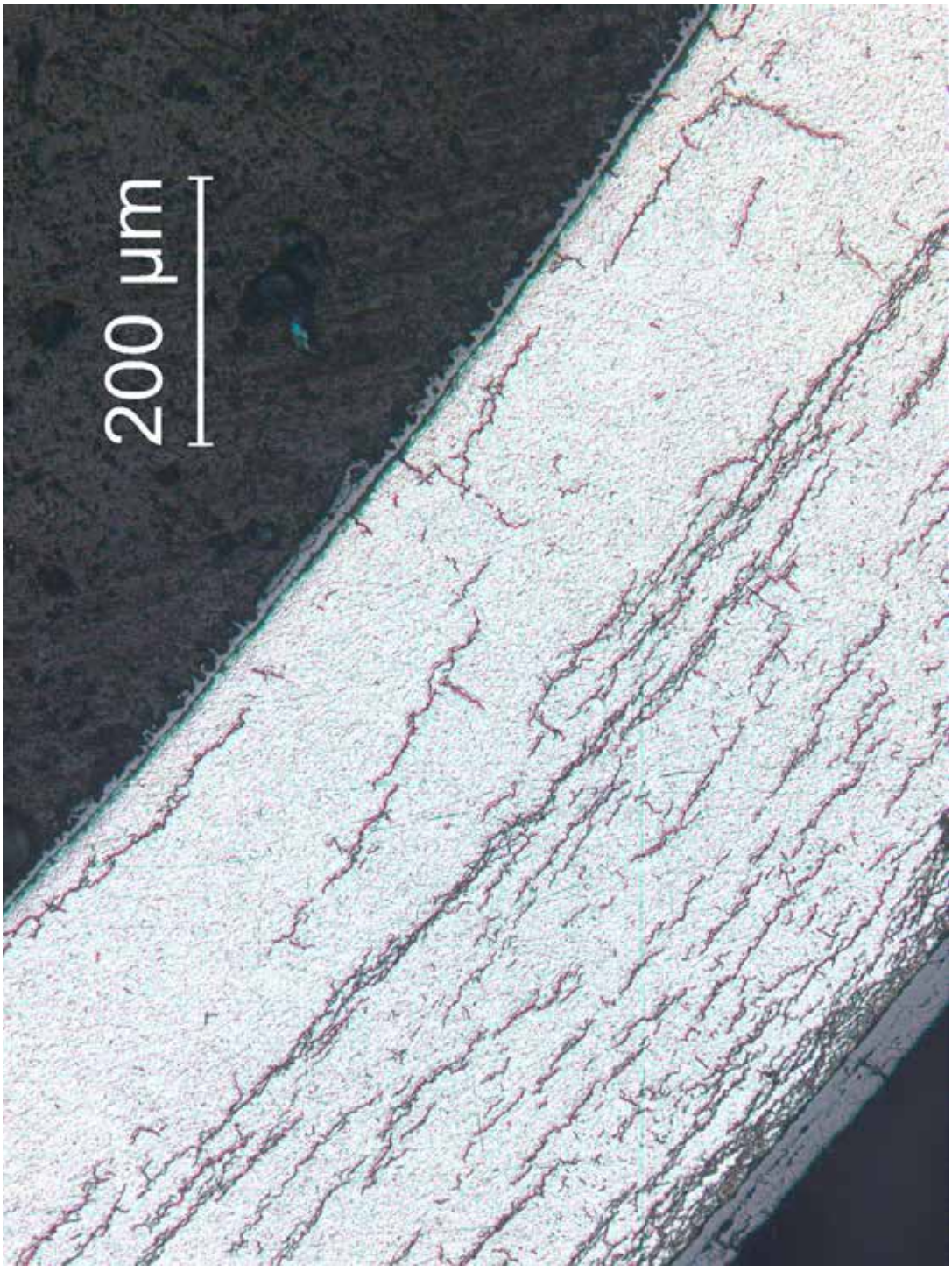

Figure A.25: Image (100X) of ZIRLO™ sample 646D6 in Area 25 from 1-cycle 350°C/87-MPa rodlet 646D.

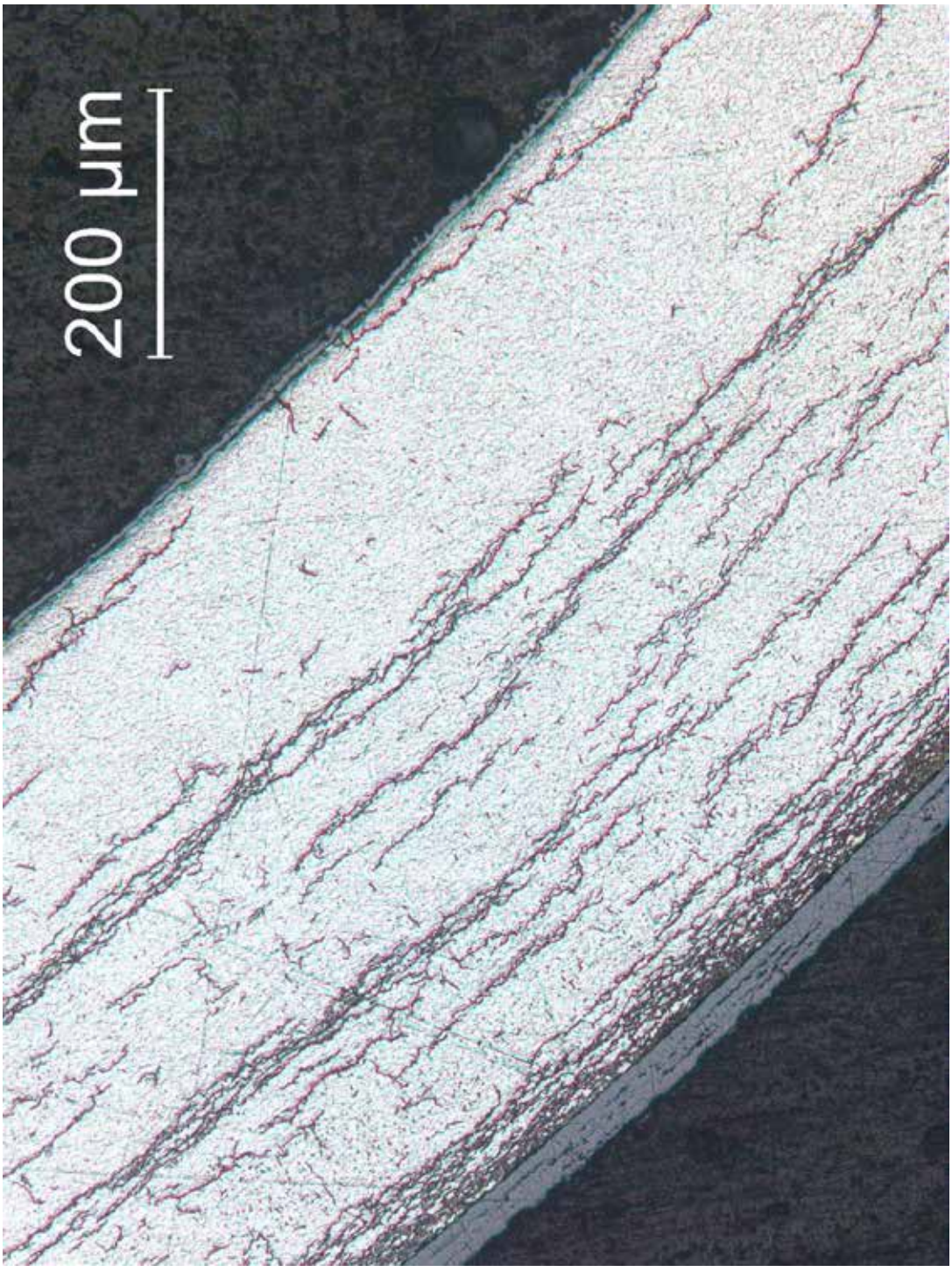

Figure A.26: Image (100X) of ZIRLO™ sample 646D6 in Area 26 from 1-cycle 350°C/87-MPa rodlet 646D..

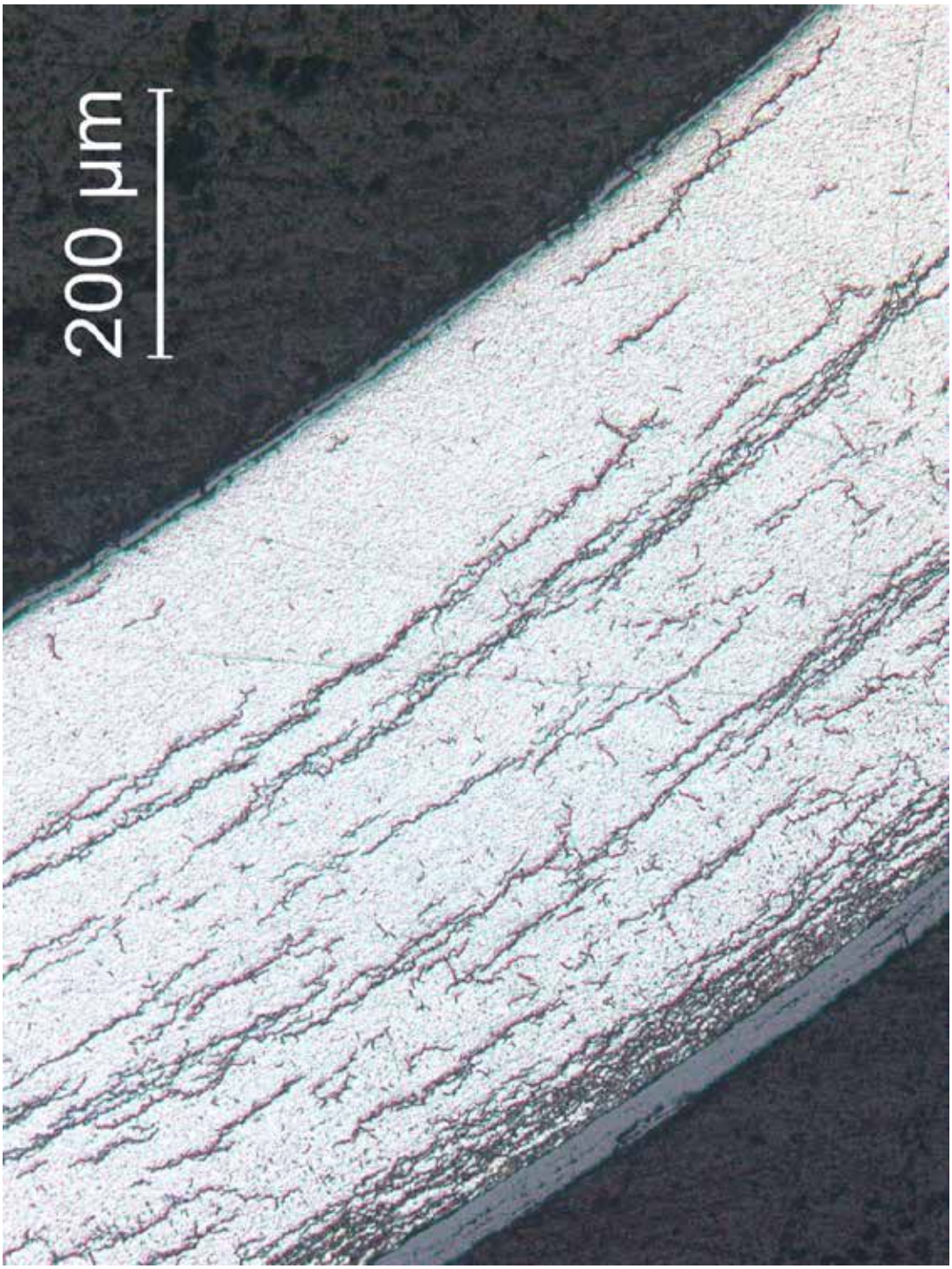

Figure A.27: Image (100X) of ZIRLO™ sample 646D6 in Area 27 from 1-cycle 350°C/87-MPa rodlet 646D.

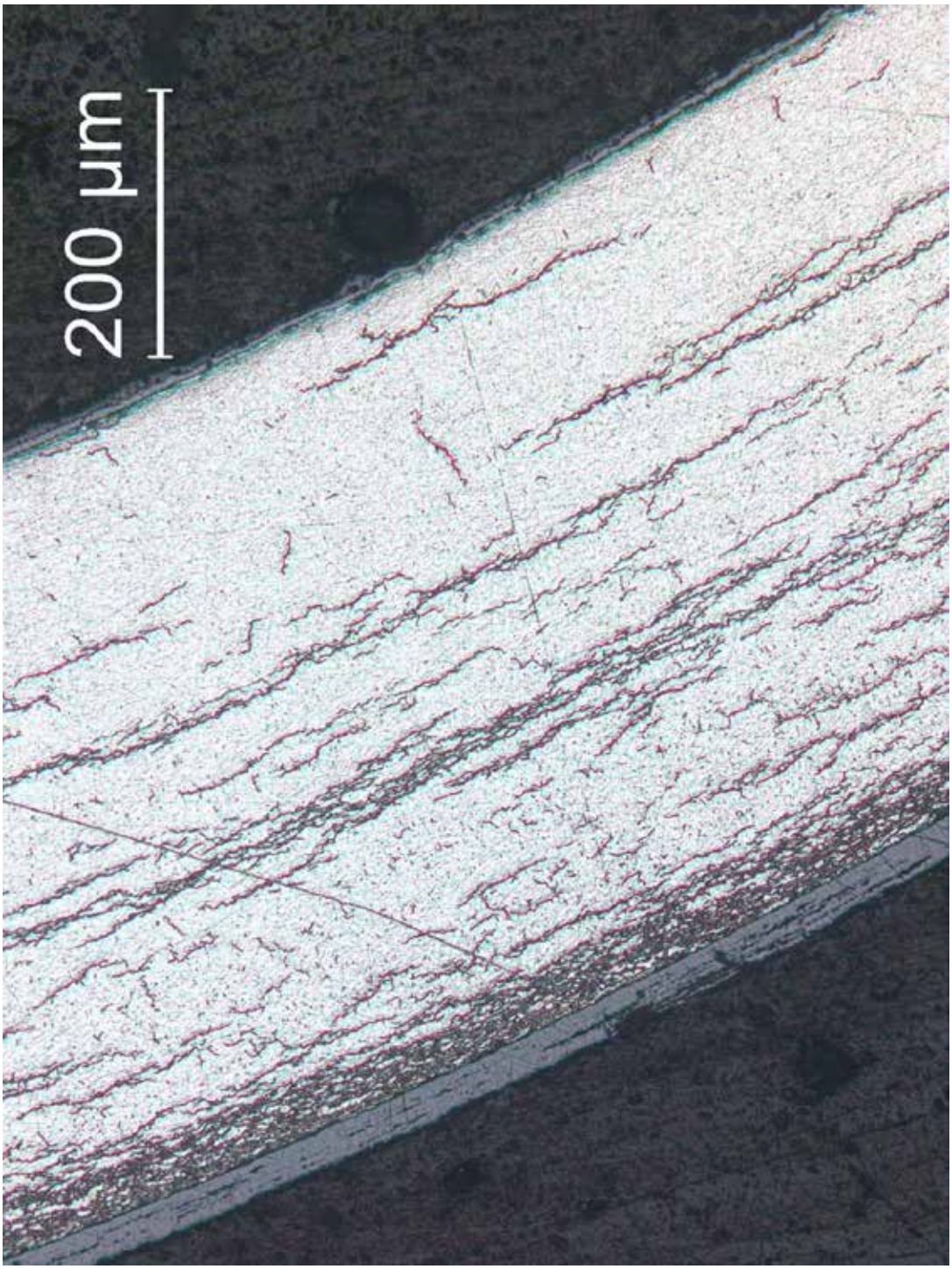

Figure A.28: Image (100X) of ZIRLO™ sample 646D6 in Area 28 from 1-cycle 350°C/87-MPa rodlet 646D.

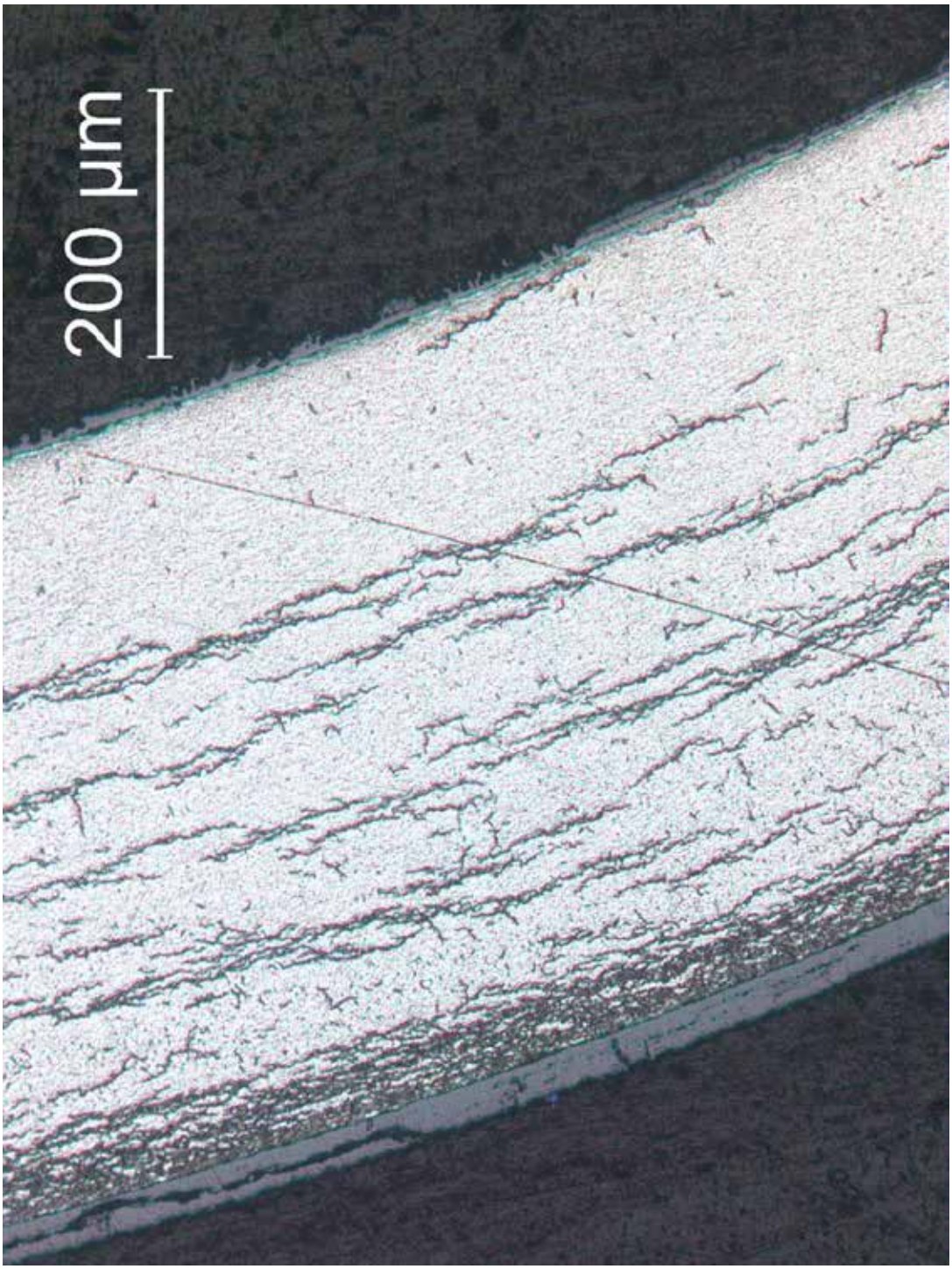

Figure A.29: Image (100X) of ZIRLO™ sample 646D6 in Area 29 from 1-cycle 350°C/87-MPa rodlet 646D.

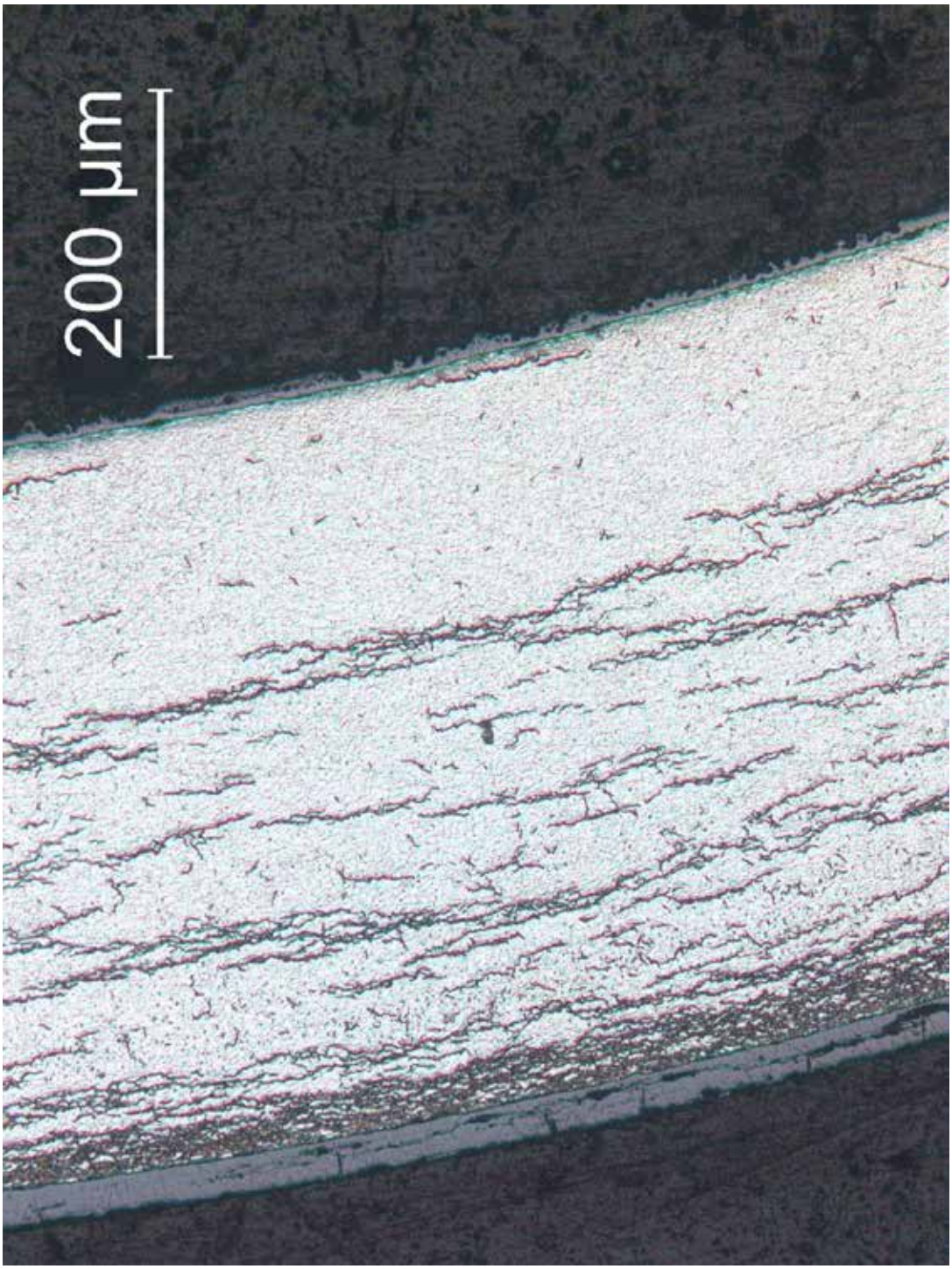

Figure A.30: Image (100X) of ZIRLO™ sample 646D6 in Area 30 from 1-cycle 350°C/87-MPa rodlet 646D.

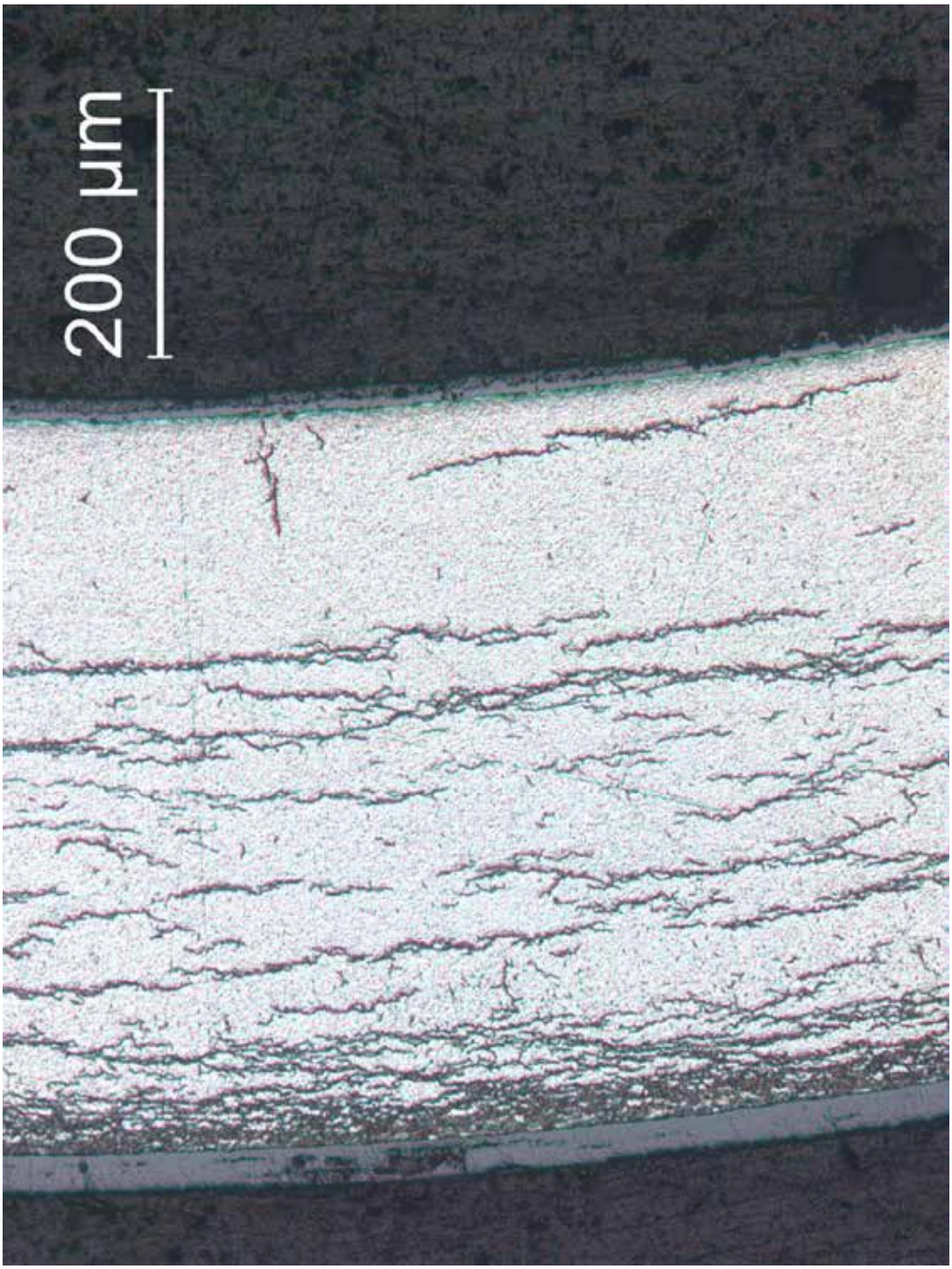

Figure A.31: Image (100X) of ZIRLO™ sample 646D6 in Area 31 from 1-cycle 350°C/87-MPa rodlet 646D.

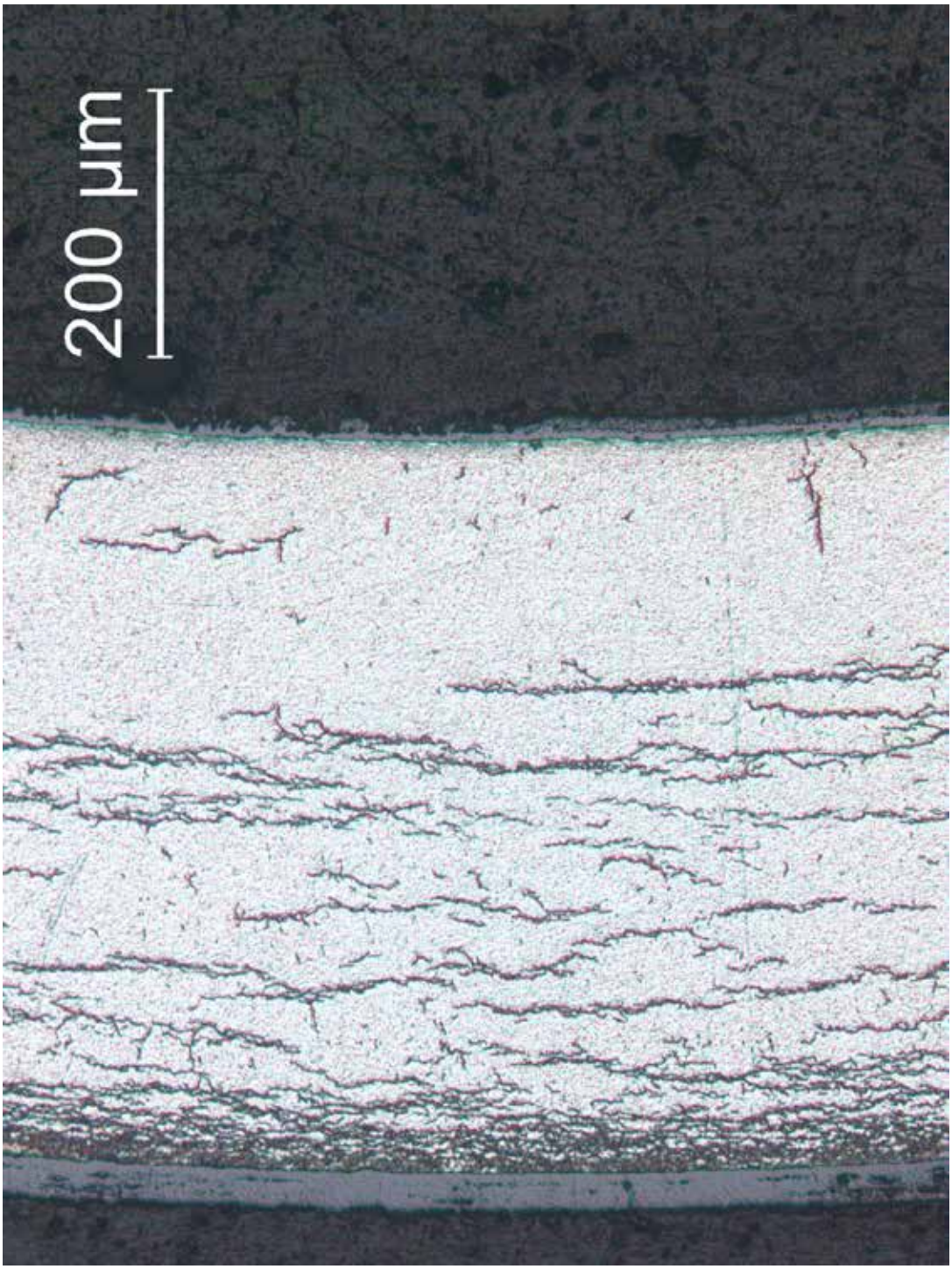

Figure A.32: Image (100X) of ZIRLO™ sample 646D6 in Area 32 from 1-cycle 350°C/87-MPa rodlet 646D.

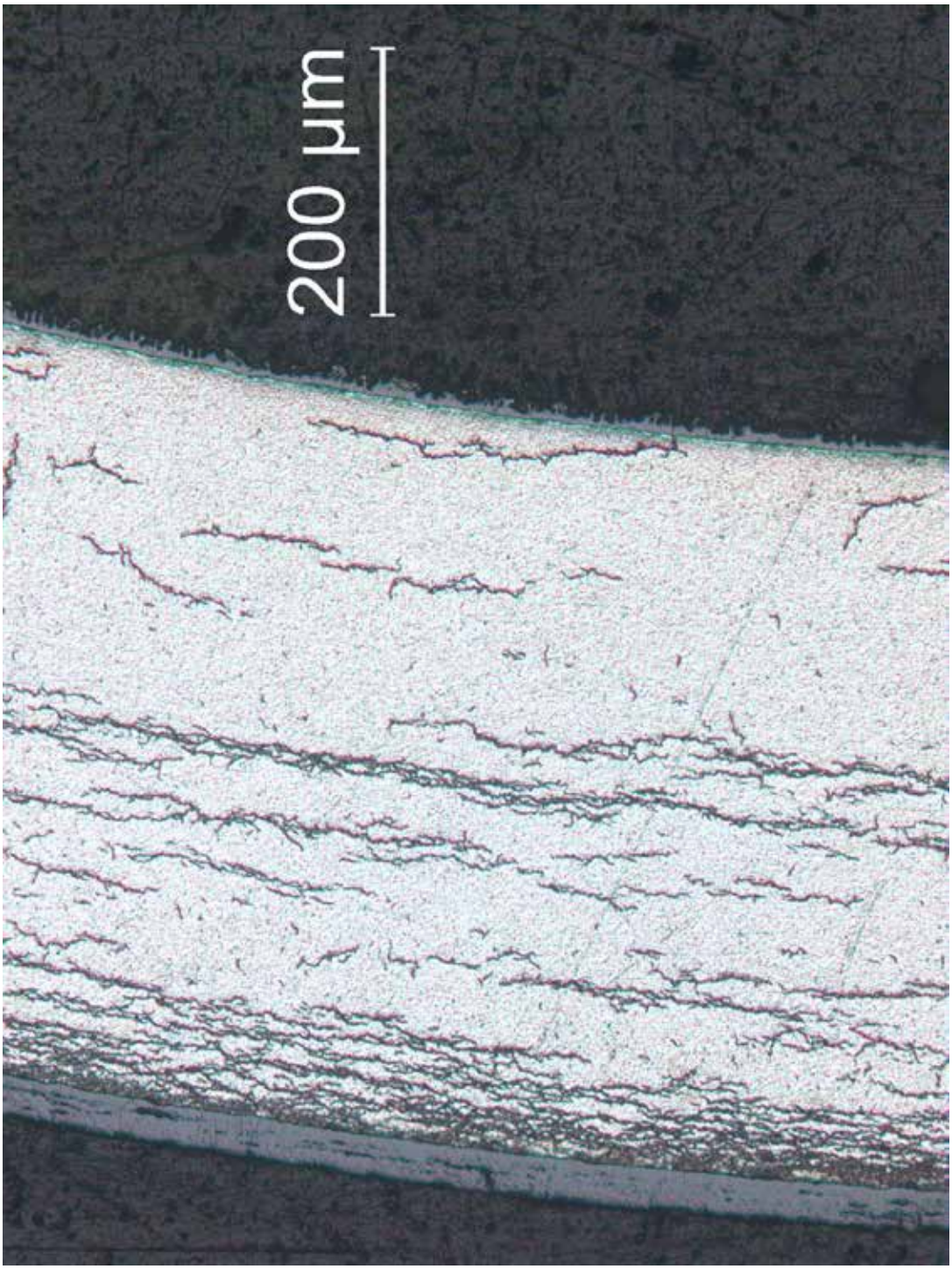

Figure A.33: Image (100X) of ZIRLO™ sample 646D6 in Area 33 from 1-cycle 350°C/87-MPa rodlet 646D.

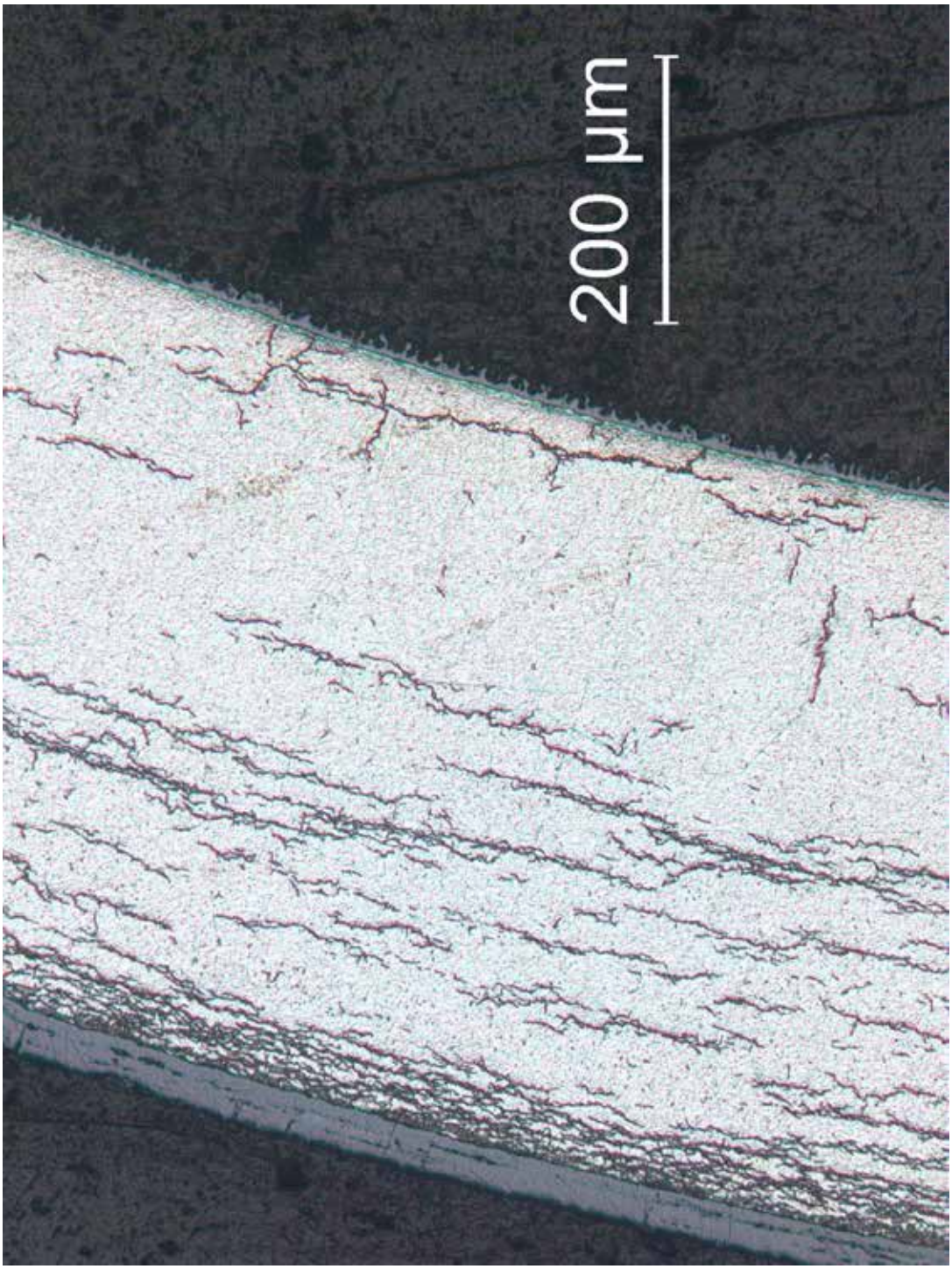

Figure A.34: Image (100X) of ZIRLO™ sample 646D6 in Area 34 from 1-cycle 350°C/87-MPa rodlet 646D.

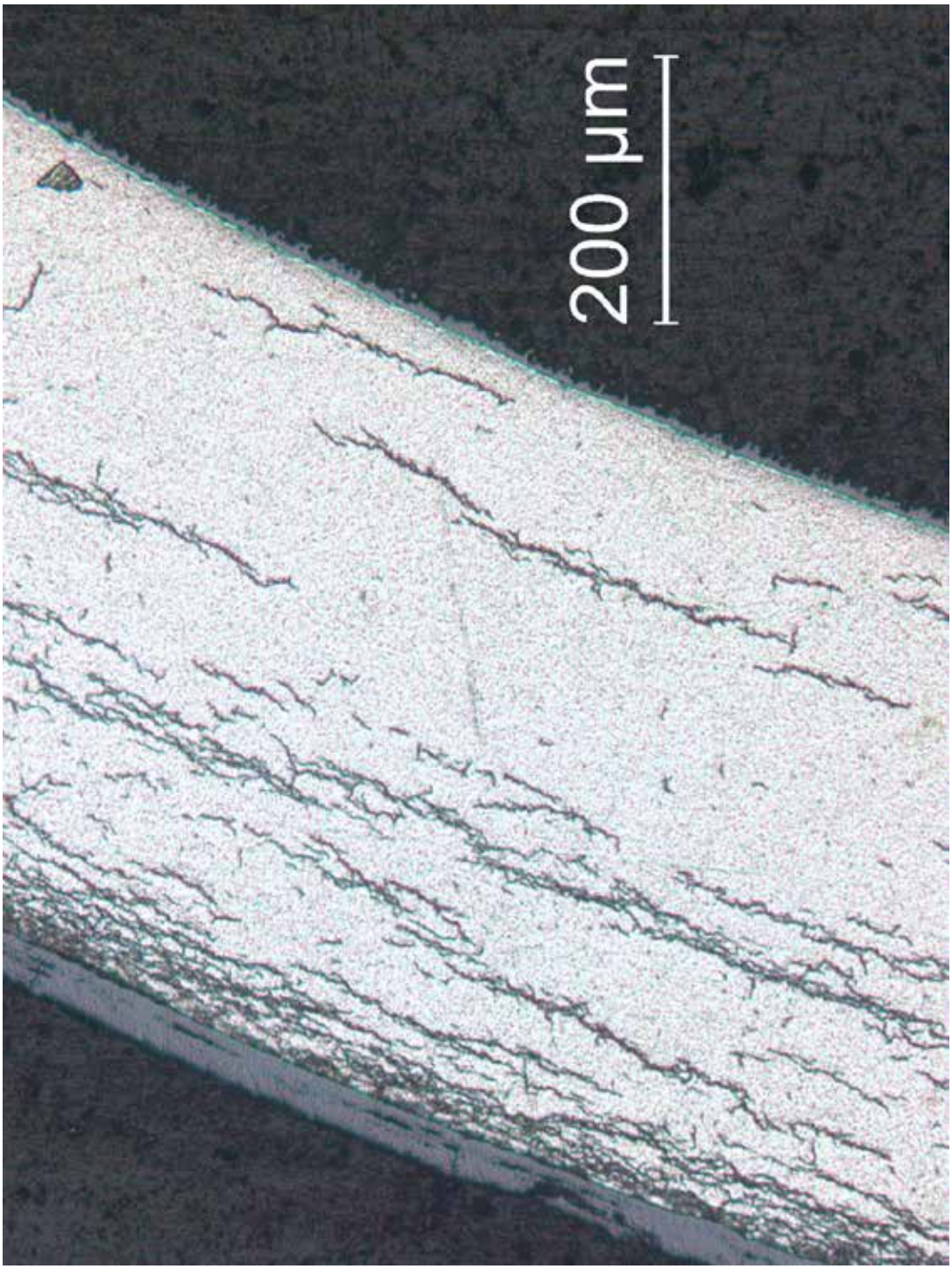

Figure A.35: Image (100X) of ZIRLO™ sample 646D6 in Area 35 from 1-cycle 350°C/87-MPa rodlet 646D.

Figure A.36: Image (100X) of ZIRLO™ sample 646D6 in Area 36 from 1-cycle 350°C/87-MPa rodlet 646D.

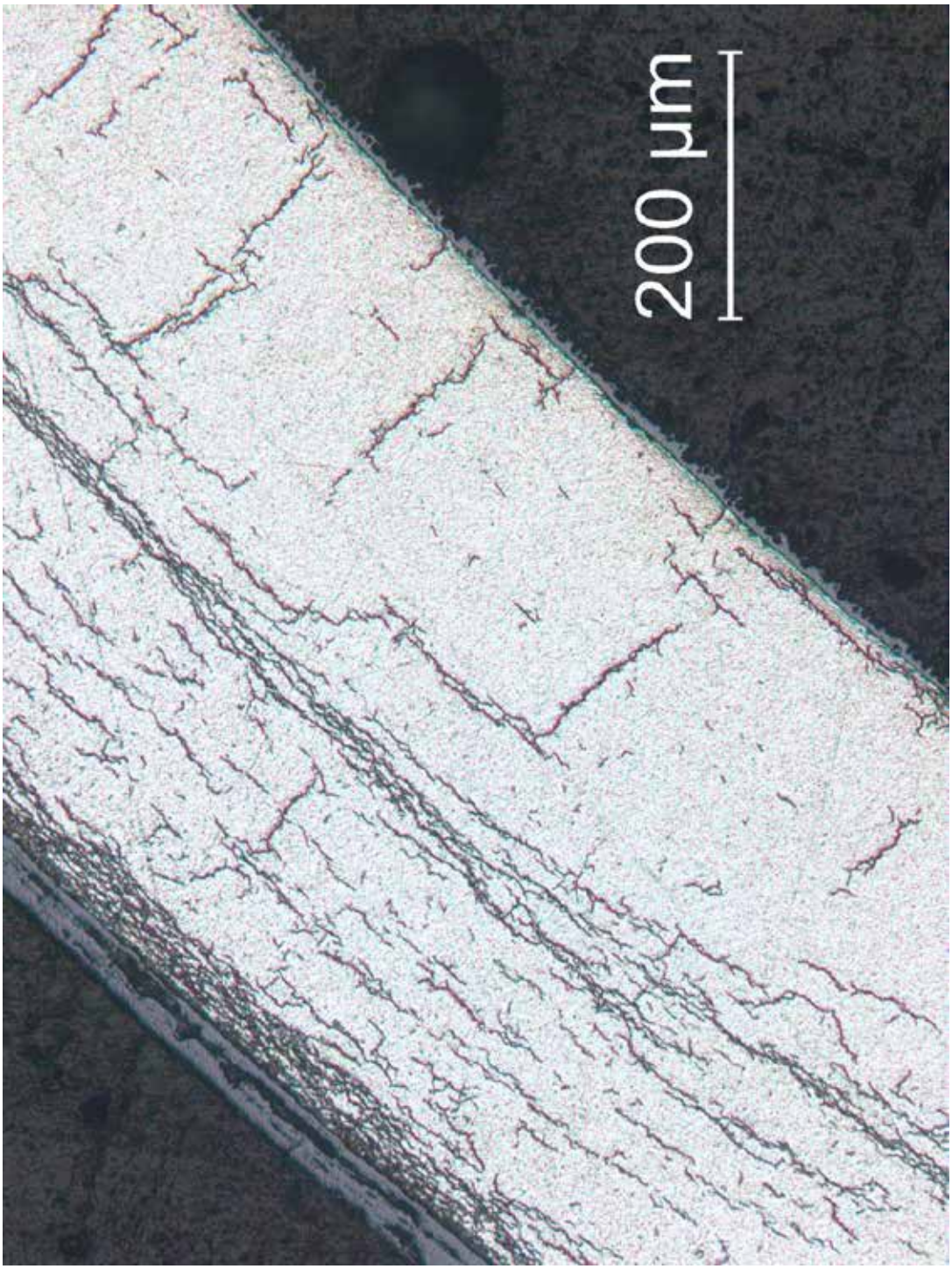

Figure A.37: Image (100X) of ZIRLO™ sample 646D6 in Area 37 from 1-cycle 350°C/87-MPa rodlet 646D.

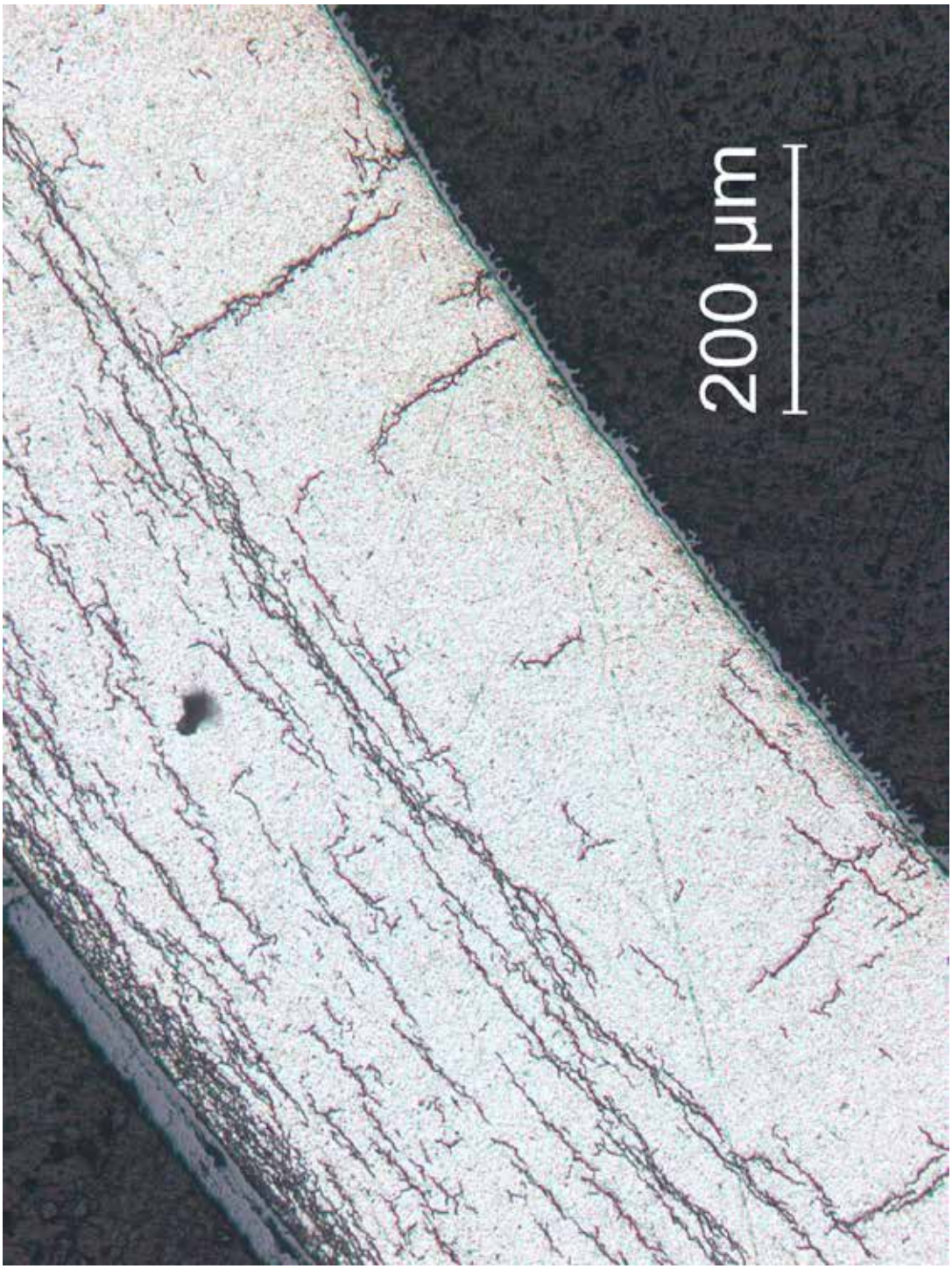

Figure A.38: Image (100X) of ZIRLO™ sample 646D6 in Area 38 from 1-cycle 350°C/87-MPa rodlet 646D.

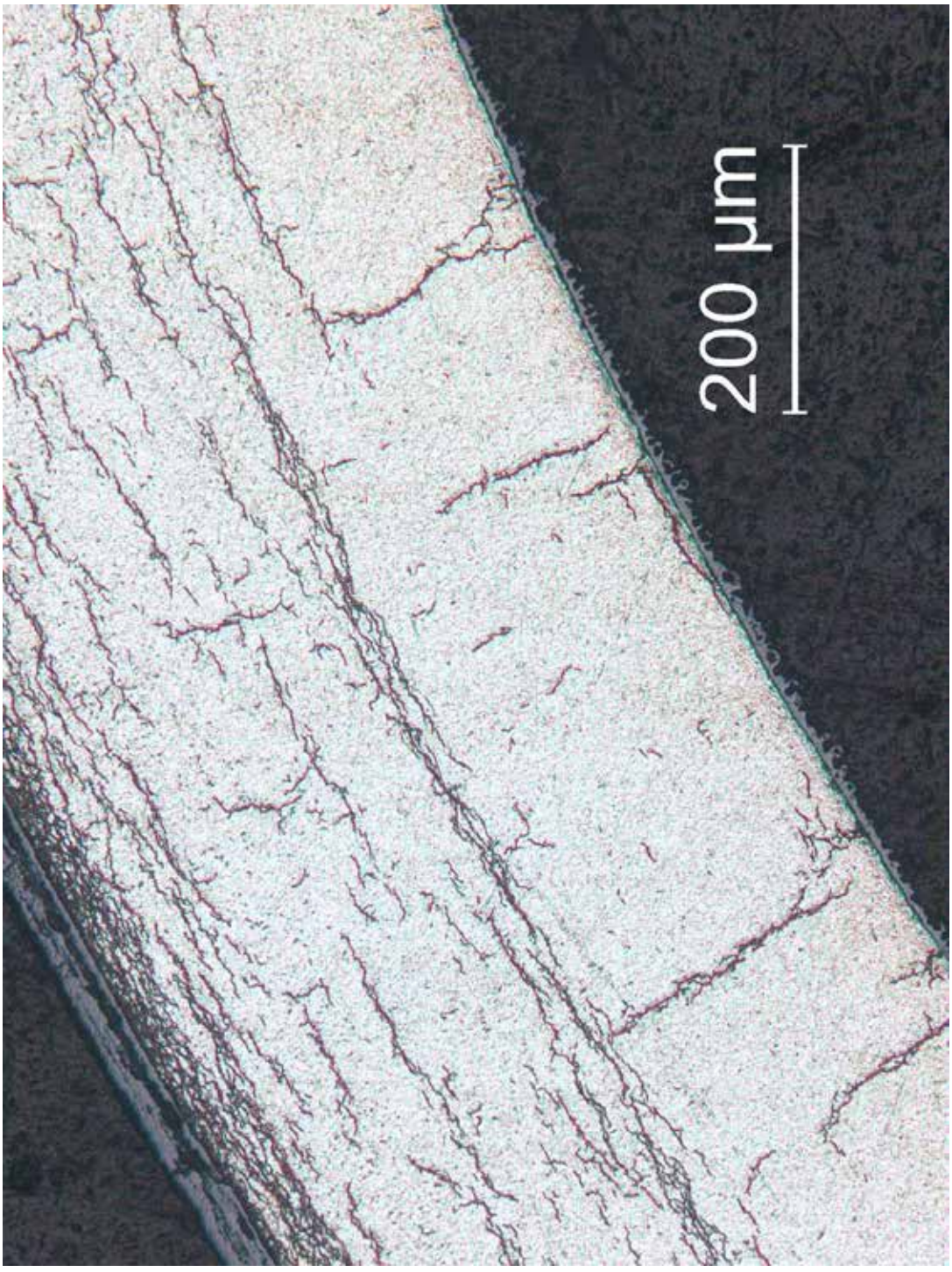

Figure A.39: Image (100X) of ZIRLO™ sample 646D6 in Area 39 from 1-cycle 350°C/87-MPa rodlet 646D.

Figure A.40: Image (100X) of ZIRLO™ sample 646D6 in Area 40 from 1-cycle 350°C/87-MPa rodlet 646D.

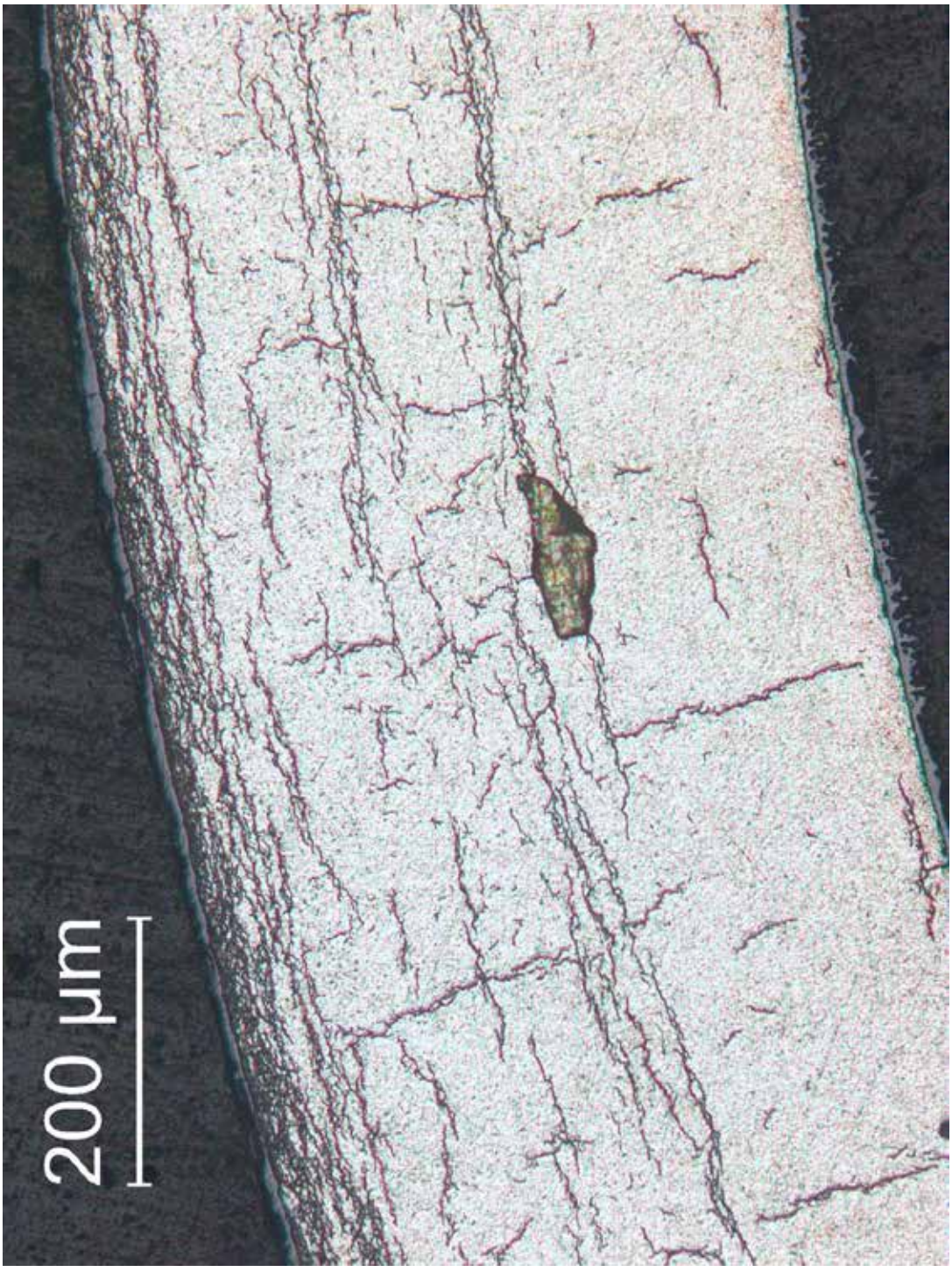

Figure A.41: Image (100X) of ZIRLO™ sample 646D6 in Area 41 from 1-cycle 350°C/87-MPa rodlet 646D.

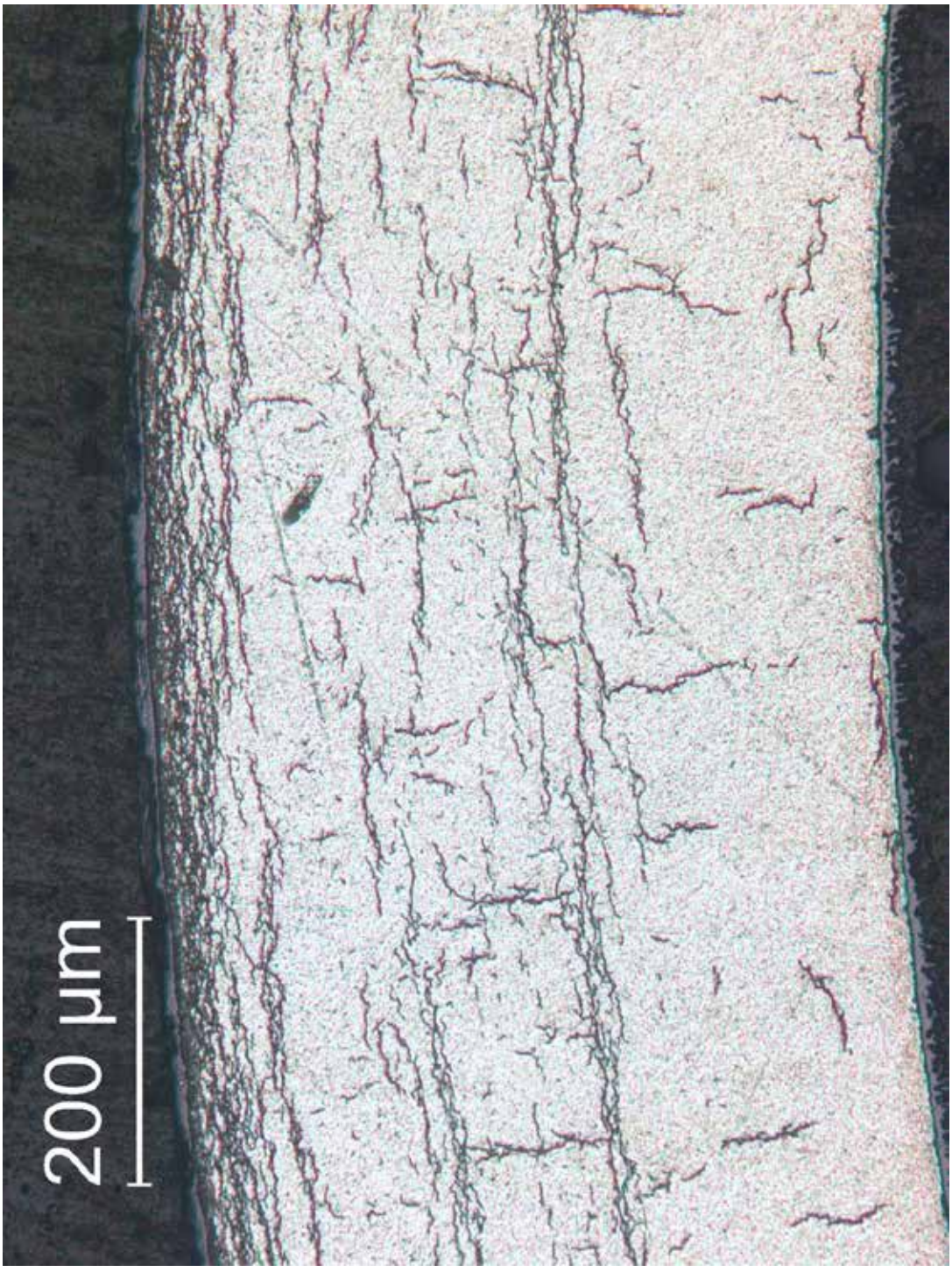

Figure A.42: Image (100X) of ZIRLO™ sample 646D6 in Area 42 from 1-cycle 350°C/87-MPa rodlet 646D.